



Development of new tools for eelgrass monitoring in Natura 2000 areas

Nielsen, Mette M.; Thomasberger, Aris D.; Svane, Niels; Thompson, Fletcher; Hansen, Flemming T.

Publication date:
2023

Document Version
Publisher's PDF, also known as Version of record

[Link back to DTU Orbit](#)

Citation (APA):
Nielsen, M. M., Thomasberger, A. D., Svane, N., Thompson, F., & Hansen, F. T. (2023). *Development of new tools for eelgrass monitoring in Natura 2000 areas*. DTU Aqua. DTU Aqua-rapport No. 437-2023

General rights

Copyright and moral rights for the publications made accessible in the public portal are retained by the authors and/or other copyright owners and it is a condition of accessing publications that users recognise and abide by the legal requirements associated with these rights.

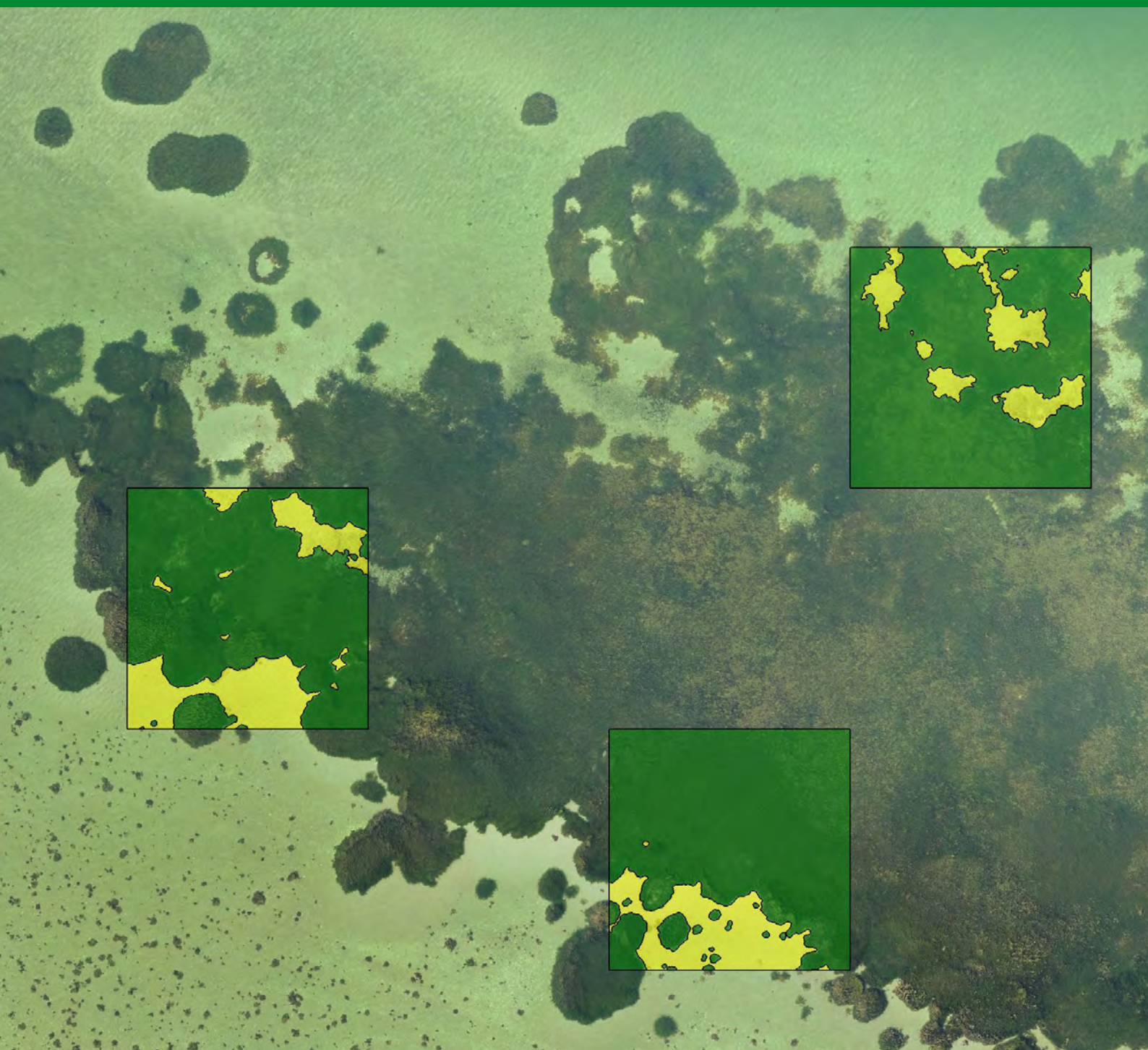
- Users may download and print one copy of any publication from the public portal for the purpose of private study or research.
- You may not further distribute the material or use it for any profit-making activity or commercial gain
- You may freely distribute the URL identifying the publication in the public portal

If you believe that this document breaches copyright please contact us providing details, and we will remove access to the work immediately and investigate your claim.

Development of new tools for eelgrass monitoring in Natura 2000 areas

Mette M. Nielsen (Ed.), Aris D. Thomasberger, Niels Svane, Fletcher Thompson and Flemming T. Hansen

DTU Aqua Report no. 437-2023



Development of new tools for eelgrass monitoring in Natura 2000 areas

Mette M. Nielsen¹ (Ed.), Aris D. Thomasberger¹, Niels Svane², Fletcher Thompson¹ and Flemming T. Hansen¹

¹ Technical University of Denmark, DTU Aqua

² University of Southern Denmark, Department of Biology

DTU Aqua Report no. 437-2023

Colophon

Title:	Development of new tools for eelgrass monitoring in Natura 2000 areas
Authors:	Mette M. Nielsen ¹ (Ed.), Aris D. Thomasberger ¹ , Niels Svane ² , Fletcher Thompson ¹ and Flemming T. Hansen ¹ ¹ Technical University of Denmark, DTU Aqua ² University of Southern Denmark, Department of Biology
DTU Aqua Report no.:	437-2023
Year:	Scientific work finalized May 2023. Report published December 2023
Reference:	Nielsen, M.M., Thomasberger, A.D., Svane, N., Thompson, F. & Hansen, F.T. (2023). Development of new tools for eelgrass monitoring in Natura 2000 areas. DTU Aqua Report no. 437-2023. National Institute of Aquatic Resources, Technical University of Denmark. 96 pp.
Quality assurance:	The report has been reviewed by Professor Jens Kjerulf Petersen, DTU Aqua and Professor Mogens Flindt, SDU
Cover photo:	Eelgrass bed in Horsens Fjord obtained in July 2021 from 100m altitude drone flight. Subsections classified into eelgrass (green) and sand (yellow). Photo: Aris Thomasberger
Published by:	National Institute of Aquatic Resources, Øroddevej 80, 7900 Nykøbing Mors, Denmark
Download:	www.aqua.dtu.dk/publikationer
ISSN:	1395-8216
ISBN:	978-87-7481-370-5

DTU Aqua Reports contain results from research projects, reviews of specific topics, expositions for authorities etc. Unless stated in the colophon, the reports are not peer reviewed, which means that the content has not been reviewed by researchers outside the project group.

Preface

This report presents the results from the project “Udvikling af værktøjer til omkostningseffektiv monitoring af ålegræs i Natura-2000 områder” (ref.no. 33113-B-19-141), which received financial support from the European Maritime and Fisheries Fund and the Danish Ministry for Food, Agriculture and Fisheries (“Ministeriet for Fødevarer, Landbrug og Fiskeri”) in the program “Fiskeri, natur og miljø - marin biodiversitet og økosystemer”. The project period was from June 2019 to May 2023.

All published DTU Aqua research reports can be downloaded in electronic format from the DTU Aqua webpage: www.aqua.dtu.dk/Publikationer.

Original texts and illustrations from this report may be reproduced for non-commercial purposes provided that clear source information is provided.

Nykøbing Mors, December 2023

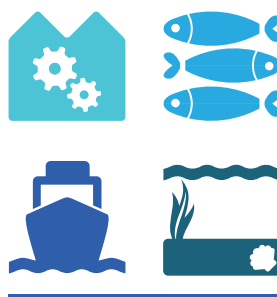
Mette Møller Nielsen
Project manager

DTU Aqua
Section for Coastal Ecology
Øroddevej 80
7900 Nykøbing Mors
Ph.: +45 96 69 02 83
post@skaldyrcenter.dk
aqua.dtu.dk/english/research/coastal-ecology



Den Europæiske Union
Den Europæiske Hav- og Fiskerifond

HAV & FISK



Content

Dansk resumé	5
English summary	8
1. Introduction.....	11
1.1 The Danish case – bottom dredging in Natura-2000 sites.....	11
1.2 Monitoring of submerged aquatic vegetation.....	11
1.3 Project aim and approach	15
2. Monitoring eelgrass with Unoccupied Aerial Vehicles (WP1)	16
2.1 Large-scale mapping.....	17
2.2 Monitoring eelgrass in deep or turbid waters using different platform and sensor systems..	20
2.3 Change detection	27
2.4 Evaluating stressors.....	33
2.5 Ground truthing using drone platforms.....	44
2.6 Image analysis	51
2.7 Discussion and recommendations.....	54
3. Underwater Remotely Operated Vehicles (WP2)	58
3.1 Background	58
3.2 Results	62
3.3 Discussion.....	69
4. Improving existing GIS models for eelgrass distribution (WP3).....	71
4.1 Improved interpolation of data into model layers.....	72
4.2 Further improvement of model layers – light and shear stress.....	77
4.3 Implementing drone-data into GIS models	87
5. Conclusions and recommendations	91
References	95

Dansk resumé

Ålegræs er en vigtig økosystemkomponent i det marine miljø, der dels skaber vigtige yngel- og opvækstområder for fisk og bunddyr og dels medvirker til at stabilisere havbunden og bl.a. derfor anvendes ålegræs som en vigtig indikator for den økologiske tilstand i marine vandområder. Traditionelt set er overvågningsprogrammer for ålegræs funderet i dykker- og video-undersøgelser, som på trods af at være solide videnskabelige metoder, er kendetegnet ved dels at være tidskrævende, og dels at have begrænset brug på større skala. I de senere år har en teknologisk udvikling indenfor brugen af droner til miljøovervågning dog åbnet nye muligheder, således kortlægning af ålegræs kan udvikles mod en mere præcis og arealbaseret tilgang.

For at undersøge mulighederne for at integrere droneteknologi som redskab i overvågningen af ålegræs – fx ifm. konsekvensvurderinger af fiskeri i Natura 2000 områder eller ifm. 3. generationsvandplanerne – har vi i dette projekt testet brugen af henholdsvis luftbårne droner (*unoccupied aerial vehicles* [UAV]) og undervandsdroner (*remotely operated vehicles* [ROV]) og *autonomous underwater vehicles* [AUV]) til at kortlægge ålegræs i forskellige typer af vandområder i danske farvande. Derudover er det undersøgt, hvorvidt et tidligere udviklet GIS-værktøj, der bruges til bestemmelse af ålegræssets potentielle udbredelse ifm. konsekvensvurderinger af fiskeri i Natura 2000 områder, kan optimeres ved bl.a. at implementere drone-baserede data og forbedre interpolationen af forskellige input-lag

Undersøgelserne viste, at brugen af luftbårne droner kan være et middel til at opnå bedre data-nøjagtighed, lavere ressourceforbrug og øget kost-effektivitet end det er tilfældet ved traditionelle kampagne-programmer baseret på punktobservationer og video-undersøgelser. Konkret anbefaler vi på baggrund af en række del-undersøgelser i projektet, der dækker forskellige aspekter indenfor drone-kortlægning, et robust, alsidigt og omkostnings-effektivt setup. Del-undersøgelserne beskæftigede sig med følgende temaer: monitoring på bassin-skala (afsnit 2.1), monitoring på dybt eller i uklart vand (afsnit 2.2), identifikation af sæsonbestemte og stress-relaterede ændringer (afsnit 2.3), identifikation og analyse af diverse stressfaktorer, der påvirker ålegræsset (afsnit 2.4), indsamling af data til *ground truthing* (afsnit 2.5) og metoder til billedanalyse (afsnit 2.6).

Det anbefalede setup adresserer samtlige af disse aspekter indenfor ålegræs-monitoring og er baseret på en let multi-rotor drone med et højopløseligt RGB-kamera i kombination med et RTK modul for høj geopræcision. Med setuppet der blev anvendt i dette studie (DJI Phantom 4 RTK) var det således muligt at kortlægge et område på 300 hektar i et lavvandet fjordområde på 6,5 timer i felten (afsnit 2.1). Foruden dronen anbefales software til henholdsvis planlægning og udførsel af drone-flyvningerne, til billedanalyse, samt et GIS software. Desuden kan et system med et drone-opereret sænkbart undervandskamera kobles på setuppet til indsamling af *ground truthing* data. I projektet blev flere sådanne systemer testet med den konklusion at et enkelt modulært system, der kan kobles direkte på selvsamme drone, der anvendes til kortlægningen, er en fuld valid og funktionel løsning til indsamling af valideringsdata ifm. en kortlægningsmission (afsnit 2.5). En større drone-platform (DJI Matrice 600) blev desuden testet og fundet nyttigt ift. at tilkoble forskellige loggere til systemet.

I monitoringsprogrammer, der dækker større områder såsom de årlige konsekvensvurderinger af muslingefiskeri i Natura 2000 områder, viser resultaterne, at ved kun at fokusere på de dybere områder med de traditionelle video-baserede metoder og i stedet udføre kortlægningen på de lavere vanddybder med droner, så opnås ikke alene en tidsbesparelse af kortlægningen, men også en kortlægning med signifikant bedre rummelig opløsning og højere geografisk nøjagtighed.

En sammenligning af forskellige sensor-systemer viste at brugen af konventionelle RGB-kameraer med høj opløsning langt overgår mere avancerede multi-spektrale sensorer med lavere opløsning i områder med enten dybt eller uklart vand (afsnit 2.2). Dog kan en mere avanceret multispektral sensor let tilføjes de lette multi-rotor droner, hvis en sådan ønskes anvendt for eksempel ved kortlægning af fritlagt ålegræs (ved lavvande) eller i områder med klart/lavt vand under gunstige forhold.

Identifikation af ændringer af ålegræssets tilstand på bed-skala blev fundet muligt med brug af RTK-funktionen på den anvendte drone (RTK=*real time kinetics*). Med denne funktion opnås data med tilstrækkelig høj geografisk præcision til at kunne følge udviklingen af specifikke bed-områder uden den tidskrævende opgave at udlægge referencepunkter i området for præcis geolokalisering. Desuden muliggjorde metoden kvantificering og kvalificering af stressorer, der påvirker ålegræsset, hvormed en mere holistisk beskrivelse af et område, der også inddrager økologiske processers indflydelse på ålegræsset kan opnås (afsnit 2.3).

I projektet blev brugen af objektbaseret billedanalyse (OBIA=*object-based image analysis*) til databehandling af det drone-indsamlede data undersøgt. Resultaterne viste, at denne type billedanalyse er særdeles brugbar til at analysere dronebaserede data af høj opløselighed og resultaterne i afsnit 2.6, der omhandler dette kan bruges som en guideline til hvordan man processerer sit data og som støtte til at vælge de rette algoritmer for klassificering.

Undervandsdronerne (ROV og AUV), der blev testet i projektet (afsnit 3) viste sig at være gode alternative redskaber til monitoring af ålegræs i områder, der ikke umiddelbart er tilgængelige for de luftbårne droner – fx i dybe farvande eller områder med høj turbiditet. AUV-systemerne gav umiddelbare gode data af stabil karakter selv på dybt vand og over lange strækningen, mens ROV-systemerne havde udfordringer med geopræciseringen af data. ROV-systemet var dog enkelt at operere og giver desuden mulighed for at følge optagelserne live, om end dette samtidigt betyder at deres rækkevidde er begrænset til længden på kablet. Den største udfordring ved at kortlægge ålegræs med undervandsdroner er dog ufravigeligt problemer med korrekt geopræcisering af data.

Arbejdet omkring optimering af GIS værktøjet, der anvendes i konsekvensvurderinger for fiskeri i Natura 2000 områder til at udpege potentielle ålegræsområder, viste at nøjagtigheden af de data-lag, der baseres på enten punktobservationer fra felten eller fra simulerede modeller kunne forbedres væsentligt ved opgradering af de anvendte interpolationsmetoder (afsnit 4.1). Desuden blev der for model-lagene lys og forskydningsspænding fundet yderligere muligheder for forbedring. Resultaterne viser bl.a. hvordan en genberegning af lyssvækkelseskoefficienten i kombination med forbedret batymetri-data øger nøjagtigheden af model-laget for lys. For det simulerede data-lag for forskydningsspænding anbefales en metode til at opnå en tilsvarende højere nøjagtighed, baseret på input fra de hydrodynamiske modeller udviklet til Miljøstyrelsen og

en mere præcis repræsentation af batymetri (afsnit 4.2). Slutteligt blev det vist at implementering af drone-baserede data-lag for ålegræs fremfor interpolerede lag baseret på punktobservationer, giver et yderligere potentiale for forbedring af GIS værktøjet (afsnit 4.3).

Med dette projekt konkluderer vi at drone-baseret ålegræs-kortlægning kan og bør inkluderes i fremtidige monitoringsprogrammer og vi giver klare anbefalinger for det nødvendige setup herfor, som sikrer datasammenlignelighed og høj brugervenlighed og som samtidig er robust og kost-effektivt. I et fremtidigt scenarie, hvor der udelukkende fokuseres på monitoring på stor skala i faste overvågningsprogrammer, bør systemer som fastvingedroner eller hybrid-droner desuden dog undersøges.

English summary

The importance of eelgrass beds as a coastal marine habitat and provider of a wide range of ecosystem services has for decades motivated researchers and managers to investigate abundance and growth dynamics to understand linkages to human perturbations, secure protection and allow restoration. In European coastal waters, eelgrass monitoring campaigns traditionally involve diver observations and/or video recordings. While these techniques provide very useful data, they are rather time consuming, labor-intensive, and limited in their spatial coverage.

Technical innovations in recent years in the field of drone technology have opened up for new approaches to eelgrass monitoring, allowing to shift from point specific measurements to area based monitoring, without compromising the spatial resolution needed.

To investigate the possibility of integrating drone technology into national eelgrass monitoring programs, such as the environmental impact assessments within Natura 2000 areas or the 3rd generation water plans, the functionality of unoccupied aerial vehicles (UAVs), remotely operated vehicles (ROVs) and autonomous underwater vehicles (AUVs) for eelgrass mapping purposes was tested in Danish water bodies of different characteristics. Furthermore, it was tested, if and how a formerly developed GIS tool used as part of the environmental impact assessments in Natura 2000 areas can be optimized by incorporating information on eelgrass distribution obtained by UAVs as well as by improving currently used methods of including point specific observation from video transects and improving certain model derived layers themselves.

Testing UAVs in different monitoring scenarios showed, that accuracy, time, and cost efficiency of traditional in-water eelgrass monitoring campaigns can be improved in many cases, if supported by UAV-based monitoring methods. A recommendation of a robust, versatile, and cost-efficient set-up could be given after having conducted field studies that addressed different aspects of UAV based monitoring. These aspects included large-scale monitoring (section 2.1), monitoring in deep or turbid waters (section 2.2), detection of seasonal and stress related change (section 2.3), detection and analysis of stressors affecting eelgrass populations (section 2.4), the collection of ground truthing data (section 2.5) and the image analysis process (section 2.6).

The suggested set-up to address these aspects of eelgrass monitoring is based around a light-weight multi-rotor UAV equipped with a high resolution RGB camera and an RTK module. With the multi-rotor UAV used in this project (DJI Phantom 4 RTK) it required 6.5 hours of field work to monitor 300 ha of shallow water habitats (section 2.1). Suggested software packages include a flight mission planning software, image processing and analysis software as well as GIS software. An optional UAV-based underwater camera system can be added if ground truthing data needs to be collected.

Different UAV-based underwater camera systems were tested for the purpose of efficient ground truthing data collection. A low-tech solution presented in section 2.5, could be quickly mounted to the same low weight multirotor UAV (DJI Phantom 4 RTK) used for the aerial monitoring and proved to be a good solution for the efficient collection of ground truthing data after or

before a survey mission. A larger ground truthing system carried by a multirotor UAV (DJI Matrice 600) was successfully tested for the application of additional loggers.

In relation to large-scale monitoring programs, such as the environmental impact assessments in Natura 2000 areas, the results showed that by focusing on deeper waters with the traditional video-based methods and instead use UAVs to monitor eelgrass in shallow areas, not only fewer resources are spent but also the quality of the produced information in terms of spatial accuracy and resolution can be significantly improved.

A comparison of different sensors showed that high spatial resolution of conventional RGB cameras is superior to more advanced narrow band but lower resolution multispectral cameras when monitoring submerged eelgrass in turbid or deep waters (section 2.2). Nonetheless, if a multispectral sensor is the sensor of choice, for example when monitoring exposed eelgrass or when working in environments with clear and shallow water during favorable environmental conditions on a smaller scale, the additional sensor can be added to the multirotor UAV.

Monitoring of small-scale changes within eelgrass beds was made possible by the RTK (real-time kinematic) functionality of the used UAVs. The spatial accuracy of the obtained data increased to such an extent, that an overlay and comparison of images taken at different time points became possible without the need for labor intensive distribution of ground control points and georectification processes.

The developed tools and suggested set-up proved to be an accurate and feasible method not only for the detection of eelgrass, but also for the classification and quantification of stressors impacting eelgrass beds, which enabled a more holistic description of study areas and the ecological processes acting within them on an unprecedented temporal and spatial scale (section 2.3).

The analysis of the data obtained in this project was done using an object-based image analysis (OBIA) approach. This approach proved to be useful when analyzing UAV-based high resolution imagery and the results from section 2.6 can be used as a guideline for the image analysis process and a support for the classification algorithm choice.

The tested underwater systems (ROV and AUV) (section 3) proved to be a viable complementary tool for the operation in areas that pose difficulties for UAV-based eelgrass detection due to water depth or turbidity by providing imagery of very high resolution from close distance to the seabed. The AUV provided stable control at larger water depths and relatively long transects in comparison to the ROV but was subject to drift and was occasionally difficult to locate and recover. On the other hand, the ROV provided immediate video quality feedback and was easy to control but was limited in range by the tether and a less stable platform. The biggest challenge to underwater seabed imaging and mapping remains the precision and accuracy of the positioning system.

The formerly developed layer-based GIS tool, which is used for the evaluation of areas with a high eelgrass reestablishment potential as part of the environmental impact assessments in Natura 2000 areas, could be optimized by adopting improved interpolation methods used to create the input layers that are based on either point specific field observations or model derived

layers (section 4.1). A further possibility of improvement was found to be related to the model layers representing benthic light and shear stress. A re-analysis of simulated light attenuation coefficients combined with bathymetry data of higher spatial resolution for example improved the benthic light layer. For the simulated layer representing shear stress, a re-calculation was suggested, based on input from the hydrodynamic models developed for Danish Environmental Protection Agency and a more accurate bathymetry representation (section 4.2). The implementation of a UAV-based eelgrass distribution layer, as a more accurate alternative to the layer based on the interpolation of point observations, showed to have additional potential of improving the GIS-tool (section 4.3).

With this project we conclude that UAV-based eelgrass mapping can and should be incorporated into future eelgrass monitoring programs and we suggest a setup that facilitate repeatability, data comparability and easiness of its application while being robust and cost-efficient. However, in the future, other platforms, such as fixed-wing or hybrid UAVs can be recommended for long-term reoccurring survey campaigns, when focusing solely on large-scale monitoring of eelgrass beds.

1. Introduction

Eelgrass beds function as key marine habitats by providing a wide range of important ecosystem services. They stabilize sediments and reduce erosion and therefore act as a natural buffer against coastal storms and waves. They absorb nutrients like nitrogen and phosphorus from the water, help to mitigate the impacts of eutrophication, and improve water quality. They mitigate climate change by absorbing and sequestering atmospheric carbon dioxide. They also improve water clarity by trapping suspended particles, enhancing light penetration to the seafloor, and promoting the growth of other marine organisms. And finally, they support complex food webs and serve as shelter, hatching and nursery grounds for many commercially and recreationally important aquatic species, including fish, invertebrates, and waterfowl. Due to the many ecosystem services and functions eelgrass provides, it is a key indicator species when assessing marine water quality in Europe and its distribution is a key parameter in coastal water management.

1.1 The Danish case – bottom dredging in Natura-2000 sites

The national monitoring of eelgrass in Denmark focuses on presence/absence, coverage, and distributional depth limit on designated transects in Danish fjords and coastal zones, whereas areal distribution is less often considered, except for a few exceptions – one being in relation to bivalve fisheries inside Natura 2000 areas. In Denmark, mussel and oyster fisheries in Natura 2000 areas are regulated by the Danish mussel policy securing a sustainable fishery that complies with the EU directives. The mussel policy requires that environmental impact assessments (EIA's) must be conducted before any dredge-fishing activities in the Natura 2000 areas are allowed. The EIA's are done annually and as no impact of the fishery on eelgrass is accepted, eelgrass monitoring is a central part of the assessments considering both existing eelgrass beds as well as areas for potential future development of the eelgrass.

Different methods have been used to predict eelgrass presence and development over time ranging from simple correlations between e.g. eelgrass depth limit and nitrogen loading or light availability to statistical multi-parameter approaches, geo-statistical and geospatial techniques and a wide range of ecological/dynamic models (e.g. Nielsen et al. 2002, Greeve & Krause-Jensen 2005, Carstensen et al. 2013, Flindt et al. 2016, Kuusemäe et al. 2016, Stæhr et al. 2019). In the EIA's, two approaches are currently applied: 1) video monitoring and 2) modelling, but many other options are in play when monitoring submerged marine vegetation.

1.2 Monitoring of submerged aquatic vegetation

To gather information on spatial distribution, habitat structure and health status of eelgrass, many benthic monitoring programs, such as the Danish marine monitoring program, use in situ visual field surveys and video-based techniques. Moreover, in-air methods involving satellite-, plane- and UAV-based (Unoccupied Aerial Vehicle) photogrammetry as well as ship- and underwater drone-based video recordings, echo-sounding and acoustic techniques are being used in various eelgrass monitoring programs. These methods vary in their cost and easiness of application as well as their sensitivity to specific weather conditions such as cloud cover or turbid and deep waters. Furthermore, the provided data differs in spatial resolution, temporal resolution, areal coverage, depth limit and the amount of required validation data, attributing each technique with different strengths and limitations. For example, the ability of satellites and

planes to collect data over extensive areas ($\geq \text{km}$) comes with the expense of limited spatial resolution (dm-m) resulting in less information on biological details. UAVs on the other hand, can provide data of higher spatial resolution (mm-cm), providing more biological detail, however, compared to planes and satellites, they cover relatively small areas (m-km). Techniques involving echo sounding can provide data with a similar biological detail as UAVs, operate in a similar spatial extend, but are however often not applicable in shallow waters, while having the advantage of being less sensitive to turbid and deep waters than in-air methods. The smallest areal coverage is obtained when using in-water methods involving divers, ROVs or video-based techniques, which however provide data of highest spatial resolution. Therefore, it is important to recognize that no single technology can fully address all needs. Instead, the various technologies can complement each other. For instance, UAVs can serve a dual purpose by facilitating the training and validation of satellite- and plane-based classification models as well as conducting monitoring campaigns with high temporal and spatial resolution over medium-sized areas. On the other hand, satellites and planes can provide data over extensive areas while identifying specific regions that require finer detail from UAVs. Divers, underwater drones and vessel-based videos are a great tool to validate UAV based methods or acoustic techniques and the best choice for monitoring campaigns conducted in deep and turbid water or when highest biological detail is required on a small scale.

The following section will briefly introduce the most common monitoring techniques used to map and monitor eelgrasses while a comprehensive overview of techniques used to monitor SAV (submerged Aquatic Vegetation) (Fig. 1.1), including eelgrass, is given by Lønborg et al. (2022).



Figure 1.1. Most common monitoring techniques used to map and monitoring seagrasses.
From Lønborg et al. 2022.

Diver observations and video based surveys

Diver-based monitoring of eelgrass typically involves a diver, that is towed or freely swims along a predefined transect of limited width. This observer visually assesses and records specific vari-

ables along the transect, which may encompass aspects such as species composition, coverage, and signs of disturbances. To accurately map eelgrass distribution, divers may use surface GPS devices or underwater navigation techniques to georeference their survey sites, which helps to create spatially accurate maps of the eelgrass. Underwater video-based surveys follow a similar approach, but instead of having an observer, a camera is towed behind a boat to capture continuous video footage of the seafloor. While there is little post-survey data processing necessary for the diver-based approach, the post-survey data processing and extraction from videos is often conducted manually and therefore often time-consuming, and at risk of subjective assessments. Significant progress in the field of machine learning and video analysis shows however promising potential for increasing the post-survey automation. The data provided by diver observations and video-based surveys have, together with the in-water drones that will be described in the next section, the highest spatial resolution compared to all mentioned monitoring techniques. This comes however at the expense of spatial extent, which leads to high financial costs and time demand required to monitor larger areas. A common method used to circumvent this problem is to interpolate between the point specific data gathered by in-water techniques to create distribution maps over larger areas. While this works well in areas of continuous eelgrass meadows, misclassification is likely to occur in areas dominated by patchy and fragmented beds. The interpolation method will be discussed in greater detail in chapter 4. An important advantage of the in-water techniques is that they are less weather dependent and able to detect the eelgrass depth limit.

In-water drones

In-water-based drones operate with a similar spatial extent and resolution as the diver- and video-based methods. In-water drones can be grouped into three categories: autonomous underwater vehicles (AUVs), remote operated vehicles (ROVs) and automated surface vehicles (ASVs). Additionally, to camera-, light- and navigation systems, most in-water drones can be equipped with side-scan sonar or multi-beam echo sounders, which provide additional opportunities for mapping and characterization of habitats. ROVs are tethered to the point of operation and receive power and instruction from this tether. An advantage of using an ROV is the ability to stop and hover to collect more specific data of an object or area of interest. AUVs and ASVs are entirely unattached, with their own navigation, power, and data storage equipment onboard. All underwater drones can capture high-resolution imagery of the seafloor, while the sonar systems provide bathymetric data and topography of the underwater environment.

Post-survey sensor fusion and integration can combine imagery and bathymetric data to create a cohesive dataset that represents the seafloor and seagrass distribution. The ASV is the most weather dependent of the in-water drones, as it operates from the surface, while ROVs and AUVs are fully submerged during the monitoring and therefore less affected by, for example, wave action. Like the diver and video sled-based method, the ROV and AUV operate close to the seafloor and are therefore able to detect the seagrass depth limit as well as to distinguish between different species and provide information on additional variables (e.g. epiphyte coverage). The spatial extent of their operation is low, which limits in-water drone-based surveys to small, targeted areas.

Echo-sounding/acoustic techniques

Acoustic methods cover a large range of techniques that produce high-resolution images of the seafloor, including eelgrass beds. Based on differences in acoustic reflectivity, the sonar images

can reveal the shape, structure, distribution, and depth limit of eelgrass, depending on the technique used. An advantage of acoustic methods is that they are not limited by light availability and can therefore be used in turbid and deep waters, where other monitoring approaches might be limited. Weather sensitivity of acoustic techniques is likewise relatively low. However, a common aspect among all acoustic methods is their heavy reliance on calibration with *in situ* data. Automated processing of acoustic data has been significantly advanced with the development of various analytical routines and specialized software.

Unoccupied aerial vehicles (UAVs)

The use of UAVs in eelgrass monitoring campaigns has gained significant attention in recent years. UAVs can be grouped into three categories: (1) multirotor, (2) fixed wing and (3) transitional (hybrid). This diversity offers a broad spectrum of applications due to the various functionalities it provides concerning flight performance, endurance, range, payload, and control options. UAVs can capture aerial imagery with high spatial and temporal resolution over large areas in a relatively short time, providing a more comprehensive view of eelgrass distribution than in-water techniques. UAVs follow preprogrammed transects and capture imagery, that with the use of photogrammetry software is aligned to create high-resolution orthomosaics. Next to the high-resolution RGB (Red, Green, Blue) cameras that most UAVs are equipped with, additional sensors such as multispectral or hyperspectral cameras can be mounted, capturing data in multiple spectral bands, which can help to distinguish eelgrass from other vegetation or substrate. Low operational costs and automated flight operations allow UAV surveys of eelgrass habitats with a high temporal resolution. This can be useful for tracking small-scale changes in distribution, health, stressor presence, and other parameters over time. The high spatial resolution of UAV-based imagery lowers the need for extensive ground validation data, compared to low-resolution imagery obtained from traditional air-and space-borne remote sensing. A limiting factor for the use of UAVs for eelgrass monitoring are the environmental conditions above as well as below water. While above water, waves and sun reflection at the surface can have a negative impact on the image quality, underwater conditions with high turbidity decrease the contrast between eelgrass and the surrounding substrate. Post-processing of UAV-based imagery requires adequate skills but can be automated to a large extent using machine learning techniques.

Plane-based monitoring

The use of plane-based orthophotos for land surveys and mapping has a long tradition. Equipped with digital cameras, planes can capture aerial imagery over large areas in a relatively high spatial resolution. The resolution of the imagery depends on the flight altitude and camera specifications, however, is usually not high enough to allow for species level identification or SAV depth limit. On the other hand, plane-based surveys can cover large areas and are therefore useful for large-scale monitoring campaigns. While planes are effective for large-scale eelgrass surveys, they have limitations in terms of costs, logistics and weather conditions and surveys are usually limited to shallower areas of the water bodies. Furthermore, a considerable amount of ground validation is needed to train and validate the classification of imagery over large areas, which requires additional field surveys.

Satellite remote sensing

Use of satellite imagery to monitor and map SAV provides a tool that allows for extensive spatial coverage but the limitation of satellite based SAV mapping lies in the spatial resolution, which

especially in heterogeneous or patchy meadows may not capture small-scale variations. Additionally, atmospheric conditions, waves, sun glint, water turbidity and the presence of suspended matter can affect the quality and accuracy of satellite imagery and requires a considerable amount of correction techniques. However, on many occasions, satellite data can provide useful input to seagrass mapping. Eelgrass mapping using optical satellite imagery is typically approached in two ways: either through visual inspection and interpretation by specialists or by employing supervised classification algorithms, the latter of which demands a substantial volume of appropriate training data which is typically obtained via other techniques such as UAVs.

1.3 Project aim and approach

The main objective of the project was to develop new optimized methods for the mapping and monitoring of eelgrass within Natura 2000 areas where dredge fishing regulated by the Danish Mussel policy is allowed. The methods should secure a professionally sound area-based mapping, crucial for the management of the mussel policy, so that it does not end up in a dilemma between the precautionary principle in relation to the protection of the eelgrass and the utilization of the shellfish resource for fishing. Besides Natura 2000 areas, the methods developed in the project would as well be relevant in other management practices, e.g., in relation to the 3rd generation water plans. Thus, the aim of the project was to provide new knowledge for eelgrass monitoring, and mapping in relation to management over a wide range of action areas.

In particular, the project focussed on investigating the possibility of implementing drone technology for future mapping work - primarily using unoccupied aerial vehicles (UAVs), but also, though with less emphasis, using in-water methods, such as ROV's and AUV's. To develop a method as useful as possible for Danish waters in general, the project focussed on different water bodies with different characteristics – exemplified by turbid conditions in the Limfjorden with very low water visibility and thus, eelgrass at low water depths (2-4 m), to more clear water areas at the east coast of Jutland, with eelgrass at deeper water depths (6-8 m).

Additionally, an objective of the project was to optimize and develop the GIS models that have been developed previously for selected water bodies as a part of EIA's in Natura 2000 areas subjected to bivalve fishery, to improve the accuracy and thereby the applicability of those GIS models in the management of the areas. Eventually, by combining precise geo-localized mapping carried out with drone technology with dynamic models for the eelgrass distribution, the main project aim was to provide new cost-effective methods for mapping eelgrass in relation to future EIA's in Natura 2000 areas subjected dredge fishing.

Based on the above-mentioned main objectives, the project was split in three main work packages (WP's) focussing on different tools for improved eelgrass mapping: WP1) Unoccupied aerial vehicles (UAVs), WP2) In-water drones, and WP3) Models. These WP's are treated independently in the following chapters 2-4, with the work of WP1 constituting most of the report.

2. Monitoring eelgrass with Unoccupied Aerial Vehicles (WP1)

UAV-based monitoring can produce data of high spatial resolution over relatively large areas in a time and labor efficient way. The application of UAVs in eelgrass mapping campaigns can thus in the long term be expected to make monitoring more efficient, detailed, and cost-efficient. However, before implementation into Danish management practices, further studies, tests and optimizations of processes and methods are needed to make UAV monitoring of eelgrass applicable in a standardized way and on a wider scale. In a former EMFF project (Management of mussel fishery in Horsens Fjord and Lillebælt (Nielsen et al. 2019) DTU Aqua has investigated the possibility of using UAVs for eelgrass mapping in collaboration with the DTU Space DroneCenter. The results from this were promising, albeit preliminary. In another previous project, SDU has investigated the effectiveness of UAVs for mapping coastal waters in and around Odense Fjord, and has, among other things, collected detailed information on eelgrass distribution (Svane 2020).

The overall aim of work package 1 was therefore to further develop and optimize UAV-based eelgrass monitoring methods as a geo-accurate and cost-efficient alternative to current methods based on video transects that are both resource intensive and partly based on point observations. To do so, several important themes that must be taken into consideration when monitoring eelgrass using UAVs were investigated in depth.

Large-scale monitoring (section 2.1): The investigation of UAV-based monitoring of eelgrass on a larger scale was done with a focus on estimating the effort and time needed to cover a certain area as well as to identify limitations of the methodology, or in other words; identify environments in which the traditional video-based monitoring methodology would be superior.

Monitoring in deep or turbid waters (section 2.2): The possibilities and limitations of eelgrass monitoring in challenging environments with deep or turbid waters was tested by using and comparing different sensors (multispectral and RGB) in different water bodies.

Detection of seasonal and stress related change of eelgrass beds (section 2.3): The monitoring of seasonal and stress related change in eelgrass bed extension using UAV-derived imagery was tested with a focus on providing spatially accurate information on small-scale changes.

Detection and analysis of stressors affecting eelgrass populations (section 2.4): To improve and standardize UAV-based monitoring of stressors affecting eelgrass populations, the analysis techniques based on SDU's former investigations were further developed by looking into possibilities of detecting and quantifying impact related to epiphytes, macroalgae, sediment mobility and infauna.

Ground truthing data collection (section 2.5): For improving efficiency and automation of ground truthing data collection, different UAV-mounted underwater camera systems were developed and tested.

Image analysis process (section 2.6): The need for a solid foundation for the image analysis process was addressed by testing different classification algorithms using images obtained from different altitudes and during different environmental conditions combined with training sample sets of different sizes.

The gained experience and resulting information from these investigations is presented in detail in the following sections 2.1-2.6 and meant to serve as a decision-making support in form of guidelines and protocols when planning to incorporate UAVs into eelgrass monitoring campaigns.

2.1 Large-scale mapping

The potential of UAVs in supporting such large-scale eelgrass monitoring campaigns by providing data of high spatial resolution and accuracy over extensive areas in a cost and labor effective way, was tested in Lovns Broad (Fig. 2.1).

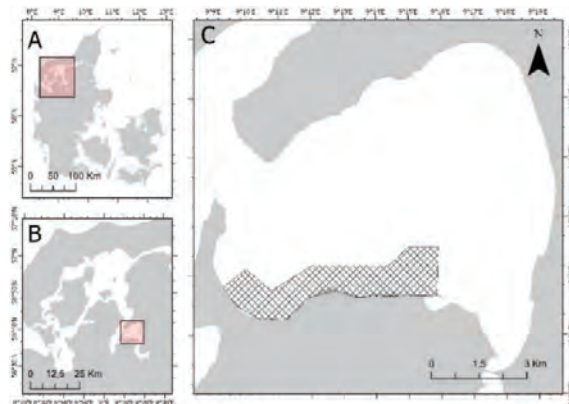


Figure 2.1. Study area indicated with hatched fill situated along the southern coast of Lovns Broad (C) in the Limfjorden (B), Denmark (A).

The study area is located along the southern coast of the broad and characterized by mixed eelgrass/mussel habitats and different growth forms of eelgrass beds until a depth of around 2 m, followed by pure mussel beds and sandy bottom at greater depths. The area chosen for large-scale mapping spanned over 6.5 km in east-west direction and between 0.3 and 1 km in north-south direction, covering a total of 300 ha. After testing different sensor options for eelgrass detection in these turbid waters (section 2.2), the UAV model DJI Phantom 4 RTK was chosen. The payload was a 20 million effective pixels 1-inch CMOS sensor-equipped RGB camera with a 84° field of view, 8.8 mm/24 mm focal length, and f. 2.8–11 aperture. Flight altitude was set to 100 m, resulting in a Ground Sample Distance (GSD) of 27.41 mm and single image dimensions of 150 × 100 m. All images were taken with a nadir-viewing angle (90°). To cover the entire area, 164 transects with image front and side overlaps of 75% were flown by one pilot on May 16, 2022, which resulted in a total flight distance of 87 km. With a flight speed of 6 m/s, this amounted to a total flight time of 4 hours, excluding take-off and landing procedures when battery changes were needed. All relevant flight parameters were programmed using the flight mission planning software UgCS ver. 4.7.685. Figure 2.2 shows flight route and flight parameters in the user-interface of the UgCS software.

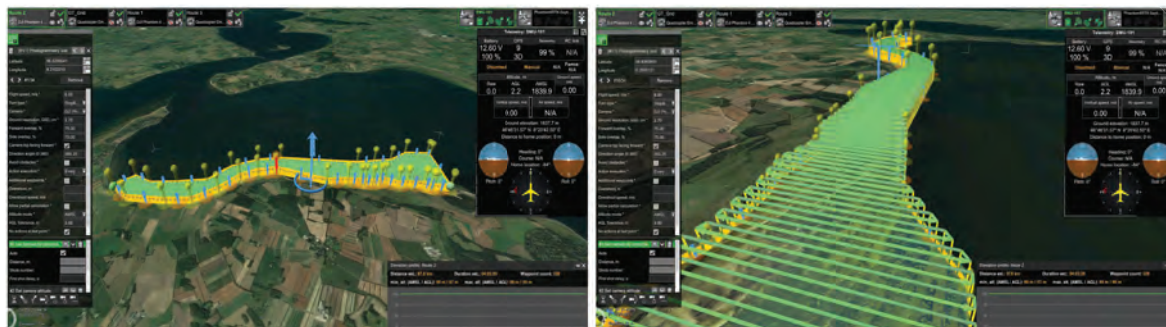


Figure 2.2 Large-scale monitoring flight route in the user-interface of the UgCS software.

The high capacity 4S LiPo (lithium-polymer) batteries of 5350– 5870 mAh used, provided a practical flight time of 22–28 min. To avoid draining the batteries and allowing for safe return when battery change was needed, the flight time allocated for image acquisition was limited to 15 minutes per flight, which resulted in a total of 16 conducted flights. The total in-field time of the monitoring mission was 6.5 hours, including set-up of the equipment and battery change in-between flights. Due to the large area covered, the pilot had to be mobile and follow the drone along the coast from the furthestmost eastern transect, where the mission was started, to the furthestmost western transect, where the mission ended. This allowed the UAV to always remain in the pilot's visual line of sight and reduced the flight time spent on battery changes.

The monitoring mission resulted in 3752 single images, that were stitched into 3 georeferenced orthomosaics, using the image processing software Agisoft Metashape Professional ver. 1.7.4. Image analysis was conducted subsequently, using the object-based image analysis approach outlined in section 2.6 (image analysis). Examples of created orthomosaics, classification results and visible detail in the images of the monitored habitats can be seen in figure 2.3 and 2.4.

The image processing (data organization and the creation of the orthomosaic) took around 5 hours, while the image analysis around 7 hours, both done on a 64-bit operating system, with Intel Core™ i9-7900 CPU @ 3.30 GHz and 64 GB RAM. Of the 12 hours of post survey work, 8 hours were pure computer processing time, thus, not requiring human resources as such.

The high spatial resolution of the images allowed for a detailed classification of the study area, which revealed 170 ha sand, 50 ha mussel and 80 ha eelgrass cover. The images obtained during the survey furthermore had a very high spatial accuracy of ± 2 cm. This is thanks to the UAVs on-board high-precision GNSS receiver, that allowed for a continuous in-flight correction of the UAV's position - a process called real-time kinematic (RTK) correction. Such high spatial accuracy becomes especially important when monitoring campaigns of the same area are conducted regularly, as it allows for the detection of small-scale changes in eelgrass distribution by comparing images and classifications of different time points to each other (see section 2.3 – Change detection).

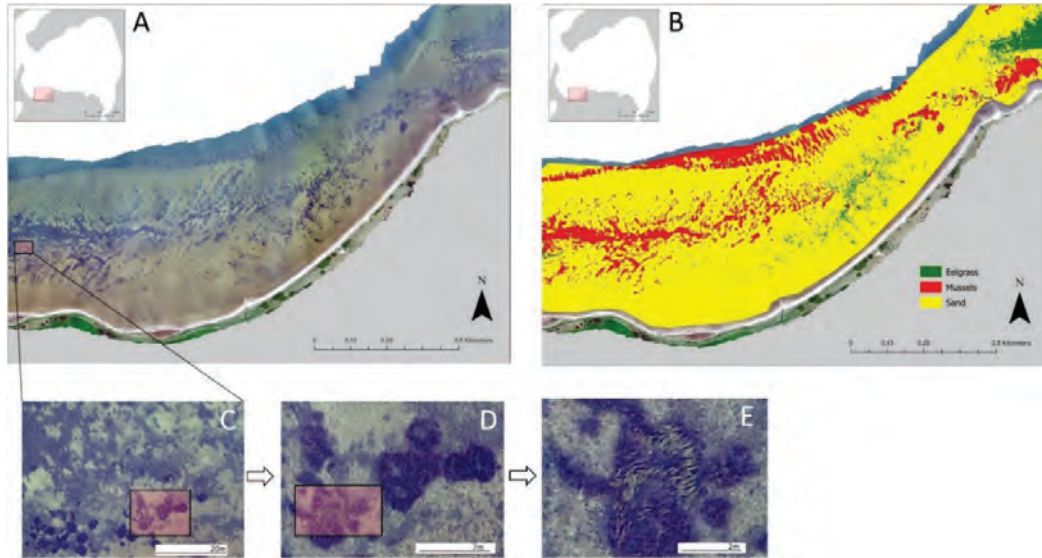


Figure 2.3. Subset of orthomosaic created from images obtained from the large-scale monitoring mission (A). Classified orthomosaic (B). Level of detail seen in the image (C-E)

The entire process, from data collection, over data processing, to data analysis and image classification was done in a highly automated way by a single person. This indicates that UAV-based monitoring of submerged eelgrass habitats could contribute to large-scale monitoring campaigns by providing data of high spatial resolution and accuracy in a labor and time efficient way. As most eelgrass populations inhabit shallow waters, the total area of interest is also limited, thus the traditional vessel, diver and ROV-based surveys (chapter 3) could focus on the deepest growth zones where UAV-camera spectra are unlikely to create distinguishable differences between habitats.

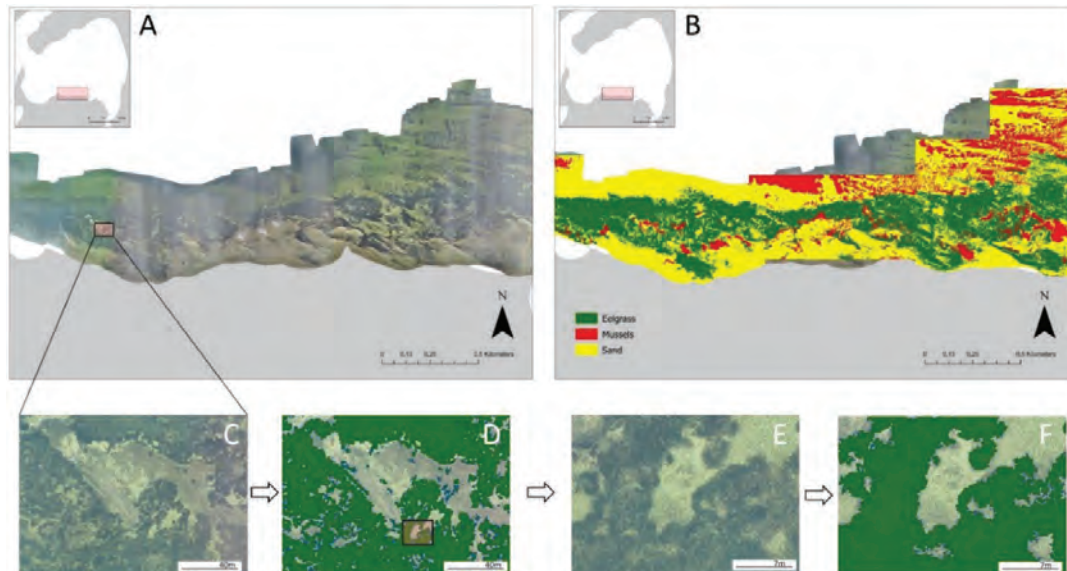


Figure 2.4. Subset of orthomosaic created from images obtained from the large-scale monitoring mission (A). Classified orthomosaic (B). Close-up of an area within the orthomosaic (C). Classification view of C (D). Close-up of an area within D (E). Classification view of E (F).

Some limitations, however, need to be considered. In the chosen study area, it was possible for the pilot to follow the UAV along the shore as well as to find access points to the coast, reachable by car. In areas where it is not possible to access the coast due to environmental barriers or otherwise restricted areas, large-scale monitoring from shore might not be possible. In these cases, a vessel can be sailed into the study area to serve as take-off and landing platform, which would however increase the cost per unit area due to the additional personal and equipment needed. An increase in monitored area could be achieved by applying a fixed-wing UAV instead of a lightweight copter UAV, as the one used in this field study. Due to efficient aerodynamics and long flight times (~60 min), fixed-wing UAVs can cover areas of approximately 600 ha/day. What needs to be taken into consideration when working with fixed-wing UAVs is, however, the need for adequate take-off and landing sites. This issue is solved by hybrid UAVs, which start vertically and only change to a horizontal flight position at a certain height. Both fixed-wing and hybrid UAVs come, however, with significantly higher acquisition costs and additional permits needed to fly beyond the visual line of sight.

2.2 Monitoring eelgrass in deep or turbid waters using different platform and sensor systems

Deep and/or turbid waters pose a significant challenge for UAV-based monitoring, as suspended particles scatter and absorb light, reducing visibility and making it difficult to obtain accurate data on submerged features such as eelgrass. A way to enhance depth penetration in such conditions could be the application of multispectral sensors. While conventional red, green, and blue (RGB) sensors detect light in the visible wavelength's spectrum (400–700 nm) with three broad and partially overlapping bands, multispectral sensors detect and measure the reflectance of light at specific wavelengths using narrow bandwidths which potentially allows them to mitigate the adverse effects of turbidity and depth. In this project, the following four sensors were tested for their usefulness of detecting eelgrass in turbid and deep waters (three multispectral and one RGB sensor):

1. DJI Multispectral sensor (2 MP x 5 images)
2. Multispectral MicaSense RedEdge sensor (1.2 MP x 5 images)
3. Multispectral MicaSense RedEdge-MX sensor (1.2 MP x 5 images)
4. DJI Phantom 4 standard RGB sensor (20MP)

Sensors 1, 3 and 4 were carried by UAVs of the model DJI Phantom 4, while sensor 2 was carried by a DJI Matrice 600 UAV. Table 2.1 lists the bandwidths of the tested sensors.

Table 2.1. Bands and bandwidths of the sensors used.

	1) DJI Multispectral	2) MicaSense RedEdge	3) MicaSense RedEdge-MX	4) DJI RGB
Blue	450 nm \pm 16 nm	475 nm \pm 16 nm	444 nm \pm 14 nm	~ 470 nm
Green	560 nm \pm 16 nm	560 nm \pm 13.5 nm	531 nm \pm 7 nm	~ 545 nm
Red	650 nm \pm 16 nm	668 nm \pm 7 nm	650 nm \pm 8 nm	~ 660 nm
Red Edge	730 nm \pm 16 nm	717 nm \pm 6 nm	705 nm \pm 5 nm	
Near Infrared	840 nm \pm 26 nm	842 nm \pm 28.5 nm	740 nm \pm 7 nm	

For the detection of submerged eelgrass in turbid or deep water the red edge and near infrared bands that usually are used for terrestrial vegetation detection are of less importance. This is

because longer wavelengths get quickly absorbed by water, especially when high amounts of suspended particles are present. It is instead the narrow bandwidths of multispectral sensors that have the potential of fitting the wavelength of light spectrum that gets reflected from the substrate. Especially narrow bands around the lower limit of the visible spectrum, such as the blue band of the MicaSense RedEdge-MX sensor, are of interest due to their shorter wavelength and therefore deeper water penetration abilities. A limitation of using multispectral sensors is however the lower spatial image resolution. To test, if the advantage of narrow bandwidths gets overruled by high spatial resolution when detecting eelgrass in deep or turbid waters, the conventional RGB sensor was added to the experiment.

2.2.1 Turbid waters

Three sensors were tested for eelgrass monitoring in turbid waters – two multispectral sensors (MicaSense RedEdge and DJI Multispectral) as well as the conventional DJI RGB sensor. Three sites in Lovns Broad were chosen for the experiment (Fig. 2.5). Lovns Broad is situated in the Limfjorden and characterized by high eutrophication levels and frequent algal blooms. Site 1 was located along the northern coast of the broad. Eelgrass and blue mussels occur here on sandy substrate in scattered mixed habitats until a depth of approximately 2 m, followed by mussel habitats in deeper waters. Site 2 was likewise situated along the northern coast but differed however in the habitat structure. Here a dense eelgrass bed extends from the shore to a depth of 1 m followed by sand and mussels in deeper water. Site 3 was located along the south-eastern coast of the broad. Here eelgrass and mussels are arranged in bands parallel to the coast, where eelgrass colonizes the landwards site while mussels grow on the opposite site.

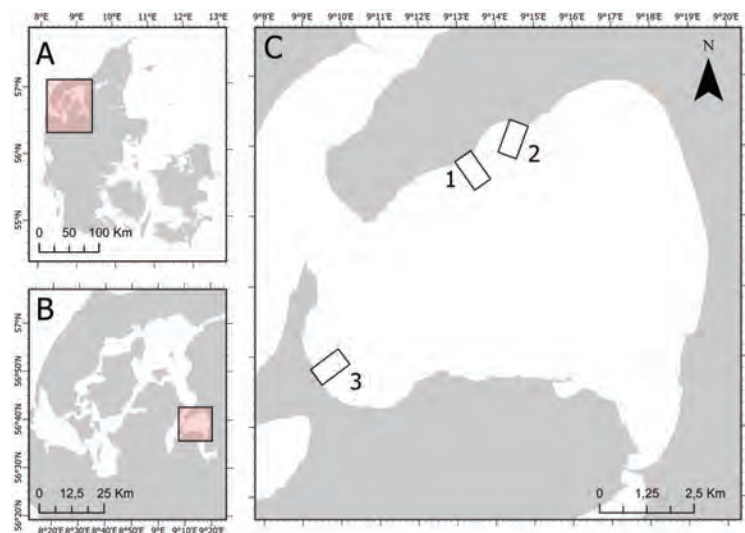


Figure 2.5. Study areas 1, 2 and 3 in Lovns Broad (C), situated in the Limfjorden (B), Denmark (A).

Three flights were conducted with each sensor at the three study sites on May 18, 2021. Each of the three flights was conducted at a different altitude, depending on the spatial resolution of the sensor used. This was done so that the obtained images would have the same Ground Sample Distance (GSD), which increases comparability of the produced imagery. Table 2.2 shows details of all conducted flights in study area 1. The same arrangement was used in area 2 and 3.

Flights were planned, using the flight mission planning software UgCS ver. 4.7.685. This software allows advanced planning options such as customized payloads and multiple UAV control, and therefore was especially suited for this experiment. Three GSD values and resulting flight altitudes were chosen to test the applicability of the sensors for different tasks. Low altitude flights result in higher resolution and therefore produce data of more detail but are limited in their spatial extent. Data obtained during high altitude flights is of lower spatial resolution, providing less detail, however over larger areas. As environmental conditions during flight can have strong effects on the image quality and properties, flights were conducted simultaneously to increase comparability. Figure 2.6 shows the flight routes of the three UAVs during flight 1 in study area 1.

Table 2.2. Flight details for all flights conducted in study area 1.

	Sensor	Altitude (m)	Speed (m/s)	Front/side overlap (%)	Flight area (ha) (m)	Surveyed Area (ha) (m)	Single image dimensions (m)	Flight rows #	Distance between rows (m)	GSD (mm)	Camera triggering distance (m)	Camera triggering interval (sec)	Shots #	Flight time (minutes)
Flight #1	RGB	100	7.4	85/85	11.9 (450 x 265)	21.9 (550 x 397.5)	150 x 100	12	22.5	27.4	15	2	372	15
	P4Multispec	51.8	3.5	80/85	1.75 (350 x 50)	3.5 (384.5 x 89.82)	43.83 x 35.62	8	6.57		7.12	2	400 (x6)	15
	MicaSense RedEdge	39.5	3.8	85/85	1.75 (350 x 50)	3.1 (377.3 x 82.4)	35.07 x 26.3	10	5.27		3.95	1	900 (x5)	16
Flight #2	RGB	51.1	3.8	85/85	3.15 (370 x 85)	6.6 (418.8 x 157.11)	76.61 x 51.07	8	11.5	14	7.66	2	392	18
	P4Multispec	26.4	1.8	80/85	0.45 (250 x 18)	1 (265.72 x 39.18)	22.39 x 18.20	6	3.36		3.64	2	414 (x6)	17
	MicaSense RedEdge	20.2	2	85/85	0.5 (250 x 20)	1 (265.4 x 36.74)	17.94 x 13.44	8	2.69		2	1	1000 (x5)	18
Flight #3	RGB	10	1	79/85	0.08 (40 x 20)	0.18 (50 x 35.25)	15 x 10	10	2.25	2.72	2.1	2	200	18
	P4Multispec	79.7	5.4	80/85	4.1 (350 x 115)	7.3 (406 x 178.99)	67.50 x 54.86	12	10.13		10.97	2	396 (x6)	16
	MicaSense RedEdge	60.5	5.9	85/85	4.4 (350 x 125)	6.9 (397.1 x 174.5)	53.76 x 40.32	16	8.06		6.05	1	944 (x5)	17

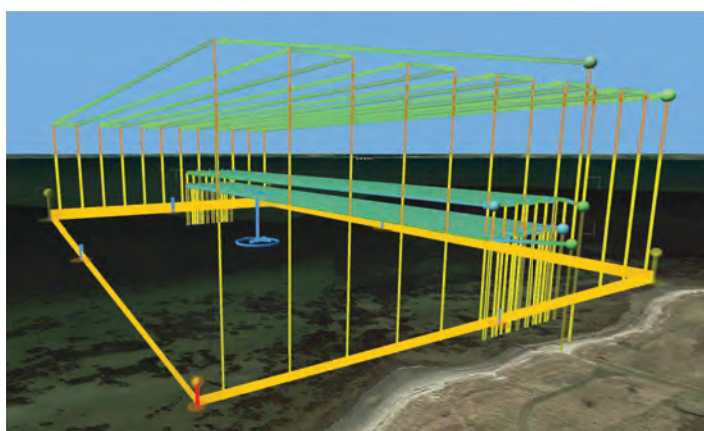


Figure 2.6. Flight routes of the three UAVs during flight 1 in study area 1.

One georeferenced orthomosaic was created for each flight (27 in total) by stitching the obtained images using the image processing software Agisoft Metashape Professional ver. 1.7.4. The resulting orthomosaics were calibrated in reflectance for each band, using the MicaSense reflectance panel and/or data obtained by the UAV mounted downwelling light sensors. The corrected images were subsequently analyzed by applying the image analysis workflow described in section 2.6 on image analysis using the eCognition Developer software ver. 10.1.

As expected, the red edge and near infrared bands did not prove to be beneficial for the classification of submerged eelgrass in any of the three study areas. The natural high absorption effect of water in the infrared spectrum was most likely increased by high amounts of suspended particles and organic matter, making it difficult even to obtain useful reflection values in the very shallow areas (Fig. 2.7).

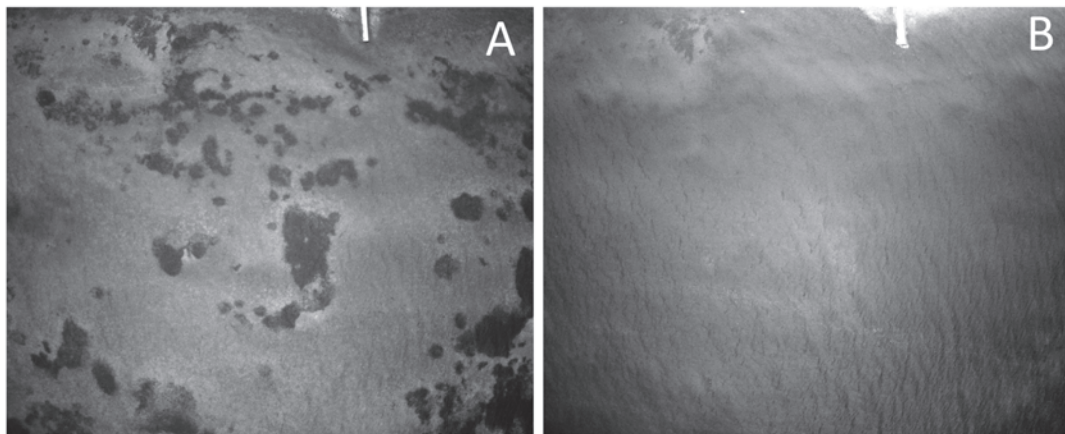


Figure 2.7. Green band image of eelgrass in very shallow water obtained with the DJI multispectral sensor (A). Red edge band of the same image (B).

In study area 1, the green bands of both multispectral sensors on the other hand proved to be useful for the detection of eelgrass, with the MicaSense RedEdge sensor showing the best separation between eelgrass and surrounding sand (Fig. 2.8C). Similar strong contrasts between eelgrass and sand were created by the green band of the DJI multispectral sensor (Fig. 2.8B). The red band of the DJI RGB sensor showed slightly lower reflectance intensities, but still allowing for good class separation (Fig. 2.8A).

However, when used for classification of submerged eelgrass, the images obtained from the DJI RGB sensor produced the highest accuracies, despite the apparently high eelgrass detection capabilities of the multispectral sensors. The reason for that is most likely the increased amount of noise visible in the images obtained by the multispectral sensors. The lower spatial resolution of the sensors requires lower flight altitudes to not lose too much detail in the image. This, however, might have increased the visibility of waves and related light scattering on the water surface. The high resolution of the RGB sensor on the other side allowed for higher flight altitudes, which smoothened out the negative effects of waves. This is visualized in figure 2.9, which shows a subset of the orthopictures created from images obtained by the three sensors in study area 1. All images have the same spatial resolution of 27.4 mm/pixel (flight 1, table 2.2). To obtain this resolution, the RGB sensor had to be flown at 100 m altitude (left), the DJI multispectral

sensor at 52 m (middle) and the MicaSense RedEdge multispectral sensor at 40 m (right). The increasing noise becomes visible from left to right. The higher flight altitude of the RGB sensor carrying UAV furthermore advantageously reduces survey time by providing larger single image dimensions of 150x100 m compared to 42x36 m and 25x26 m produced by the DJI multispectral and the MicaSense RedEdge multispectral sensor respectively.

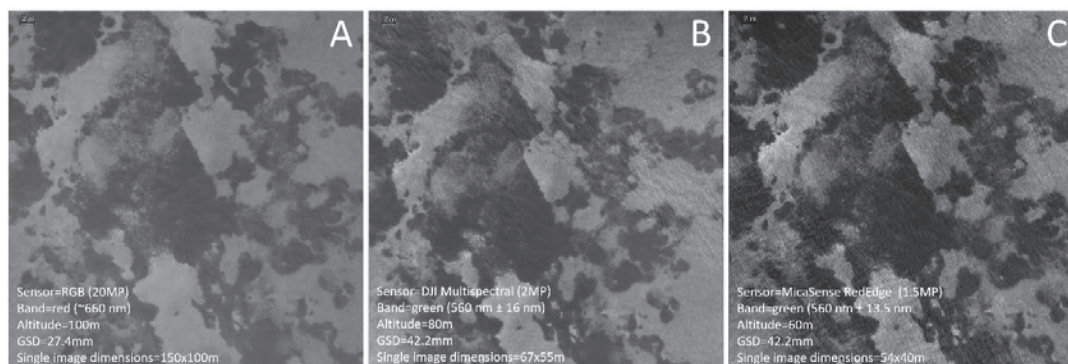


Figure 2.8. Images of study area 1 obtained from the sensor bands with highest eelgrass reflectance values: Red band of the DJI RGB sensor (A). Green band of the DJI Multispectral sensor (B). Green band of the Micasense RedEdge multispectral sensor.

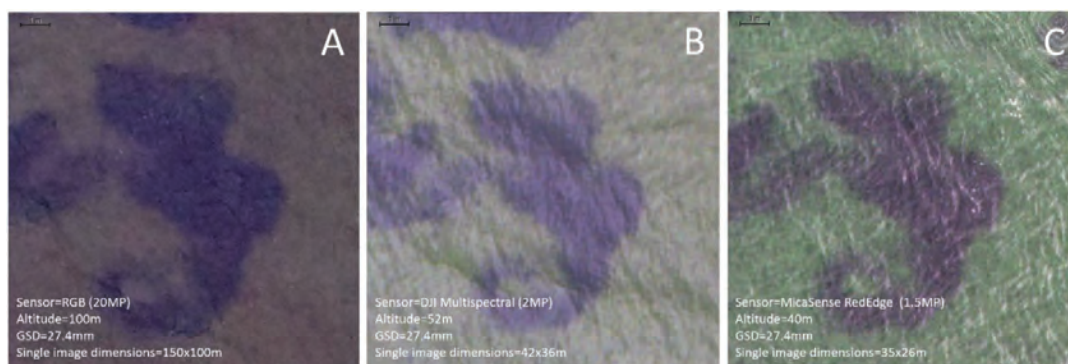


Figure 2.9. Subset of the orthophotos created from the RGB bands of the images obtained by the three sensors in study area one: RGB sensor (A), DJI multispectral sensor (B), MicaSense RedEdge, (C) multispectral sensor.

In study area 2 and 3, image quality of both multispectral cameras was compromised by sun glint to such an extent that no reliable reflectance values could be obtained while the images obtained by the RGB sensor allowed eelgrass detection in at least some areas.

The results show that multispectral sensors can be useful to detect eelgrass in turbid waters, such as in Lovns Broad in the Limfjorden. However, they also have shown to be more sensitive to environmental conditions, especially those affecting the water surface, such as wind and light reflections. The conditions during data collection of this field experiment created so much noise in the multispectral imagery, that the higher resolution of the conventional RGB sensor overruled the advantage of narrow bandwidth. Higher flight altitudes of the multispectral sensors might have provided better results, however to the cost of spatial resolution. Significantly better results are to be expected when data collection is done at times of low to no wind. In conclu-

sion, the results of the experiment indicate that multispectral sensors have the potential to improve eelgrass detection in turbid waters, but only during certain favorable environmental conditions. The lower sensitivity, the significantly higher image resolution, and the resulting ability of covering more area in less time, makes the conventional RGB sensor a more reliable tool, when mapping eelgrass in turbid environments.

2.2.2 Deep waters

Three sensors were tested for eelgrass monitoring in deep waters – two multispectral sensors (MicaSense RedEdge MX and DJI Multispectral) as well as the conventional DJI RGB sensor. The study site chosen for this task was situated along the southern coast of Endelave island (Fig. 2.10). Here, eelgrass beds grow on sandy bottoms until a known depth of around 5.5 m.

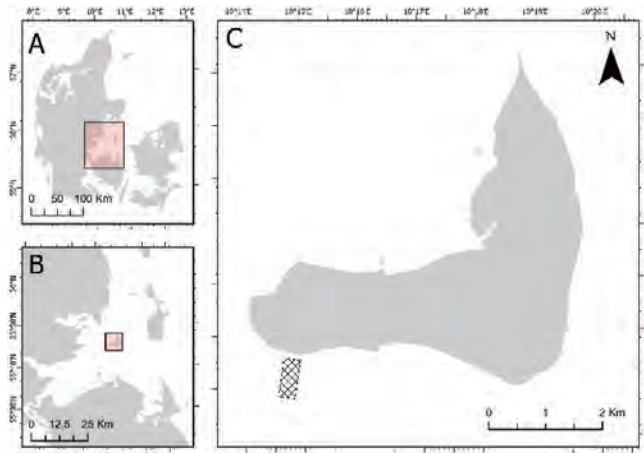


Figure 2.10. Study area situated along the southern coast of Endelave (C), situated in the Kattegat (B), Denmark (A).

One flight was conducted with each set-up on July 28, 2022. Due to drone pilot resources, only one flight was conducted at the time, in contrast to the tests in turbid waters covered above. The RGB sensor was flown at 100 m altitude, resulting in a spatial resolution of 27.4 mm/pixel and a single image dimension of 150x100 m. The DJI multispectral sensor was flown at 66 m, resulting in a spatial resolution of 35mm/pixel and a single image dimension of 54x44 m. The MicaSense RedEdge-MX multispectral sensor was flown at 50 m, likewise, resulting in a spatial resolution of 35mm/pixel, while single image dimension was 43x32 m. The MicaSense RedEdge-MX multispectral sensor was attached to the DJI Phantom 4 RTK platform, using a mount kit developed by Sky Flight Robotics. The additional payload reduced the UAVs flight time from 25 minutes to 13-15 minutes. Flights were planned, using the flight mission planning software UgCS ver. 4.7.685. This software allows advanced planning options such as customized payloads and multiple UAV control, and therefore was especially suited for this experiment. Figure 2.11 shows the flight path of the Phantom 4 RTK equipped with the conventional RGB sensor.

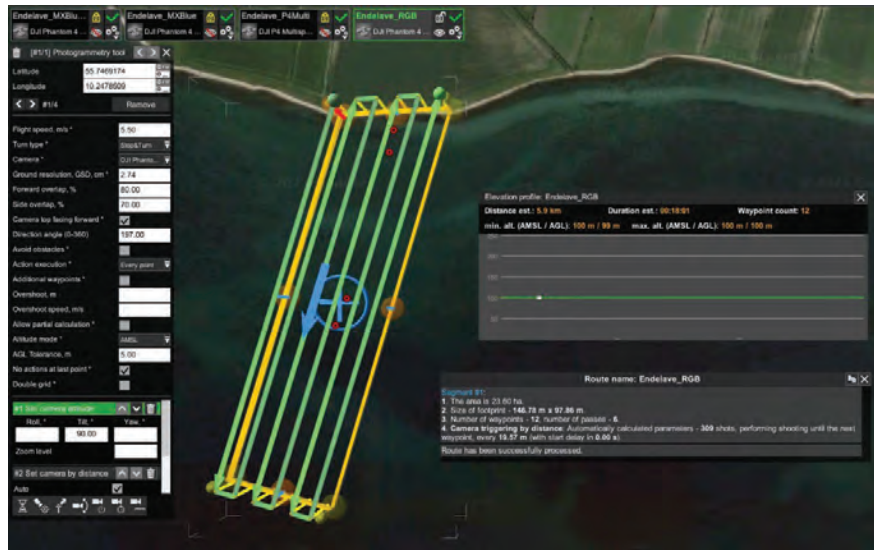


Figure 2.11. Flightpath of platform/sensor combination 2 from the coast of Endelave.

One georeferenced orthomosaic was created for each flight by stitching the obtained images using the image processing software Agisoft Metashape Professional ver. 1.7.4. From the 1178 composite 5 band images obtained by the MicaSense RedEdge-MX multispectral sensor, only 41 images, which inherited at least some land features, could be stitched together. This is most likely due to a wind induced agitated water surface, creating noise on the images in form of reflections and distortions. The analysis of single images did furthermore not show any beneficial effect of using the narrow blue band ($444 \text{ nm} \pm 14 \text{ nm}$) provided by this sensor to detect deep eelgrass patches. The hypothesis was that this band could penetrate deeper into the water column and therefore be used for monitoring eelgrass at greater depths. An orthomosaic could be created using the images obtained by the DJI Multispectral sensor, however, none of the bands were useful for eelgrass detection due to the quick absorption of long-wave radiation with depth and reduced image quality caused by sun reflections at the water surface. Yet again, the RGB sensor proved to be the best tool to map and monitor eelgrass in this field study. The data provided by this sensor allowed for eelgrass detection until a depth of around 5.5 m, which was measured and confirmed by a UAV mounted underwater camera system, presented in section 2.5 (ground truthing). Figure 2.12 illustrates eelgrass detection at around 5.5 m based on the RGB sensor derived data. Areas that were deeper than 5.5 m had to be excluded from the analysis, as no sensor was able to detect signals of reflecting surfaces due to light absorption of the water column. If eelgrass occurred in deeper water than the detected patch at 5.5 m depth remains unknown, which points out the limitation of in-air based monitoring methods of deep eelgrass using passive sensors.

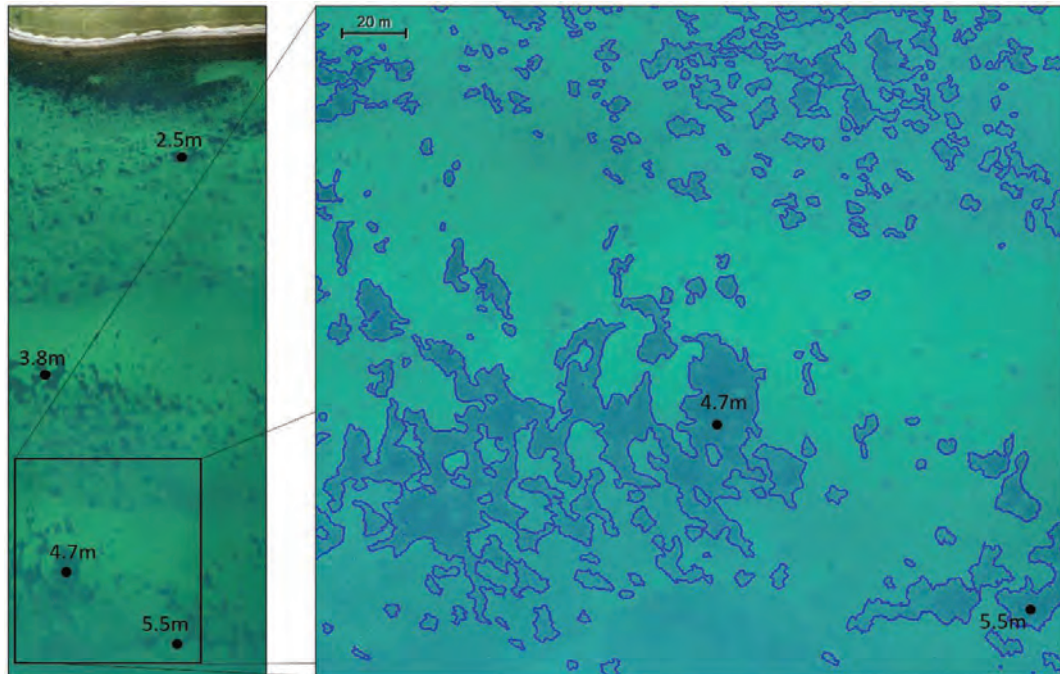


Figure 2.12. Detection of deep eelgrass using the RGB sensor. Points indicate depth measurements obtained with a UAV mounted underwater camera system (see section 2.5 on ground truthing).

2.3 Change detection

Change detection studies play an important role in eelgrass monitoring, as they help to understand the dynamic nature of these important habitats. By analyzing data collected at different times, researchers can identify alterations in eelgrass distribution, health, and overall habitat conditions over time. In this way, temporal variability, the status of restoration efforts as well as the impact of destructive events can be studied.

To test the application of UAV-based change detection of eelgrass beds, a 2 ha large study area in the Limfjorden was chosen (Fig. 2.13). In this area, eelgrass beds grow on a sandy bottom to a maximum depth of 2.5 m. The area is characterized by eutrophication, resulting in events of oxygen depletion, and generally reduced benthic light availability. Other pressure factors such as waves, ice cover during winter, high water temperatures during summer, sediment bioturbation by lugworms as well as anthropogenic destruction from fishing gear and boating result in the partial fragmentation of eelgrass beds.

The UAV platform used in this change detection study was a consumer-grade, low-weight quadcopter of the type DJI Phantom 4 RTK, equipped with the standard in-built 20MP RGB camera. In total, 24 flights were conducted to study the small-scale changes of the eelgrass bed over 17 months. The data obtained by five of these 24 flights is presented here. Four flights, conducted in early April and late August of 2021 and 2022 were used to document seasonal gain and loss of eelgrass cover, while the data of an additional flight conducted in March 2021 was used to document the delayed impact of an ice cover period, occurred in February 2021. All flights were performed at an altitude of 100 m, resulting in a ground sample distance of 27.4 mm. Flight route and flight parameters were identical for all flights and were planned and executed using

the flight mission planning software UgCS ver. 4.7.685. This allowed a high level of automation and repeatability during data collection, which is important in monitoring campaigns that require high temporal resolution. One georeferenced orthomosaic was created from the images obtained during each flight, using the image processing software Agisoft Metashape Professional ver. 1.7.4. Subsequently, the images were analyzed using the object-based image analysis workflow presented in section 2.6 (image analysis). By doing so, it was possible to achieve classification accuracy levels of 90-95% for all images. The remaining misclassified areas were manually corrected based on visual interpretation and expert knowledge (Fig. 2.14).

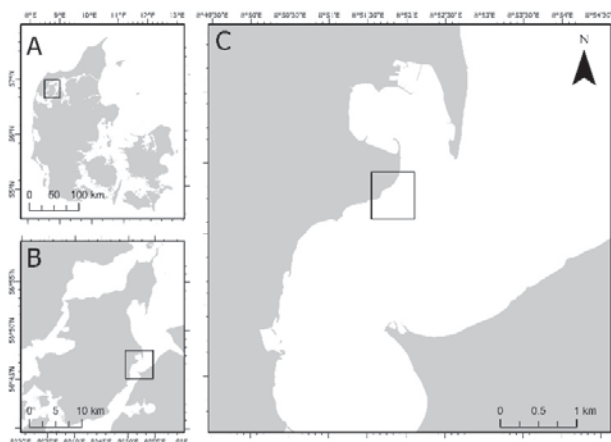


Figure 2.13. Study area (C) situated along the eastern coast of the island Mors (B) in the Limfjorden, Denmark (A).

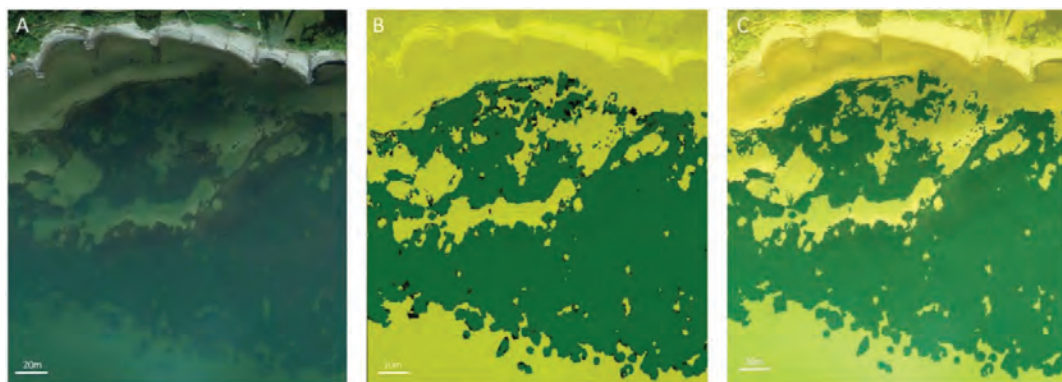


Figure 2.14. (A) Original orthomosaic obtained in August 2021. (B) Classified image using OBIA with eelgrass (green), sand (yellow) and misclassified areas (black). (C) Manually corrected classification used for change detection

A high classification accuracy is critical when aiming to detect even subtle changes in seagrass distribution and health. Equally important is the spatial accuracy of the images. Positioning and orientation of a consumer grade UAV and its sensors are usually generated by an on-board global navigation satellite system (GNSS) positional receiver, which enables georeferencing of the collected images with an accuracy of $\pm 2-10$ m. This can be precise enough for large scale monitoring missions, however not when comparing a large number of images for small scale change detection. In this case spatial accuracy needs to be brought down to cm level, which can be achieved with the deployment of ground control points (GCPs) at precisely measured

and marked locations that are strategically distributed across the study area and subsequently used to geometrically correct the location of the collected images. However, deploying GCPs and geo-rectifying the images is a labor-intensive task and often not possible in environments dominated by water due to the lack of suitable static surfaces. A way to minimize the need for GCPs while still maintaining accuracy on a cm level is the use of UAVs equipped with an on-board high-precision GNSS receiver. In this way, a UAV's positioning data is corrected during flight (real-time kinematic [RTK]) or after the flight (Post-processed kinematic [PPK]) by correction processes that make use of additional positioning data recorded by a mobile base station or a network of permanently installed geodetic stations. The latter option was used in this project, which required a subscription to a network RTK correction service. This allowed for a spatial accuracy of ± 2 cm without the need for installing a mobile base station during each flight or placing GCPs in the study area.

The high classification and spatial accuracies made it possible to detect small scale changes in the monitored eelgrass bed. Figure 2.15 shows an example of such small-scale changes over time. The change detection was performed in the eCognition Developer software ver. 10.1, by overlaying and comparing the classification outputs with each other. Figure 2.16 visualizes the workflow.

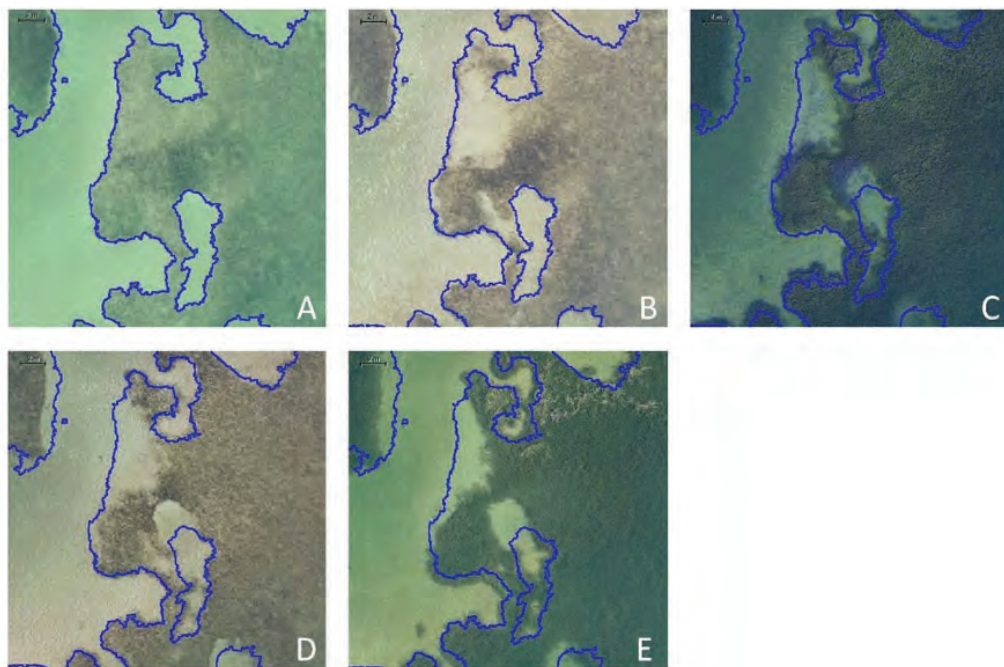


Figure 2.15. Subset of the original orthophotos (20x20 m), showing small scale changes over time. A) March 2021, B) April 2021, C) August 2021, D) Apr 2022 and E) Aug 2022. The outline of the eelgrass bed from March 2021 (A) is shown in blue.

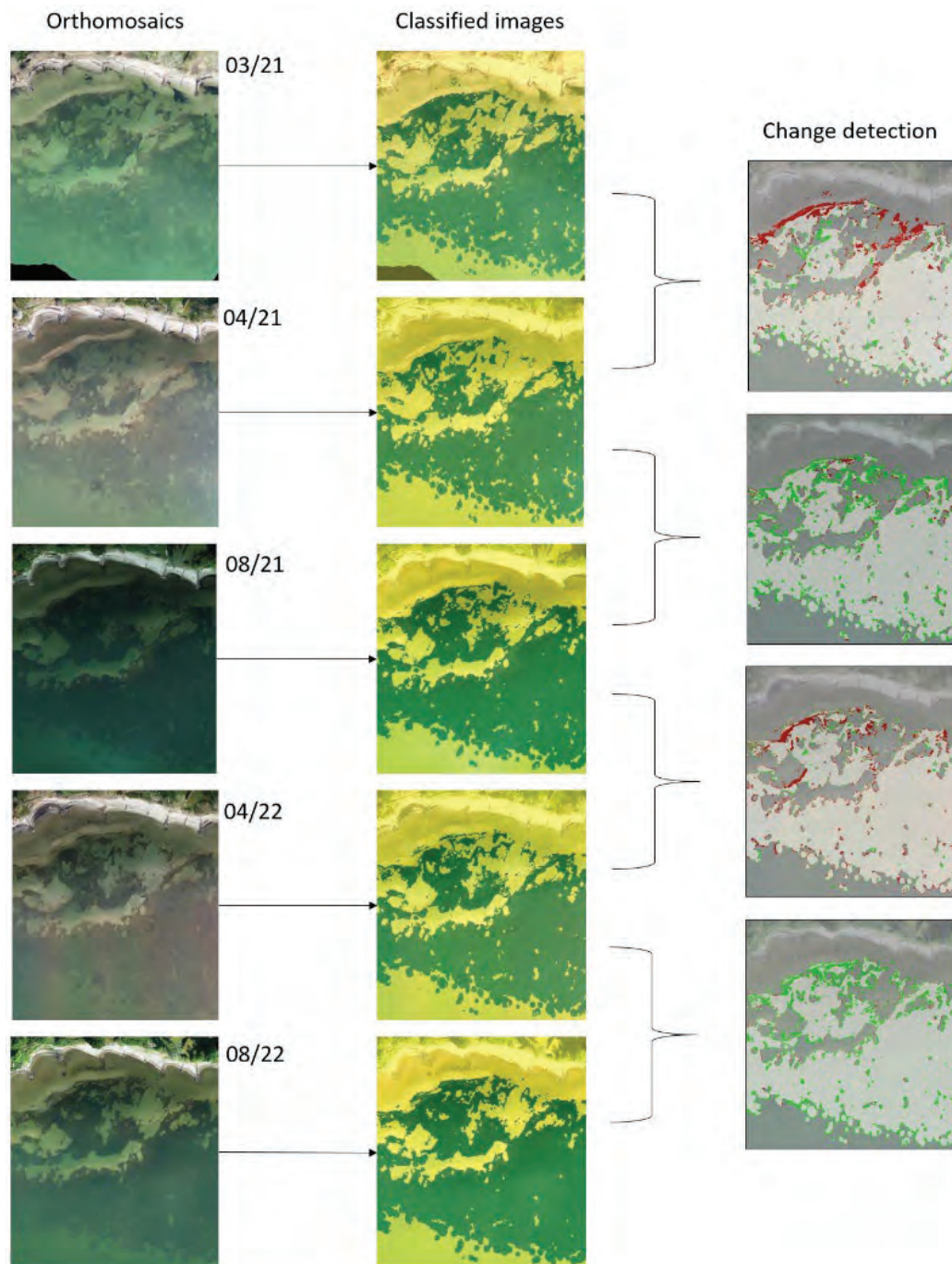


Figure 2.16. Original images are shown in the left column, resulting classifications in the middle column and maps visualizing eelgrass gain (green), loss (red) and areas of no change (grey) in the right column.

The results show that seasonality related changes in eelgrass bed cover, as well as the effects of stressors (in this case ice cover) can be monitored at high detail over relatively large areas in an easy and economically feasible way due to the high spatial resolution, spatial accuracy and

temporal flexibility provided by UAVs. Figure 2.17 visualizes eelgrass cover gain and loss between time steps. Interestingly, the impact of the ice cover event that occurred in February 2021 could only be detected with a delay of 1.5 months on the image obtained in April 2021, as the image obtained in March 2021 did not show significant change.

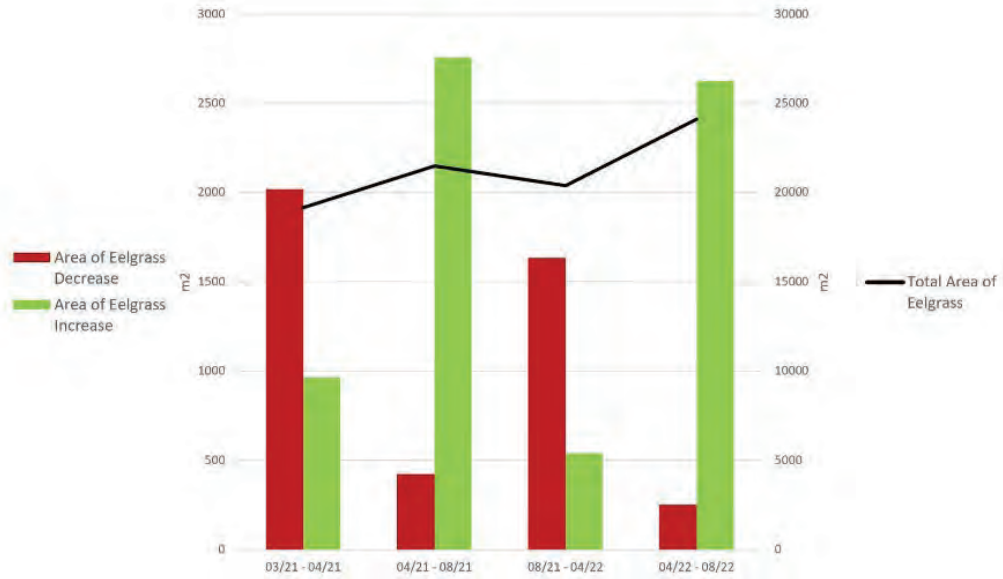


Figure 2.17. Eelgrass cover gain and loss between time steps.

The fact that the state of the eelgrass bed, in terms of density and possibility of visual detection, allowed to map and monitor its extent early in the year and during a state of minimum biomass, raises the question if eelgrass monitoring campaigns should better be conducted during this early period in the year, instead of later in the year, closer to its biomass maximum, as it is done in many campaigns at the moment. The benefit of conducting monitoring earlier in the year are the lower levels of phytoplankton in the water column as well as significantly less epiphytes potentially overgrowing the eelgrass, which on many occasions make the detection more difficult and labor intensive in late summer months. From the conducted experiment it was learned that the eelgrass bed extent was about 15% lower at the beginning of the growth season, which helps to estimate and predict its cover to the peak of the growth phase.

Case: Transplantation of eelgrass in Horsens Fjord

A direct application of UAV-based change detection procedures can be found in the context of eelgrass restoration. Here, eelgrass is transplanted to an area as shoots that with time will spread and form into full grown beds. An example of this is the case of Horsens Fjord.

A case study of change detection in a large-scale eelgrass transplant in Horsens Fjord (established in 2017 by SDU) was conducted on imagery from the growth season 2019, 2020 and 2021 (Fig. 2.18). A complete area of 30 ha including natural eelgrass patches was mapped and the transplanted section (1 ha) chosen for analysis. The area was mapped in 100 m altitude for creation of an orthomosaic and in 5 m altitude for ground truthing using a DJI Phantom 4 Pro with a standard 20 MP RGB camera.

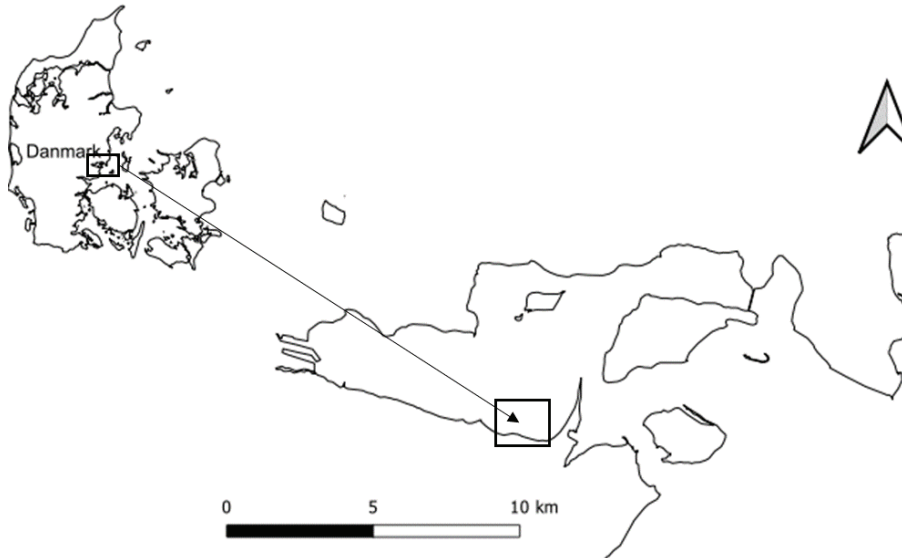


Figure 2.18. The study area of transplanted eelgrass in Horsens Fjord, Denmark.

The orthomosaics were then classified into the classes Bare bottom, Eelgrass and Macroalgae in order to measure the specific areas per class using 20 training samples per class and a supervised classifier (here SVM) with a >90% accuracy (Fig. 2.19).



Figure 2.19. Classified section of the transplanted eelgrass bed in Horsens Fjord. Top: The classified maps from 2019, 2020 and 2021 showing the classes: Eelgrass, Bare bottom and Macroalgae. Middle: The yearly measured areas of eelgrass and macroalgae. Bottom: Example of a ground truthing image obtained in 5 m altitude.

The initial 17.000 transplanted shoots (Lange et al., 2022) planted in 2017 had in 2019 developed into dense patches of a total area of 1324 m². The complete transplant further developed with an expansion of 61% in 2020 and further with 52% in 2021 resulting in a total area of 3225 m². Using the UAV-based method and image analysis, a complete assessment of the transplant state was made possible by enabling separation into eelgrass and surrounding macroalgae, and

identification of sections of lower growth (high stress) like in the South-Western corner. Using this method makes monitoring of transplantation success possible even at very high shoot numbers complementing diver-based monitoring of these large eelgrass patches.

2.4 Evaluating stressors

Eelgrass beds are constantly exposed to stress from the surrounding environment such as sediment mobility, opportunistic algae species, or epiphytes, or mobile perennial macroalgae. The effects of these stressors on the eelgrass beds are well known and well described but quantifying the stressors and evaluating their impact can be a hurdle on a large scale (landscape scale). By implementing UAV-based techniques it is possible to obtain very high-resolution imagery and thus map the coastal areas in a fast, precise, cost-efficient, and consistent way. This data combined with advanced image analysis (see also section 2.6) enables detailed studies of the coastal zone, changes in coverage and biomass, stress-impact, and restoration potential. Eelgrass stressor estimation and quantification is highly important regarding management as the processes impacting eelgrass are determining the extent of the eelgrass beds and the potential for restoration. Thus, both eelgrass coverage mapping and stressor assessment are vital in eelgrass management.

In this study, a method for classifying and quantifying a range of stressors acting on coastal eelgrass beds is proposed. For this, a series of part-studies have been conducted:

- Quantification of filamentous opportunistic macroalgae and epiphytes on close scale, extrapolating to landscape scale (section 2.4.2).
- Monitoring and quantification of mobile macroalgae such as *Fucus sp.* (section 2.4.3)
- Classification and count of fecal mounds of lugworms (section 2.4.4).

In general, landscape scale mapping should be performed in 100 meters altitude to support construction of accurate orthomosaics as base maps. In this altitude separation of eelgrass, bare bottom, and macroalgae mats is possible. For further separation into smaller units, a lower altitude is needed depending on the species/stressor of interest (Fig. 2.20). Thus, for smaller stressors (such as lugworms or small algae specimens) impact estimation must be based on many low-altitude images rather than one landscape-scale map and can then be extrapolated to the landscape level.

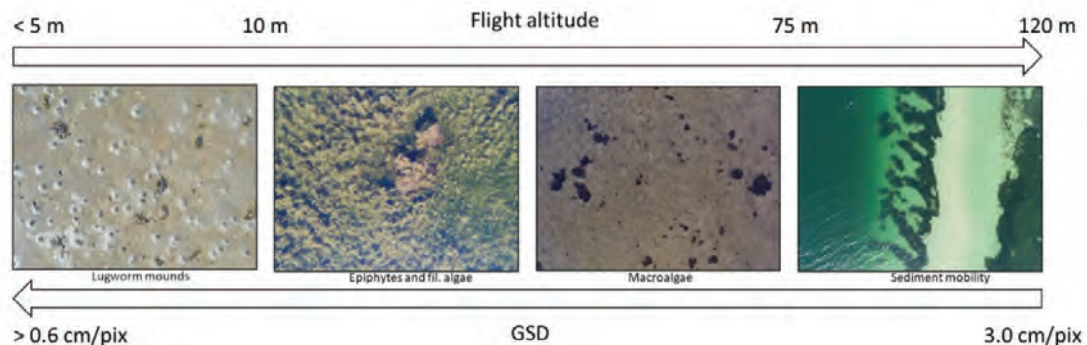


Figure 2.20. Example of stressor recognition at varying flight altitude and GSD.

In all of the part-studies in the stressor evaluation a DJI Phantom 4 Pro and Phantom 4 Advanced with a standard 20 MP RGB camera was used. The UAVs collected imagery with 80 %

overlap to secure a very high-quality data basis. In all instances the collected imagery (250-800 images) were stitched in the photogrammetry software Agisoft Metashape and the resulting orthomosaics (GSD = 2.6 cm/pix using 100 m altitude images) were analyzed by object-based image analysis in Trimble eCognition.

2.4.1 General quantification of stress in eelgrass patches

Area-specific quantification of stress-impact in eelgrass beds is based on both direct measurement of temporal growth/loss, count of individual macroalgae or measurement of algae cover, or supportive parameters such as wash-up on the beach. Direct measurement of change and fragmentation in the beds also include assessment of the number of single patches, number and size of holes in the patches, and the parameter-to-area-ratio. Ring creation is also a clear parameter of stress either being caused by algae cover or ballistic impact, or sulfide release. Thus, to be able to assess the stress-impact, type and level, a temporal scale is necessary, i.e., creating a timeseries of the area of interest. On one-time snapshots, the type and coverage of a certain stressor can be extracted or if the area characteristics contain a geographical stress-gradient – such as the coast at Enebærodde – it can be quantified (Fig. 2.21). In this area, the Western part of the eelgrass bed is partly protected by a small tongue of land while the other end is exposed to the full fetch and by dividing the area into comparative regions these can be compared based on stress parameters. The area covered by the main eelgrass population was divided into eight regions of equal size from west to east (R1-R8) for the patches on the inside towards the coast (I) and outside towards the sea (O) and the perimeter to area ratio (P/A-ratio), number of holes in the patches, number of patches and the area of holes in the beds (area fraction) was determined for maps from 2015, 2017 and 2020. 2021 and 2022 were left out as the images collected in these years were too impacted by weather and algae coverage at the times of flight.

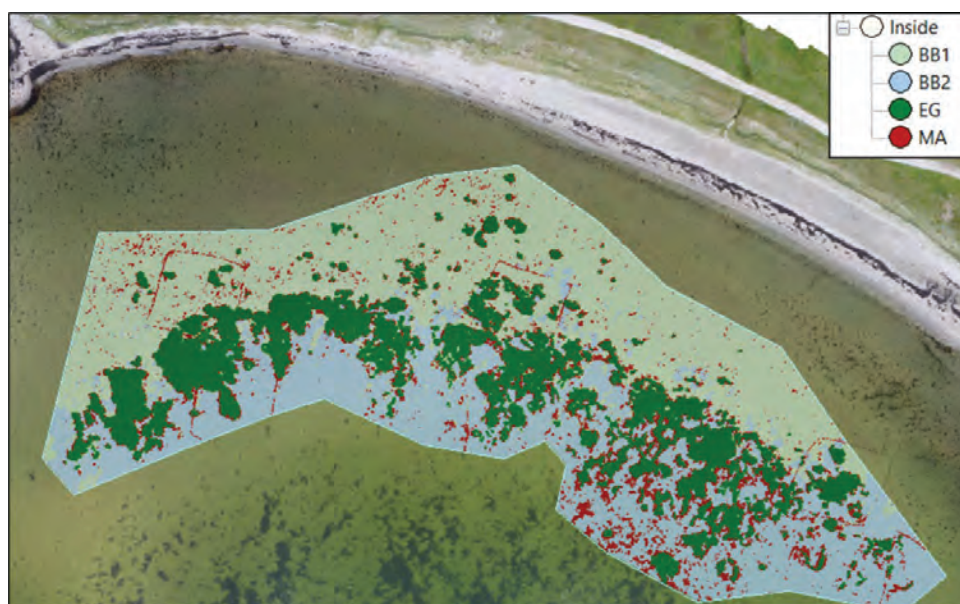


Figure 2.21. The dynamic and high-stress eelgrass area at Enebærodde in the North of Odense Fjord. Indicated are the classes Bare bottom (BB), Eelgrass (EG) and Macroalgae (MA).

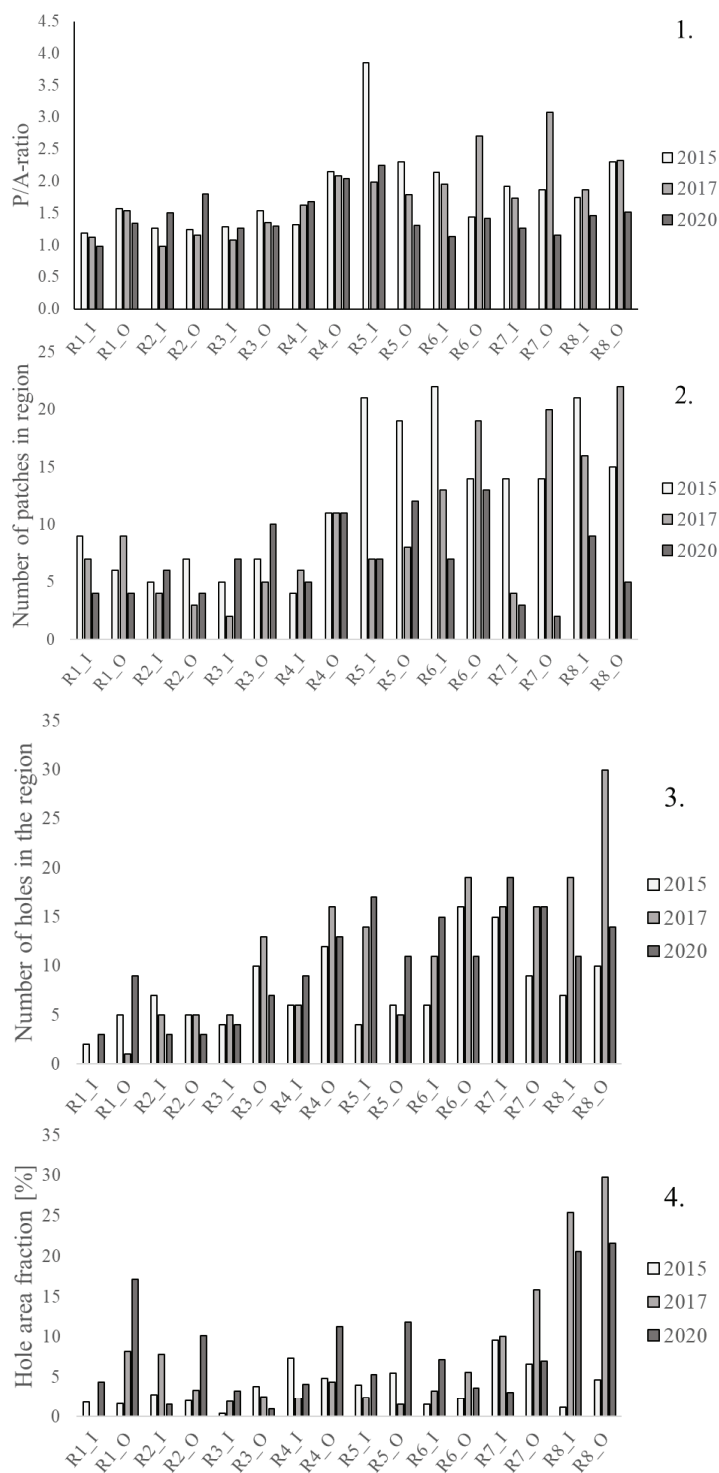


Figure 2.22. A representation of the stress gradient found at Enebærødde based on physical protection in the West. 1. P/A-ratio; 2. Number of patches in region; 3. Number of holes in the patches in the region; 4. Hole area-fraction

For all stress-descriptors the monitoring and data analysis showed a great yearly variation in all parameters, but also a general trend towards a higher stress-impact in the more exposed east but with large yearly variation in the type of descriptor: P/A ratio and number of patches show a distinct gradient in 2015-2017 while the hole-descriptors are more prominent in 2017-2020. This indicate that UAV-based data is highly applicable in exposing geographical trends and delineating changes that arise from stress impact both data-wise and visually (Fig. 2.22). More info on the processing is found in Svane et al., 2021.

To further understand the stress-impact originating from physical impact of waves, the depth-intervals combined with eelgrass area-fraction can be quantified (Fig. 2.23) as low-depth regions often have less and more fragmented eelgrass beds. This was performed at Enebærødde and combined with the classified images to create a depth-coverage relationship. It is evident that the main population is where light is sufficient for growth and wave-action is limited due to a higher depth. In the area at Enebærødde this corresponds to an MSL of 1.0-1.4 m.

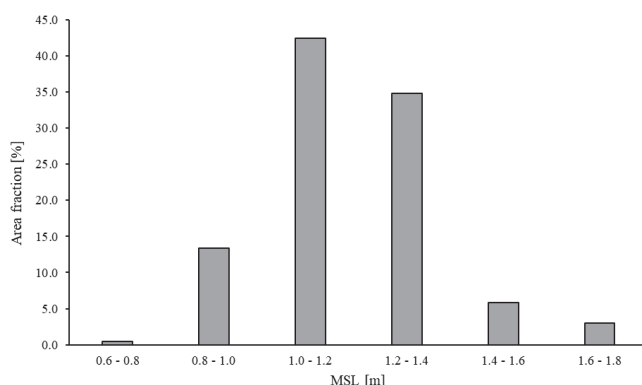


Figure 2.23. Area fractions of eelgrass in depth-intervals (MSL = Mean Sea Level) from 0.6-0.8 to 1.6-1.8 m

To assess and compare changes in bare bottom and eelgrass cover in specific areas combined with classifying present stressors it can be relevant to divide the area into sub-units of a fixed size. This aid comparative studies between different areas. This is exemplified in the following using an area with known high sediment mobility, mobile perennial macroalgae and seasonal large blooms of opportunistic filamentous algae in Dalby Bay in Northern Funen. The monitored area was divided into 10x10 m sub-units in which the present stressors were classified and quantified annually.

2.4.2 Epiphyte quantification

Epiphyte coverage was determined in three different areas of which two example classifications are presented here. To test the potential of UAV-based assessment of epiphyte coverage, field monitoring was performed in Lillebælt just south of Fænø in May 2020 and in Lunkebugten on Tåsinge in June 2022. At both times an area of approximately 15 ha was mapped and a representative sub-area for testing the methodology was selected after visualizing the data. To be able to classify and quantify epiphytes on UAV imagery, it needs to have a certain minimal coverage (15-25 cm² units). To maintain a practical mapping output, the epiphytes are therefore often mixed with general filamentous algae (if present) in the resulting classified map, as these

cannot be separated. Depending on the conditions and the size of the epiphyte/filamentous algae maps, the recommended mapping altitude is 20-50 meters (with a 20 MP sensor), but > 50 meters can be feasible depending on the resolution of the camera sensor and if the epiphyte cover is dense. Two flight procedures were tested:

- Low-altitude (< 10 m) images with **extrapolated classification** of the coverage to landscape scale (Fig. 2.24+2.25).
- 30-100 m altitude with a **direct classification** of the coverage (Fig. 2.26).

The procedure for mapping and orthomosaic creation is as stated in the earlier sections and 30 ground truthing images were obtained per station.



Figure 2.24. Base-map (100 m) with indication of recording of low-altitude (5 m) images based on imagery collected South of Fænø.

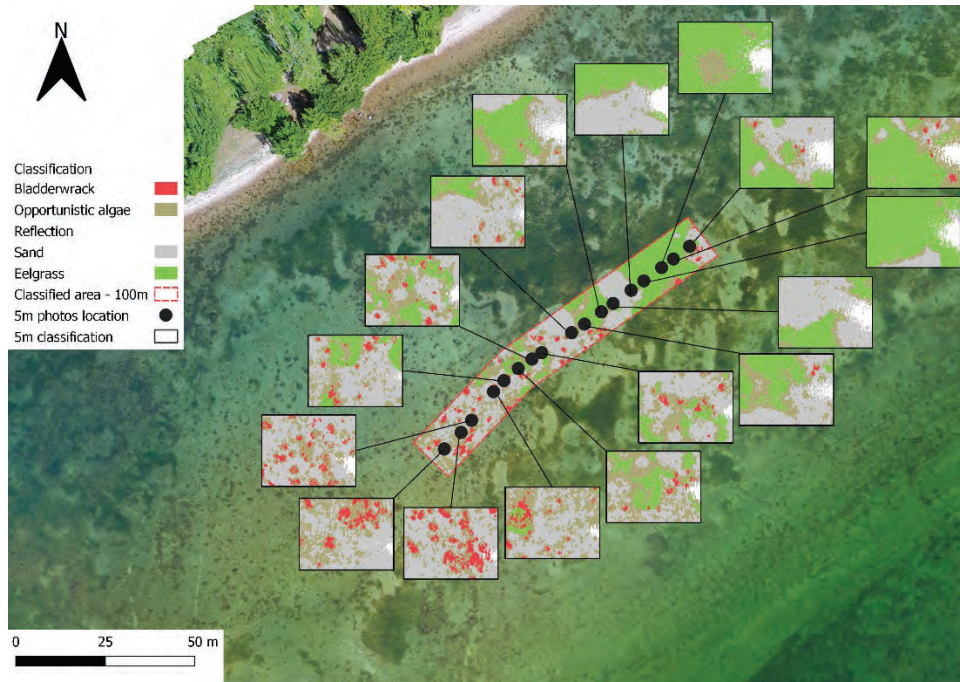


Figure 2.25. Classified output of a combination of low-altitude images and transect of the 100 m base-map

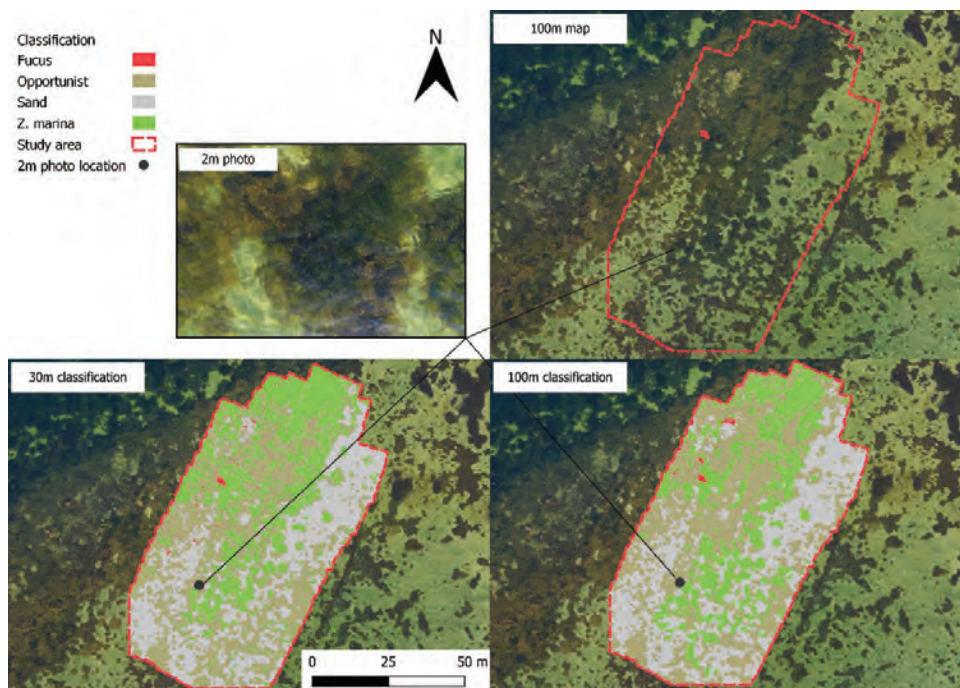


Figure 2.26. Classified output of a 30 m altitude map (lower left) and a 100 m altitude map (lower right). Top-left is a representative ground-truthing image for training. The images were obtained in Lunkebugten at Tåsinge.

The recommended procedure for classification and quantification is:

- Use an object-based image analysis workflow as suggested in section 2.1.
- Use ground truthing images as basis for training the classifier – use at least 15 per class (depending on area size) (See section 2.5 for drone-based ground truthing).
- Do manual or condition-based clean-up of the classification result (i.e. reclassification based on image object properties).

The results show that extrapolating low-altitude images (< 10m) can reach accuracies above 90% for eelgrass, macroalgae such as bladderwrack, and epiphytes/filamentous algae. The trade-off for this high classification accuracy is a lack of spatial extent. This can be mitigated by either make a number of representative, low-altitude transects throughout the area, or by mapping in higher altitudes (Fig. 2.26) but the final altitude must be chosen case-by-case based on the conditions in the area at the specific time. Additionally, the high-altitude imagery (30-100 m) requires more time for correction and refining the analysis than the low-altitude with very high resolution images. Comparing the classification based on both 5 m and 100 m (Fænø) and 30 m and 100 m (Lunkebugten) images respectively, show a small difference in epiphyte/filamentous algae cover between altitudes, but both have an accuracy above 90%. The small deviance in area is practically insignificant and the coverage output virtually equal. Thus, the error/deviance is purely thematic and so small that it is acceptable. The distribution of classes in 5 m compared to 100 m is shown in figure 2.27.

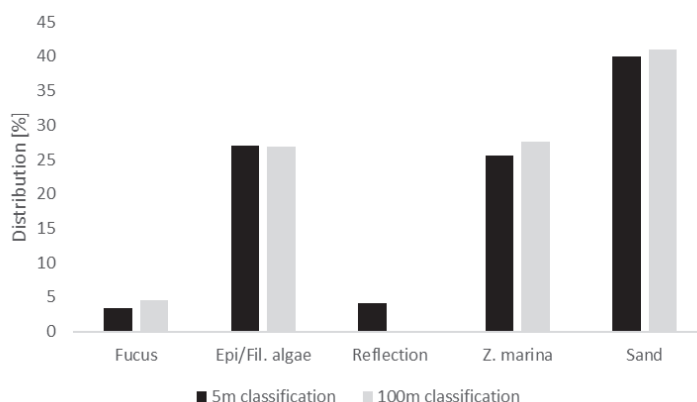


Figure 2.27. The distribution [%] of classes classified in images from 5m and the orthomosaic from 100m at Fænø.

When performing epiphyte estimation, it is sometimes necessary to record a time-series in intervals revealing both the standing biomass of stationary vegetation such as eelgrass and the mobile algae. In this case visiting the area before and after a larger wind-event might suffice and the standing stock of SAV can easily be assessed.

Discussion

As epiphytes per definition cover the leaves or appendages of other vegetation, they possess a 3D growth pattern. This depth-aspect cannot be assessed using 2D images obtained from above and field-sampling must be applied for a complete estimation of cover and biomass.

Even though UAVs provide very high-resolution images, it is also an issue to separate “real” epiphytes from general filamentous algae cover. As both act as stressors on eelgrass they are though important to quantify and by using UAV-imagery and the proposed field and analysis methodology the general coverage can be obtained with a relatively high accuracy. A combination of low-altitude images (< 10 m) and high-altitude maps (30-100 m) is recommended to create a complete and valid quantification of the eelgrass-epiphyte ratio in the monitored areas.

2.4.3 Mobile perennial macroalgae

Mobile perennial macroalgae such as bladderwrack is a cause of physical stress on eelgrass by ballistic impact resulting in uprooting of shoots or direct physical damage on leaves (Valdemarsen et al., 2010). Secondary, the macroalgae can also cause shadowing in calm conditions.

Using imagery collected monthly during the growth season in 2020, it was possible to track changes in eelgrass bed area, perimeter, P/A-ratio, shoot density (< 30 m altitude), and perennial macroalgae (here bladderwrack) cover, (Fig. 2.28). Any accumulation or growth inside or flanking the beds was easily distinguishable and can be compared to eelgrass growth or loss if the temporal resolution is sufficient. As bladderwrack grow at app. 0.45-0.48 cm/week the larger changes in coverage between months can be assumed to be based on inflow-outflow rather than growth alone, while small changes need an even higher temporal resolution to be assessed.

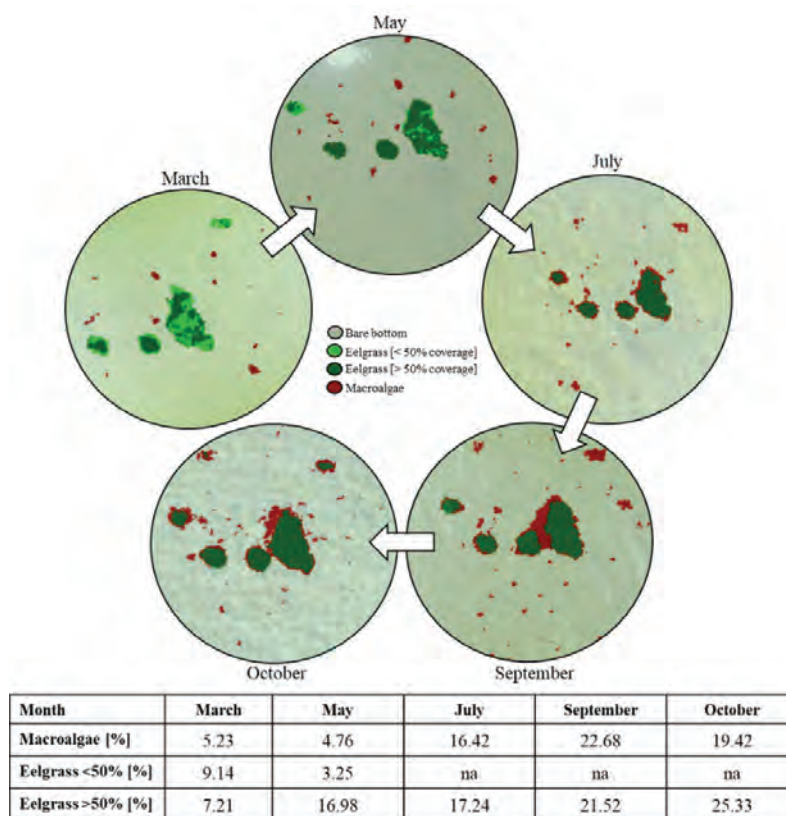


Figure 2.28. Classified sections of a 30 m orthomosaic based on images from Enebærødde, Odense Fjord, obtained in 2020. Each circle represents a month from March to October showing the change in eelgrass coverage (< 50 % and > 50 %) and macroalgae (Bladderwrack) presence. The macroalgae and eelgrass coverage is shown in the table in the bottom.

It is also possible to determine the rate of mobility if a fixed area is monitored weekly-to-monthly or the single individuals are either recognizable or can be tagged visually. In perfect conditions, the tracks or static impact (hammer-effect) from bladderwrack dragging stones are easily recognized even in 100 m altitude imagery (Fig. 2.29) and can be measured but need daily or weekly image acquisition combined with weather data for direct mobility measurement.

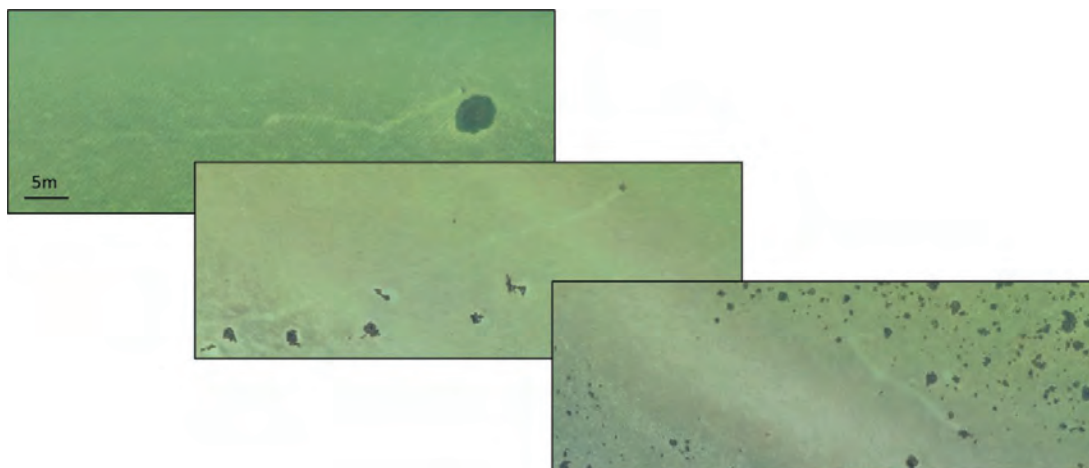


Figure 2.29. Mobile bladderwrack with distinct visual track or static impact in 100 m imagery from Horsens Fjord.

2.4.4 Additional stressor quantification

Lugworms have a negative impact on eelgrass due to their bioturbation activity, burying seeds or uprooting eelgrass shoots and seedlings (Valdemarsen et al. 2010). It has been determined that the number and size of fecal mounds can be used as a proxy for the number and biomass of lugworms (Valdemarsen et al. 2010), but a count on a landscape scale can be quite labour intensive. By applying different methods for image inspection or analysis it is possible to extract information about lugworm density at a larger scale using high-resolution drone-imagery.

Method 1: Manual marking combined with automatic count:

Map the area of interest in a maximum of 30 m altitude in perfect, still conditions, and lower if the wind-speed is between 3-5 m/s. If wind speed exceeds this, the wave-action most likely will distort the surface rendering fecal-mound monitoring impossible. After creation of an orthomosaic with a GSD of 0.85 cm/pix or lower, or collection of a number of single images, the fecal mounds can be counted manually, or marked with a coloured dot which can be counted automatically using software like ImageJ or eCognition.

Method 2: Traditional Machine Learning (ML):

Map the area of interest as described above. Perform a segmentation using a scale of 10-25 and apply an ML-algorithm such as the SVM after training with at least 25 samples. This can be aided by using shape (roundness) as a training parameter, but tests have shown a maximum of 45-65 percent accuracy using the traditional ML classifiers.

Method 3: CNN

By applying a Convolutional Neural Network algorithm, it is possible to reach higher accuracies for classification of organisms or objects that are inherently difficult to map (e.g., fecal mounds and blue mussels) (Fig. 2.30+2.31).

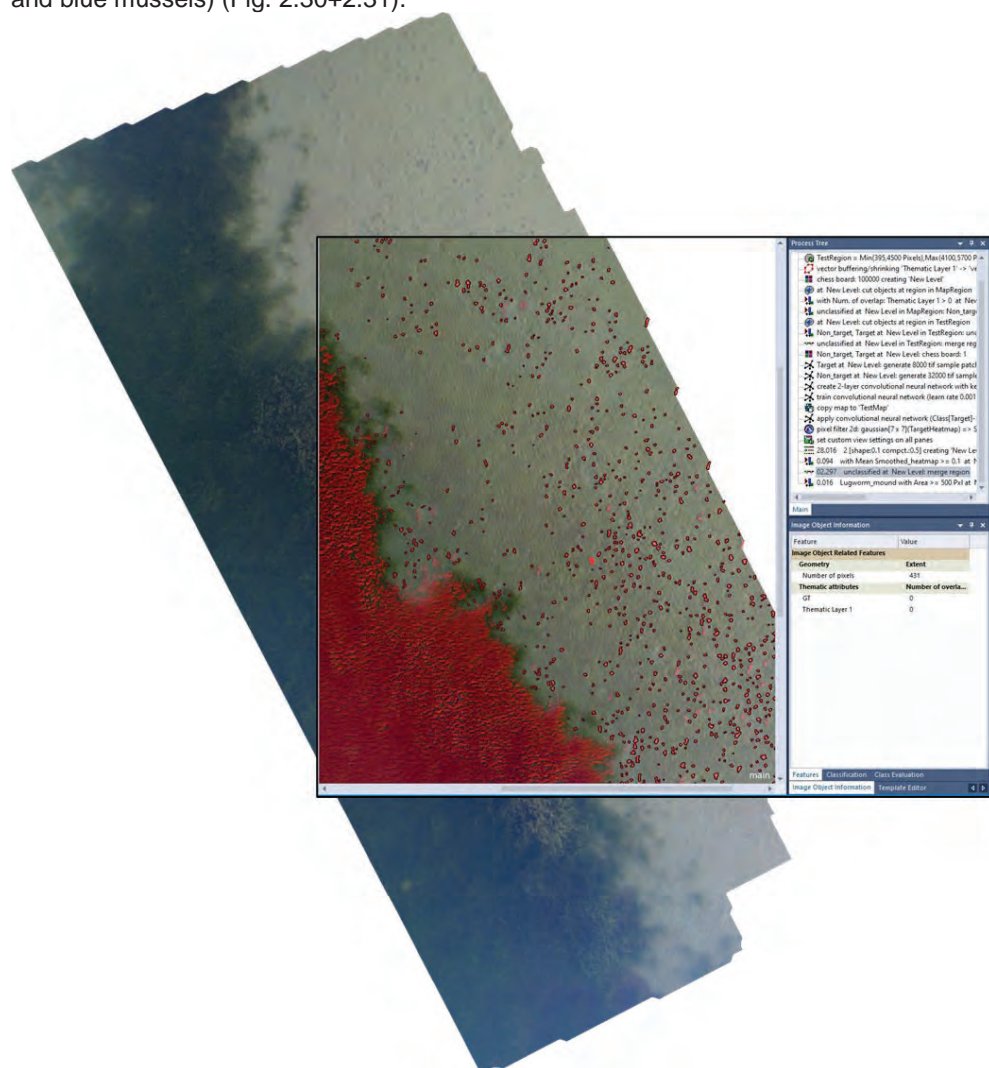


Figure 2.30. CNN-based classification of fecal mounds of lugworms in Dalby Bugt.

This method uses neural networks for assigning a class based on context and image structure in a higher degree than traditional ML. The CNN-algorithm also include an aspect of “self-learning” meaning that it gets more accurate per classification of a new image or area. Using CNN on images of fecal mounds from Dalby Bugt showed an increase in accuracy from 45-65% using traditional machine learning (here SVM) to above 90 %. In comparison with manual counting, the CNN showed a match of above 95 %. This is the same result when applying the CNN-method on imagery of blue mussel beds (Fig. 2.31).

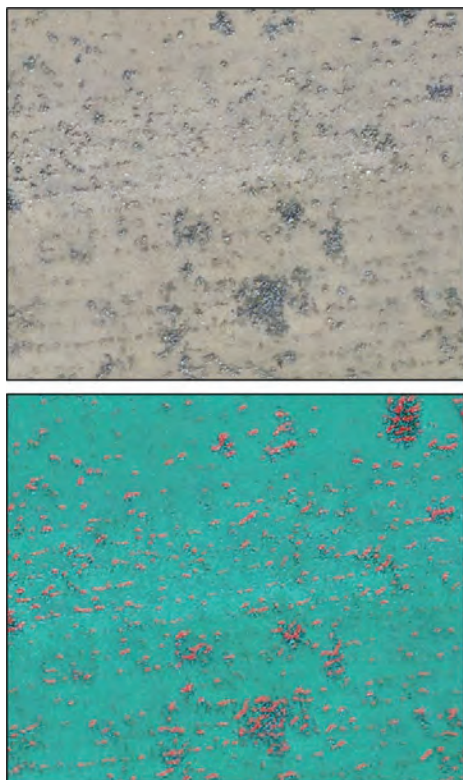













Figure 2.31. CNN-based classification of blue mussels in Gyldensteen Lagoon on Northern Fyn.

Conclusion

Using UAV-based high-resolution imagery for classification and quantification of stressors impacting eelgrass beds in Danish Coastal areas is a very accurate and feasible method. The results show that both perennial macroalgae, filamentous algae and epiphytes, and growth/loss in eelgrass are possible to define using imagery with a variable GSD (Table2.3). Using either parameters such as area change, perimeter-to-area ratio, or number of holes in the eelgrass beds, or specific coverage measurement of stressors, the UAV-imagery and image classification methods described are sufficient to describe the coastal sectors in more detail than seen before. This enables a more holistic description of the areas and the processes acting on the highly dynamic eelgrass beds on an unprecedented temporal and spatial scale.

Table 2.3. The recommended flight altitude for collection of UAV-imagery matching a specific stressor.

Monitoring altitude	Eelgrass growth/loss	Perennial macroalgae (general)	Perennial macroalgae (species)	Epiphytes/ Fil. algae (general)	Epiphytes/Fil. algae (species)	Sediment mobility	Lugworm mounds	
100 m								
75 m								
50 m								
25 m								
10 m								

2.5 Ground truthing using drone platforms

It is a recurrent issue to validate remotely sensed imagery on a larger scale using existing manual methods, especially when working in the aquatic environment. To obtain enough high-resolution ground truthing data needed for training and validation of remotely sensed imagery of submerged vegetation, traditional in-water methods involving divers, ROVs or vessel-based drop-down camera systems are usually applied. These methods are labor and cost intensive, often lack spatial accuracy or spatial extent, and are limited to areas that are accessible by boat or by divers. When environmental conditions are favorable in terms of visibility, water depth and water surface properties, UAVs can provide solid ground truthing data thanks to the very high spatial resolution of UAV-mounted camera systems combined with the ability to hover over a specific position. By lowering the UAVs altitude to a few meters above the water surface, the pilot can take close-up images of selected ground truthing points within the study area in a very efficient way. This method is however limited to areas of a maximum depth of around 1 m, while at the same time being very weather dependent, as the benthic substrate, including submerged vegetation, gets quickly blurred with increasing depth, low visibilities or wind induced movements at the water surface not allowing a clear determination of depicted species/habitat/substrate. To mitigate these issues, different UAV-based underwater camera systems were developed and tested with the aim to provide a user-friendly, cost-effective, and readily applicable method, that can be incorporated into the UAV monitoring workflow to provide close-up images of the benthic substrate before or after large scale eelgrass mapping missions.

The following UAV-based ground truthing methods were tested:

- Surface landing customized DJI Phantom 3 Pro with surface penetrating camera system.
- Surface landing of-the-shelf SwellPro 4 with surface penetrating camera system.
- DJI Phantom 4 Advanced with an underwater camera-by-wire carrying payload system.
- DJI M600 with an underwater camera-by-wire and logger setup carrying payload system.

Surface landing customized DJI Phantom 3 Pro with surface penetrating camera system

The Phantom 3 Pro with two buoyant “water-noodles” attached to the frame, and a GoPro Hero 3 mounted underneath was a working solution but only in calm weather (<4 m/s winds) and no waves. The airframe was not watertight in any way; therefore, this platform was disregarded for further testing.

Surface landing of-the-shelf SwellPro 4 with surface penetrating camera system

After initial flight tests it was concluded that the SwellPro 4 is not suited for professional field-work, as it lost connection to the live-feed camera (Wi-Fi signal drone-to-remote, and remote-to-tablet) 80-90% of the time, making it impossible to situate the drone correctly for mapping. After a series of water-landings, the drone began flying erratically, making it difficult to control and land, and was therefore disregarded for further testing.

DJI Phantom 4 Pro with an underwater camera-by-wire carrying payload system

The platform used for this setup was a DJI Phantom 4 Pro with a 20MP on-drone RGB camera. The ground truthing system attached to this UAV allowed to obtain images from a fixed distance to the substrate of 1m by an underwater camera, which was attached via a nylon string to a stand-alone payload system compatible with any DJI Phantom model. The payload systems

were 3D printed using PETG carbon fiber and designed for quick mounting in the field (Fig. 2.32). It did not interfere with the UAV camera, meaning that both systems could operate at the same time. The underwater camera used in this set up was a Paralenz Vaquita (12MP, 4K at 60fps, 1080p at 240fps, FOV (1/1.8") D108° H90° V59° lens, 18mm focal length). This underwater camera logs depth (overlay on video or images) and automatically starts recording at a pre-set depth making it exceptionally suitable for UAV-based ground truthing. Lowering of the camera was controlled by adjusting the UAVs altitude, thus, the nylon-string length needs to be adjusted accordingly to bathymetric conditions before flight. We recommend the string to have a minimum length of 5 m and at least two times the length of the water depth in the study area. In this way, the pilot can keep a safe distance between UAV and water surface. The fixed distance of 1 m that the camera has to the sea floor during data collection is controlled by a floater and counterweight system, consisting of a floater that is attached to the camera and a counterweight that is attached to the bottom end of the line. The floater and counterweight are calibrated against each other, so that the upwards force of the floater is slightly larger than the downwards force of the camera, but not larger than that of camera and counterweight combined. In this way, if the camera is fixed to the line at 1 m distance to the counterweight, the combined downwards force of the camera and the counterweight pulls down the floater when entering the water. As soon as the counterweight touches the sea floor and therefore stops pulling downwards, the floater remains in position as it has just enough force to pull the camera upwards. The distance of the camera to the sea floor can be adjusted by changing the distance between camera and counterweight.

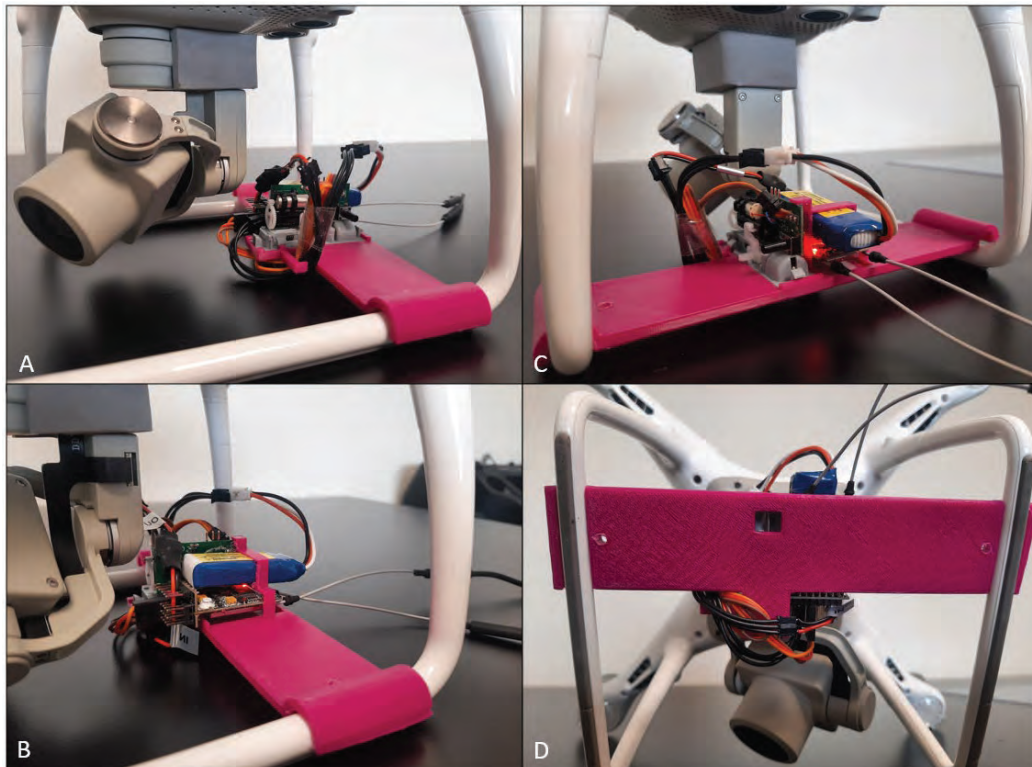


Figure 2.32. Payload system with emergency release mechanism, power supply and receiver. Views from the left (A), right (B), back side (C) and below (D).

The whole underwater camera setup was supplied with an emergency release system consisting of a receiver, transmitter, and battery, if the camera should be caught on any structures while recording. It was marked with a colored buoy for quick retrieval in case of emergency release. The weight of the payload system amounts to 275 g, which reduces the flight time of the UAV to about 15 minutes. For an efficient use of the flight time, it is therefore suggested to conduct the ground truthing mission by using a preplanned flight path. This can be done with common flight mission planning software such as UgCS (Fig. 2.33), where the flightpath, point for data collection and altitude is set in the following procedure:

- Automatic stop over sample point.
- Reduction of altitude to submerge camera.
- 5-second standstill for allowing settlement and successful recording.

When mounted on a UAV with RTK system, the sample points are of such high geographical precision that validation data for highly fragmented and scattered eelgrass beds can be collected. The design of the ground truthing systems makes data collection somewhat independent from weather conditions, though limited by the size and power of the Phantom 4 platform. Gyro- and pendulum effects caused by the hanging camera system were observed during testing. Those, however, had little to no effect on the flight performance but need to be taken into consideration during operation. In the project, the following flight characteristics of the DJI Phantom 4 setup were tested in a controlled environment:

- Taking off and landing with attached ground truthing system
- The system's impact on flight performance
- Power limitations and battery cell stability
- Release mechanism

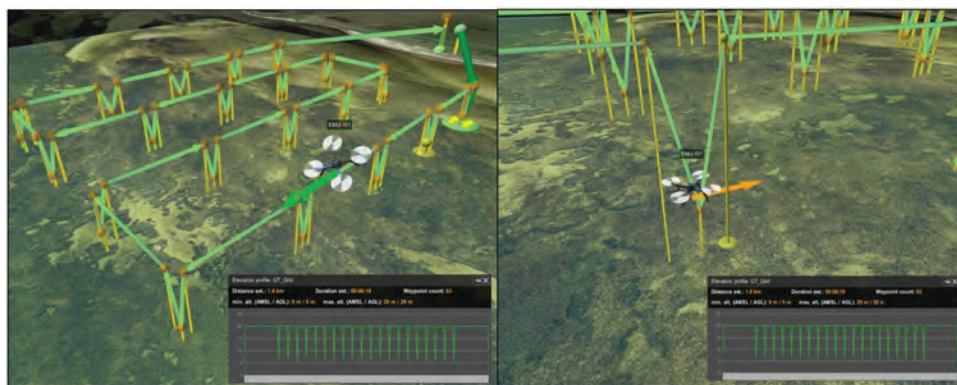


Figure 2.33. Ground truthing mission flight plan, programmed with UgCS flight planning software.

Field tests were then conducted in the Limfjorden (Lovns Broad) and in the Kattegat (Endelave). In Lovns Broad, 65 georeferenced underwater images were obtained in the depth range of 0.5m to 3 m using the described system. All images allowed a clear identification of substrate and occurring species (Fig. 2.34, left). At the study site of the coast of Endelave it was possible to detect eelgrass at depths of 5.5 m using the described system (Fig. 2.34, right).

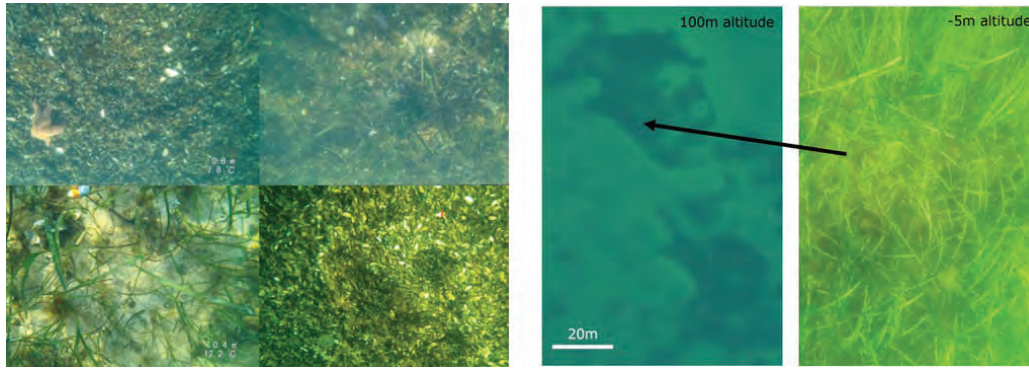


Figure 2.34. Examples of ground truthing images collected in Lovns Broad (left) and Endelave (right).

DJI M600 with an underwater camera-by-wire and logger setup carrying payload system

The UAV used in this setup was a DJI Matrice 600 (M600) with a 12MP RGB on-drone camera, 6x TB47 + 6x TB48 batteries, a flight time of app. 35 minutes per battery pack and a custom-built logger-and-camera cluster with adjustable line length (3D-printed with of-the-shelf electric motor). The maximum operational depth was 8 m. The setup used the DJI M600 channel expansion kit, where two additional servo outputs were set to lower or raise the camera and logger cluster 0.5 m per flip of the switch. The submersible camera did not interfere with the standard on-drone camera, which can be used simultaneously while sampling with the wired setup. The images from the main camera were used to georeference the underwater images. The following flight characteristics of the M600 setup were tested in a controlled environment in the project:

- Taking off and landing with the cluster attached.
- Impact on flight when spooling out line (gyro-effect).
- Any technical issues: Engine failure in the cluster setup, power limitations, instability, errors in the DJI control application, battery cell stability.

The M600 setup was then safety tested in-field under changing environmental conditions to test:

- Flight characteristics in wind-speeds > 5 m/s, 7 m/s and 12 m/s, with and without spooled out line (wind-drag).
- Flight characteristics when lowering and raising the cluster under the water surface with waves of 20-100 cm amplitude (water-drag).
- Energy consumption in changing wind conditions and during field-application.

The flight-tests were performed in Odense Fjord, at the station at Enebærodde, 23/3/2023. Sample collection was performed in Horsens Fjord 11/5/2023, Odense Fjord 28/3/2023 and 21/4/2023 and Dalby Bay 3/5/2023. At Enebærodde, it was possible to collect data points at increasing depth on bare bottom, on patch-edges, inside patches and on bare bottom in deeper water (>1.5 m) (Fig. 2.35). It was possible to separate species (eelgrass, bladderwrack, blue mussels, *Littorina* and more), assess eelgrass shoot condition and coverage, and assess bottom conditions. At no point the image quality was limited by turbidity or any other adverse effects. The application of additional loggers allowed the collection of additional data such as light and depth (Fig. 2.36).

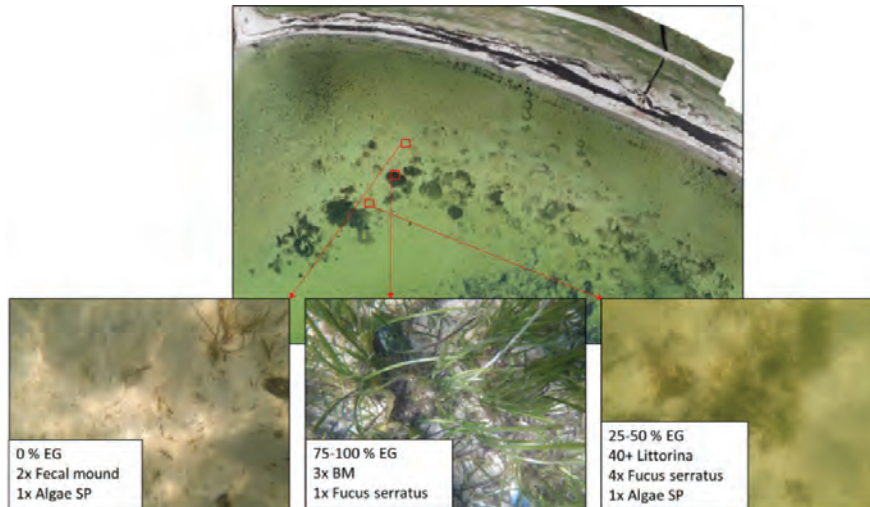


Figure 2.35. Example of drone-truthing images and image-content collected at Enebærodde. EG=eelgrass, BM=blue mussels

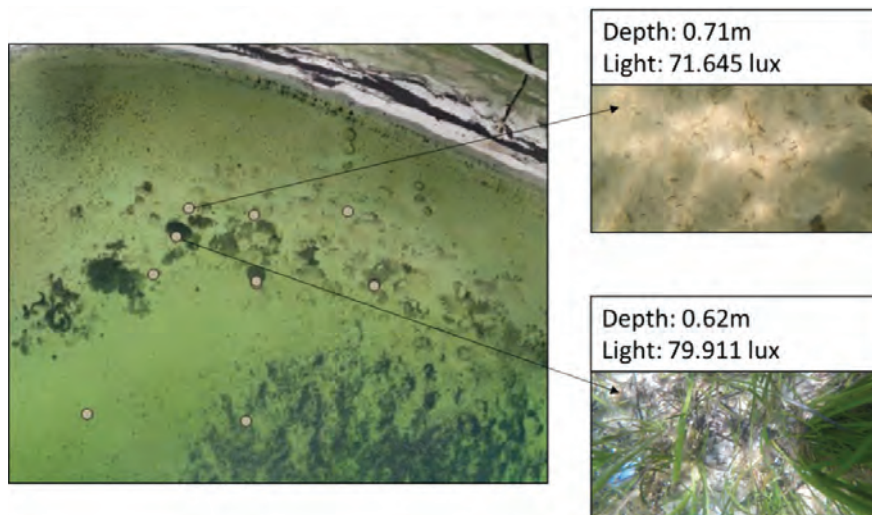


Figure 2.36. Example of additional information collected by loggers while performing drone-truthing. Here depth and light.

The image quality from image collection in Horsens Fjord (Fig. 2.37) was visually impacted by turbidity in two points, but this could be mitigated by lowering the camera gradually. At no time did the image quality severely impact the assessment of seabed type, vegetation cover, stressors, or other parameters.

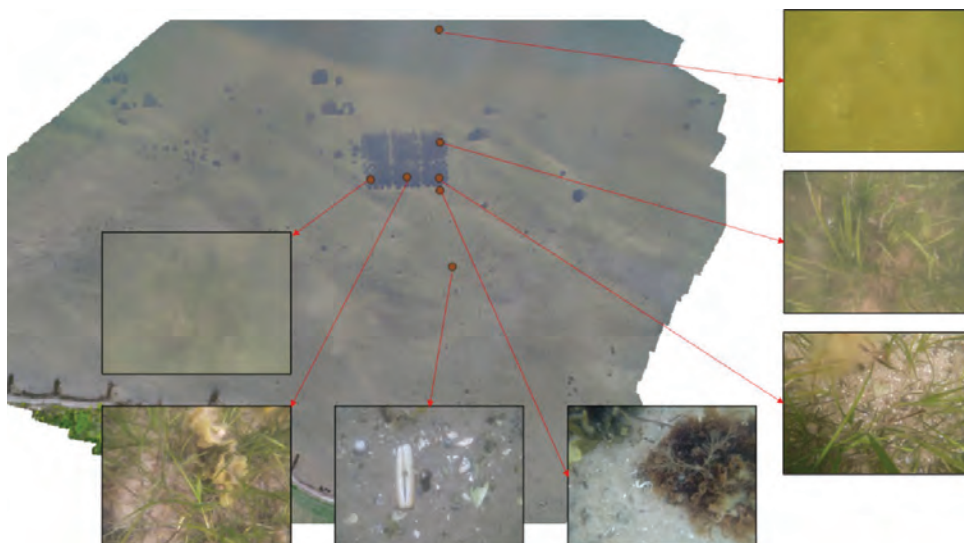


Figure 2.37. Example of drone-truthing images in a large-scale eelgrass transplantation in Horsens Fjord. In the background to the left is the 100 m orthophoto with points and arrows indicating the drone-truthing images.

In Dalby Bay, it was possible to collect data points at increasing depth (0.5-2 m) on bare bottom, on patch-edges, inside patches, in macroalgae aggregations. The environmental conditions on the day were quite adverse with high winds (8-12 m/s), wave action and resulting turbidity. As seen in the above water images (Fig. 2.38), it is difficult to assess the cover type classes even though they are quite visible in the 100 m orthophoto. The quality of the underwater images is though sufficient for determining the cover type and more. In the examples in figure 2.38, these are macroalgae (*Fucus vesiculosus* and filamentous algae) and bare bottom, and young eelgrass shoots with a coverage of app. 60% respectively.

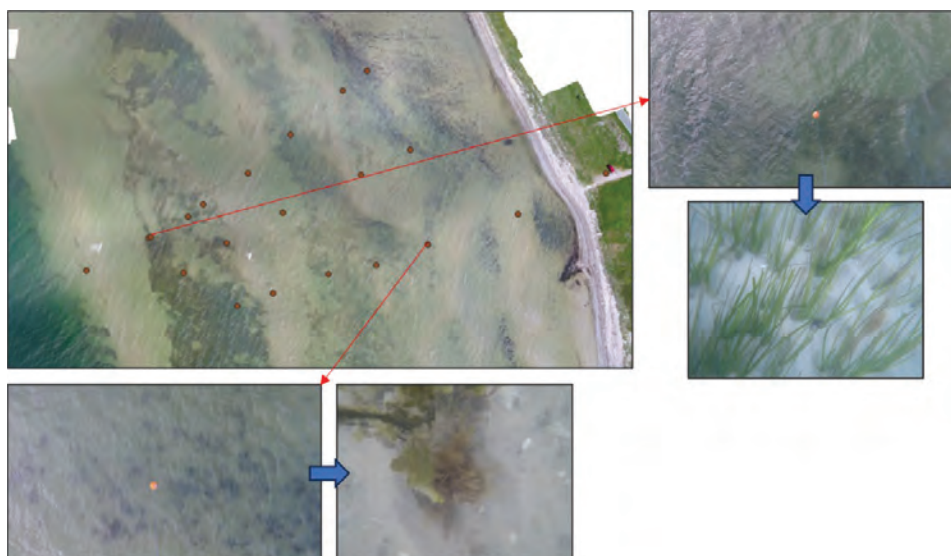


Figure 2.38. Example of drone-truthing images from Dalby Bugt. The map in the left corner shows the placement of the drone-truthing points with arrows indicating the example images. The larger images show the above-water conditions and the smaller show the underwater image-quality.

Conclusion

Using the described setups for UAV-based ground truthing in shallow water coastal habitats is a feasible way of collecting high-quality imagery for inspection, training, and validation. The spool-line system is safe in use and mitigates the gyro- or pendulum effect of a weight hanging below the drone-platform. The depth in which the setup can be used is limited to the length of the line, e.g., if an auxiliary light source and longer line is attached then the bottom conditions can be inspected at any depth. The fixed line setup is equally applicable and secures recordings at a fixed distance to the seabed at the cost of having the full length of nylon line always hanging suspended. The smaller drone-platform in the form of a Phantom 4 has pros and cons in it being cheaper, easier to use, but providing relatively short flight times (15 min). A combination of the setup of the Phantom 4 and the platform of the M600 could therefore be an option. Regarding measuring points, it is recommended to space them equally throughout the area to cover all variability – i.e., organisms and cover types. Depending on the size of the area of interest and the variability anything from 10 to 100 points should be collected.

Table 2.4: Comparison table for groundtruthing methods. * indicates that the setup can be changed to accommodate automated data collection.

	Weather sensitivity	Flight time	Camera distance to substrate	Safety	Automated data collection	Applicability
DJI Phantom 4	Medium	Low (15 min)	Adjustable	medium	Yes	High (low-tech, quick mounting)
DJI M600	Low	High (30 min)	Adjustable	high	No*	Medium

A comparison between platforms and their performance is presented in table 2.4. By adding standard loggers (e.g., HOBO or miniDOT) to the underwater camera, it is possible to determine the depth, temperature, light conditions, conductivity, and oxygen at the specific ground truthing point to further assess the environmental conditions surrounding the eelgrass beds.

Example of detailed technical workflow for groundtruthing using drone platforms

In-field:

- Create point sampling scheme (i.e., Randomly stratified) for training and validation points.
- Start ground truthing camera on either film (60fps, 4K) or image sequence (5-10 sec. intervals) if GoPro is used or use pre-set depth recording if Paralenz is used.
- Fly the drone to your desired point and take pictures with the built-in camera (for georeferencing).
- Lower camera below the surface either by spooling the line or lowering the drone.
- Stay at point for at least 5-10 seconds.
- Measure enough points for the desired application.

In-office:

- Create orthomosaic using Agisoft Metashape.
- Load orthomosaic into QGIS.
- Load images from built-in camera into QGIS using the plugin 'Import geotagged photos' to load images as vector-points as an overlay to the map.
- Save vector-points as a shape file.

- Import orthomosaic to eCognition Developer.
- Import vector-points as thematic layer.
- Make a segmentation.
- Make a classification, creating classes matching the ground-truthing imagery (i.e. eelgrass, bare bottom, algae etc.).
- Select training samples based on the vector-points (this can be automated by importing the labelled points as a TTA-mask).
- Train and classify the model and validate the result based on another set of validation-points.

2.6 Image analysis

A great advantage of UAV-based eelgrass monitoring is the possibility of collecting imagery of very high spatial resolution (mm-cm) covering relatively large areas. When working with data of such high spatial resolution, the object of interest, in this case eelgrass, is usually depicted by multiple pixels, making it impossible for a single pixel alone to reflect the object's characteristics. Therefore, it is advisable to shift the basic analysis unit from individual pixels, like it is the case with traditional pixel-based image analysis, to meaningful image objects. This is done by applying an object-based image analysis (OBIA) approach, where neighboring pixels of similar character are grouped together until they become meaningful objects. By doing so, not only spectral but also spatial, contextual, and texture features as well as hierarchical relationships of complex land-cover classes can be used to aid the classification process. While some tools, such as the image segmentation and feature selection steps, have been developed to overcome doubts related to parameter settings within the additional steps required in the OBIA workflow, the choice of adequate classifier and related hyper-parameter tuning still comes with great uncertainty and is therefore often done following a time-consuming trial and error process. Furthermore, a certain algorithm may result in a high classification accuracy in one monitoring scenario while performing poorly in another. To overcome the insecurity related to the choice of classifier, the performance of five well-established machine learning classifiers: Bayes, Decision Trees (DT), Random Trees (RT), k-Nearest Neighbor (kNN) and Support Vector Machine (SVM) was assessed in an experiment, using different hyper-parameter settings on UAV-derived imagery of a submerged eelgrass bed located in the Limfjorden, Denmark. To cover different potential scenarios of eelgrass monitoring tasks, images obtained from different altitudes (100 m, 30 m) during flights conducted during different environmental conditions (favorable, unfavorable) were used along with training sample sets of different sizes (250, 50). The overall objective of the experiment was to establish, which classifier performs best in a specific combination of environmental conditions, flight altitude, and available training sample set, while the more specific aim was to analyze, how tuning of the classifiers hyper-parameter affects the classification accuracy. A detailed description of the study can be found in Thomasberger et al. (2023) while figure 2.39 roughly illustrates the experiment setup.

The UAV platform used in this experiment was a consumer-grade, low-weight quadcopter of the type DJI Phantom 4 RTK, equipped with a 20MP RGB camera. In total, four flights were conducted in 2021. Two on 7th of April and two on 9th of September. At each date, the first flight was performed at an altitude of 100 m and the second flight at 30 m, resulting in a Ground Sample Distance (GSD) of 27.41 mm and single image dimensions of 150 × 100 m as well as 8.22 mm GSD and single image dimensions of 45 × 30 m, respectively. All images were taken with a nadir-viewing angle (90°). Image front and side overlaps were set to 75% and flight speed to 3.5 m/s during flights at 100 m altitude and 1.5 m/s during flights at 30 m altitude. One pre-programmed flight path was used for each altitude. All flights were planned and executed using the

flight mission planning software UgCS ver. 4.7.685. The flight altitudes and flight dates were chosen in order to represent four different monitoring scenarios: landscape scale studies flown at high-altitude during favorable environmental conditions (100 m_fav), landscape scale studies flown at high-altitude during less-favorable environmental conditions (100 m_unfav), small scale studies flown at low-altitude during favorable environmental conditions (30 m_fav) and small scale studies flown at low-altitude during less-favorable environmental conditions (30 m_unfav). Figure 2.40 gives an impression of the environmental condition during the UAV flights.

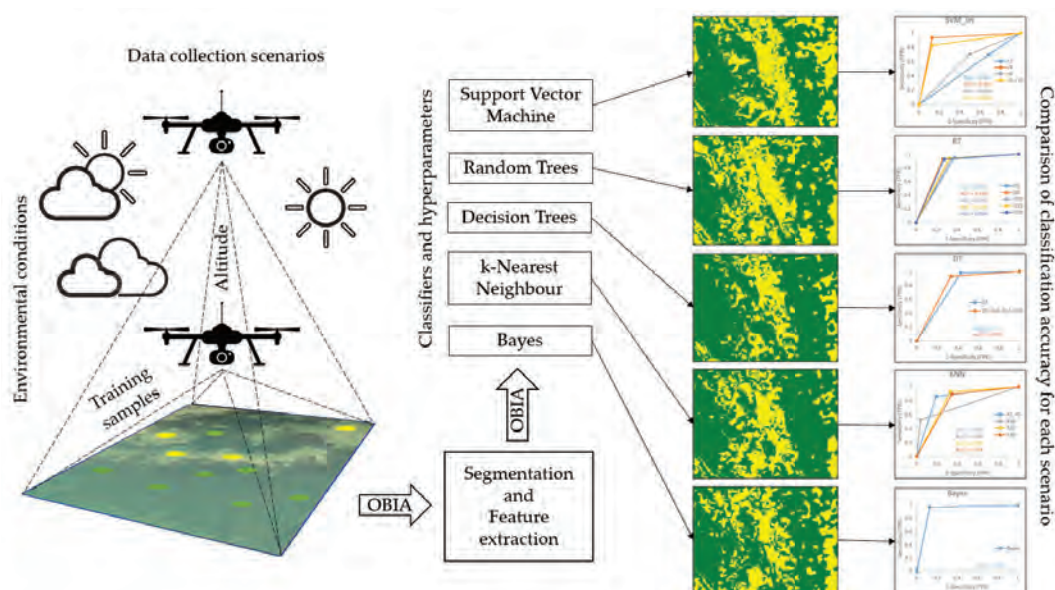


Figure 2.39. Schematic diagram of the conducted classification parameter test (Thomasberger et al., 2023).

One georeferenced orthomosaic was created for each of the four flights by stitching the obtained images using the image processing software Agisoft Metashape Professional ver. 1.7.4. For a detailed description of image segmentation, training and validation sample selection, feature space selection, tested classifiers, hyper-parameter tuning and accuracy assessment, please refer to Thomasberger et al. (2023).

The experiment resulted in 240 classification outputs (Fig. 2.41), which, as expected, confirmed that the performance of the five classifiers depends on image quality and resolution, the size of the available training data set and the algorithm-specific tuning of hyper-parameter. While in general, all classifiers were able to produce high overall accuracies (OAs), each classifier had its strengths and weaknesses in relation to the tested scenarios. The Bayes classifier produced consistently high OAs when images were obtained during favorable conditions, even when the sample set size was small. The DT and RT algorithms performed better when applied to low-altitude images. The kNN classifier was outperformed in all scenarios while still producing high OAs. Interestingly, it also performed better with fewer available training samples on the low-altitude image obtained during unfavorable conditions. The SVM classifier achieved the highest OAs most often and generally performed very well in all scenarios; however, only when the optimal hyper-parameter settings were selected.

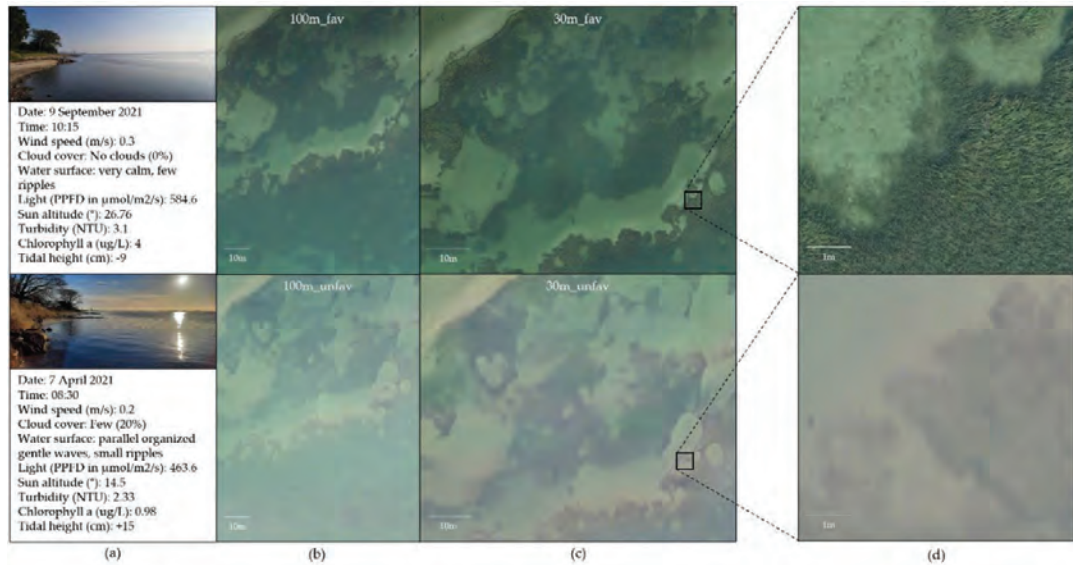


Figure 2.40. Environmental conditions during the UAV flights: a) Environmental parameters and image of the study site during UAV flights; b,c) Extent of the study area and visualization of environmental conditions during UAV flights; d) Level of details visible during different environmental conditions (Thomasberger et al., 2023).

The consistently high OAs (94%) of the Bayes classifier and the simplicity of its application made it a robust choice when images were obtained during favorable conditions, even with few available training samples. When images were obtained at low altitudes and many training samples were available, the DT and RT classifier proved to be a solid choice, as they produced consistently high OAs between 91% and 94%, if the hyper-parameter were optimally set. Very little to no hyper-parameter tuning was necessary when the kNN classifier was applied to images obtained during favorable conditions in combination with large training sample sets, as it produced OAs of >91% in all cases. Greater attention to hyper-parameter settings is needed with the SVM classifier. The high sensitivity of the algorithm requires several trial runs to identify the scenario-dependent optimal combination of hyper-parameter settings. While failing to do so could lead to the lowest performances of all tested classifiers, the highest OAs are likely to be achieved once the optimal hyper-parameter settings are identified (97% OA in this experiment). This process is more time-consuming, and therefore, depending on the respective scenario, at least one of the other tested classifiers can be used to achieve similar high OAs, if time is constrained. If the data collection unavoidably was conducted during unfavorable conditions and at high altitudes, it is important to collect enough training samples as none of the tested classifiers were able to obtain OAs higher than 73% (DT) when few training samples were available. By increasing the number of training samples, the Bayes classifier managed to reach 83% OA and the SVM classifier 84% OA, with optimal hyper-parameter settings.

Classifier	Hyper-parameter	Favourable conditions				Unfavourable conditions			
		100m altitude		30m altitude		100m altitude		30m altitude	
		250 samples	50 samples	250 samples	50 samples	250 samples	50 samples	250 samples	50 samples
		Scenario 1	Scenario 2	Scenario 3	Scenario 4	Scenario 5	Scenario 6	Scenario 7	Scenario 8
Bayes	DT Depth 1	0.94	0.94	0.94	0.94	0.83	0.61	0.90	0.77
	DT Depth 5	0.85	0.84	0.89	0.89	0.72	0.73	0.93	0.92
	DT Depth 10	0.84	0.84	0.93	0.89	0.73	0.70	0.91	0.85
	DT Depth 15	0.84	0.84	0.93	0.89	0.76	0.64	0.91	0.85
	DT Depth 20	0.84	0.84	0.93	0.89	0.76	0.64	0.91	0.85
KNN	KNN K1	0.94	0.84	0.94	0.88	0.80	0.61	0.89	0.90
	KNN K5	0.94	0.84	0.95	0.89	0.78	0.72	0.89	0.90
	KNN K10	0.94	0.82	0.93	0.89	0.75	0.72	0.89	0.90
	KNN K15	0.94	0.84	0.93	0.89	0.75	0.68	0.89	0.90
	KNN K20	0.93	0.81	0.91	0.88	0.74	0.65	0.89	0.90
RT	RT Depth 1	0.85	0.84	0.89	0.90	0.69	0.66	0.86	0.87
	RT Depth 5	0.89	0.87	0.93	0.92	0.78	0.67	0.94	0.85
	RT Depth 10	0.88	0.84	0.94	0.90	0.78	0.62	0.94	0.88
	RT Depth 15	0.88	0.85	0.94	0.89	0.79	0.62	0.94	0.88
	RT Depth 20	0.87	0.86	0.94	0.89	0.79	0.62	0.94	0.82
SVM	SVM linear_C2	0.61	0.57	0.96	0.93	0.78	0.68	0.20	0.91
	SVM linear_C4	0.89	0.91	0.96	0.93	0.43	0.67	0.18	0.91
	SVM linear_C6	0.95	0.64	0.96	0.93	0.42	0.72	0.18	0.88
	SVM linear_C8	0.69	0.84	0.97	0.93	0.68	0.50	0.18	0.91
	SVM linear_C10	0.62	0.84	0.95	0.93	0.80	0.54	0.83	0.91
	SVM rbf_g0.0001_C1	0.84	0.86	0.92	0.87	0.65	0.62	0.93	0.91
	SVM rbf_g0.0001_C1000	0.97	0.90	0.95	0.92	0.84	0.68	0.93	0.93
	SVM rbf_g0.0001_C1000000	0.82	0.89	0.95	0.89	0.56	0.46	0.74	0.93
	SVM rbf_g1_C1	0.66	0.66	0.58	0.57	0.63	0.62	0.77	0.57
	SVM rbf_g1_C1000	0.69	0.66	0.63	0.63	0.71	0.61	0.77	0.57
	SVM rbf_g1_C1000000	0.69	0.66	0.63	0.63	0.71	0.61	0.77	0.57
	SVM rbf_g1000_C1	0.66	0.66	0.57	0.57	0.62	0.62	0.51	0.51
	SVM rbf_g1000_C1000	0.67	0.66	0.58	0.57	0.63	0.62	0.51	0.51
	SVM rbf_g1000_C1000000	0.69	0.66	0.63	0.63	0.71	0.61	0.77	0.57

Figure 2.41. Overall accuracies (OA) of all 240 performed classifications. Color coding ranges from dark green to dark red and resembles the OA from high to low. (Thomasberger et al., 2023).

The high OAs produced by the different tested classifiers showed that OBIA performed on UAV-derived high-resolution imagery has great potential when used for the classification of submerged eelgrasses in temperate regions. The findings of this study are presented in detail in Thomasberger et al. (2023) and will help practitioners to create a solid OBIA workflow and selecting the appropriate classifier including algorithm-related hyper-parameter tuning for achieving the best possible classification accuracy when analyzing UAV-derived images of submerged eelgrass beds. By decreasing uncertainties and time and effort spent on choosing the best classifier set-up, the use of UAV-based techniques in coastal monitoring programs might become more widespread, resulting in more accurate spatial information about existing eelgrass habitats and their growth/decline over time.

2.7 Discussion and recommendations

Standard protocol, equipment, and costs

The results of the conducted field experiments show that accuracy, time, and cost efficiency of eelgrass monitoring campaigns can be improved, if supported by the application of UAV-based monitoring methods. To incorporate UAV-based monitoring into monitoring programs, it is however important to consider and agree on certain aspects that facilitate repeatability, data comparability and easiness of its application. Based on the findings of this project, the following setup is suggested as the most robust, widely applicable, and cost-efficient monitoring solution.

Hardware:

- Light-weight multi-rotor UAV equipped with a high resolution RGB camera and an RTK module (~45.000 DKK)
- Ground truthing setup (~5.500 DKK)

Software:

- Flight mission planning software (~5.800 DKK)
- RTK-service subscription (~6.000 DKK/year)
- Image processing software (~24.000 DKK)
- Image analysis software (~28.000 DKK)
- GIS software

Even though fixed-wing UAVs can cover larger areas due to efficient aerodynamics and long flight times, it is suggested in this context to make use of lightweight (below 25 kg) multi-rotor UAVs due to their lower acquisition cost, heavier payload capacity, vertical take-off and landing capability, easy handling, and their ability to hover in a fixed position over a point of interest. This variety of features allows for an application in a multitude of monitoring missions; from collecting ground truthing data (section 2.5) over low altitude flights for small scale change detection and stressor analysis (section 2.3 and 2.4) to large scale monitoring missions (section 2.1). If the only purpose of a survey campaign is large-scale monitoring, the investment in a fixed wing drone might however pay off. Besides the higher acquisition costs and additional permits needed to operate beyond the visual line of sight, also increased complexity of the flight mission in terms of take-off and landing and maneuverability need to be taken into consideration when using a fixed wing drone. The lightweight multi-rotor UAVs are usually equipped with RGB cameras of very high resolution (>20 MP), allowing for the detection of detail even from high altitudes. High spatial resolution of conventional RGB cameras has proven to be superior to more advanced narrow band but lower resolution multispectral cameras when monitoring submerged eelgrass in the turbid or deep waters of coastal Denmark (section 2.2). Nonetheless, if a multispectral sensor is the sensor of choice, for example when monitoring exposed eelgrass or when working in environments with clear and shallow water during favorable environmental conditions on a smaller scale, the additional sensor can be added to the UAV, in many cases, with a payload mount system for the additional costs of around 42.000 DKK.

It is also recommended to opt for a UAV with an RTK receiver module. This allows for a highly precise positioning of the UAV and increases the spatial accuracy of the obtained data to such an extent, that an overlay and comparison of images taken at different time points becomes possible without the need for labor intensive distribution of ground control points and georectification processes, which often is not a preferred option in aquatic environments. The RTK corrected data enables highly precise mapping and identification of even the smallest changes in eelgrass bed extent, as well as the highly precise collection of ground truthing data, which becomes especially important in environments of scattered growth forms or mixed habitats of, for example eelgrass, macroalgae or blue mussels. The improved spatial accuracy comes, however, at a price. A light-weight multi-rotor UAV without RTK receiver module is usually available from around 15.000 DKK while the same model, equipped with an RTK module, will cost around 45.000 DKK. Additionally, a mobile base station or a subscription to an RTK service is needed to make use of the RTK system. We suggest the latter when working in Denmark, as the country has a good coverage by a network of permanently installed geodetic stations, which the UAV can connect to with an RTK service subscription. This eliminates the need for the installation of a mobile base station (25.000 DKK) in the field before each flight. The costs for a yearly RTK-network subscription are around 6.000 DKK.

For a fast collection of ground truthing data after a survey mission, it is suggested to use a simple underwater camera system as presented in section 2.5, which can be quickly mounted to the same UAV used for the aerial monitoring. Depending on the camera used, such an arrangement will cost around 5.500 DKK. For larger ground truthing missions and the application of additional loggers, it is suggested to invest in a system carried by a larger UAV, as the Matrice 600 used in this project (section 2.5).

It is highly recommended to plan and execute flights using flight mission planning software that allows for easy export and sharing of survey missions. In this way, survey missions can be automated to a great extent and conducted by different people at different times, while being consistent in terms of flight parameters and flight routes. In this project the flight mission planning software UgCS was used. It comes with a cost of 5.800 DKK for a perpetual license, is compatible with many UAV models, and allows for customized payload arrangements. Furthermore, it runs on Windows, MacOS and Ubuntu systems and well as on Android and iOS mobile devices, which is often not the case with other mission planning software.

For aligning and combining single georeferenced images obtained during survey missions to create high-resolution orthomosaics over large areas, advanced photogrammetric software (e.g., Agisoft or Pix4D) is needed, which costs around 24.000 DKK for a perpetual license.

The analysis of the created orthomosaics in this project was done using the eCognition Developer software, which is a development environment for object-based image analysis. Rule sets for automated analysis can be created by making use of a large variety of segmentation and classification algorithms. The results from section 2.6 can be used as a guideline for the image analysis process and a support for the classification algorithm choice. A perpetual license of the eCognition Developer license costs around 28.000 DKK.

To further process, analyze or visualize the produced data in the form of maps, a GIS software is needed. Depending on the user's needs, it can be chosen between open-source solutions (e.g., QGIS) or more advanced software such as ArcGIS, that provides a wider range of features.

Conclusion

By using the set-up arrangement outlined above (excluding ground truthing), it required 6.5 hours of field work plus additional 4 hours of active post-survey processing and analysis time to map eelgrass distribution over 300 ha in an area like Lovns Broad ha, as shown in section 2.1. Due to the limitations of UAV-based monitoring in terms of water depth and turbidity, it was concluded, that, in the case of Lovns Broad, UAV-based monitoring provides accurate classification results until a depth of 2-3 m, while traditional vessel, diver and ROV-based methods are needed to provide reliable data in deeper water. For the case of Lovns Broad, this would mean that UAV-based monitoring conducted by a single person could cover the depth range of 0-3 m (1.800 ha) of the entire broad (Fig. 2.42A), with an effort of 39 hours of field work and additional 5 hours of active post survey processing and analysis time while the depth range of 0-2 m (1.400 ha) (Fig. 2.42B) would require around 30 hours of field work and slightly less post survey processing and analysis times. This would alleviate the monitoring mission by eliminating the need for traditional vessel, diver and ROV-based monitoring in shallow waters, which are the most difficult areas to operate in with a vessel, while providing eelgrass distribution data of significantly higher accuracy and resolution.

Currently, the mapping of eelgrass in Lovns Broad for the EIA's is based on video transects (Fig. 2.42) performed by a boat team of two persons with a towed camera on a sledge, followed by an after processing of one person for video analysis, data interpolation etc. In man hours this method requires approximately 60 hours for data collection and 20 hours for the after processing, in total 80 hours.

Comparing the current method to a scenario where the depth range 0-3 m of the broad are instead mapped by a UAV (44 hours), and the deeper parts (>3 m) are still based on video transect (30 hours), the mapping could be done with slightly fewer resources (6 hours). Of much more importance is however the significantly higher accuracy and resolution of the drone-based mapping compared to the current interpolation of point observations that does not always align with the actual eelgrass distribution (section 4.3).

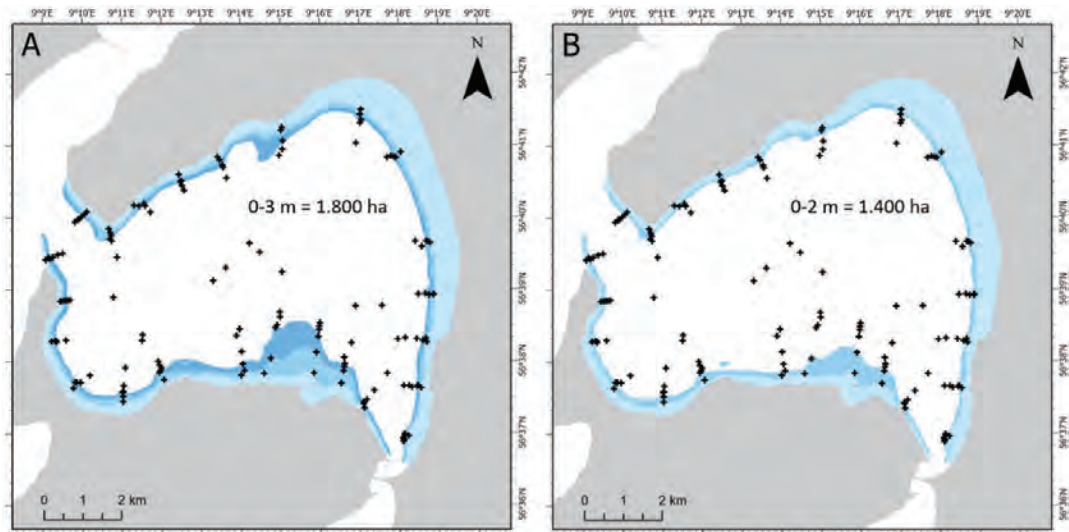


Figure 2.42. Area covering the depth ranges 0-3 m (A) and 0-2 m (B) in Lovns Broad. Crosses represent positions of video transects used in the current EIA's for the area.

3. Underwater Remotely Operated Vehicles (WP2)

3.1 Background

Water-based mapping using airborne drones can, in specific areas with unclear or deep water, potentially fail to provide an accurate mapping. In such problematic areas, there arises a need for other methods of data collection and mapping. Autonomous underwater systems such as Autonomous Underwater Vehicles (AUVs) and Remote Operated Vehicles (ROVs) may present a practical solution for these unique challenges.

The primary objective of this work package was to investigate the feasibility of employing autonomous underwater systems such as AUVs and ROVs in problematic areas where aerial or remote mapping may be ineffective. These systems minimize human operator input while simultaneously enabling high-resolution data collection with GPS. Moreover, the system could serve as a platform for additional environmental data collection if more sensors are integrated onto the platform.

In this work package, we focused on two specific areas: one where seagrass extends into greater depths (Øresund) and one area with low visibility (Limfjorden). We also examined the application of two different underwater drones, the first an AUV on loan from Atlas Maridan, the second a commercial ROV modified for semi-autonomous operation and payload developed at the Technical University of Denmark (DTU).

Øresund

The site location in the Øresund was along the southeastern coast of the island of Saltholm and to the north of the Øresund bridge to Sweden (Fig. 3.1). The target area was along the depth gradients ranging from 4 m to 7 m, with the goal of identifying the depth limit of eelgrass. In this area, the water is primarily brackish Baltic water (measured salinity 8 PSU) and has large meadows of eelgrass at depths less than 4 m. These conditions and the time of year (September 2020) meant that visibility was very good (bottom visible from surface down to 5 m) and there was a good chance for observing eelgrass at depths greater than what is typical (4 m).

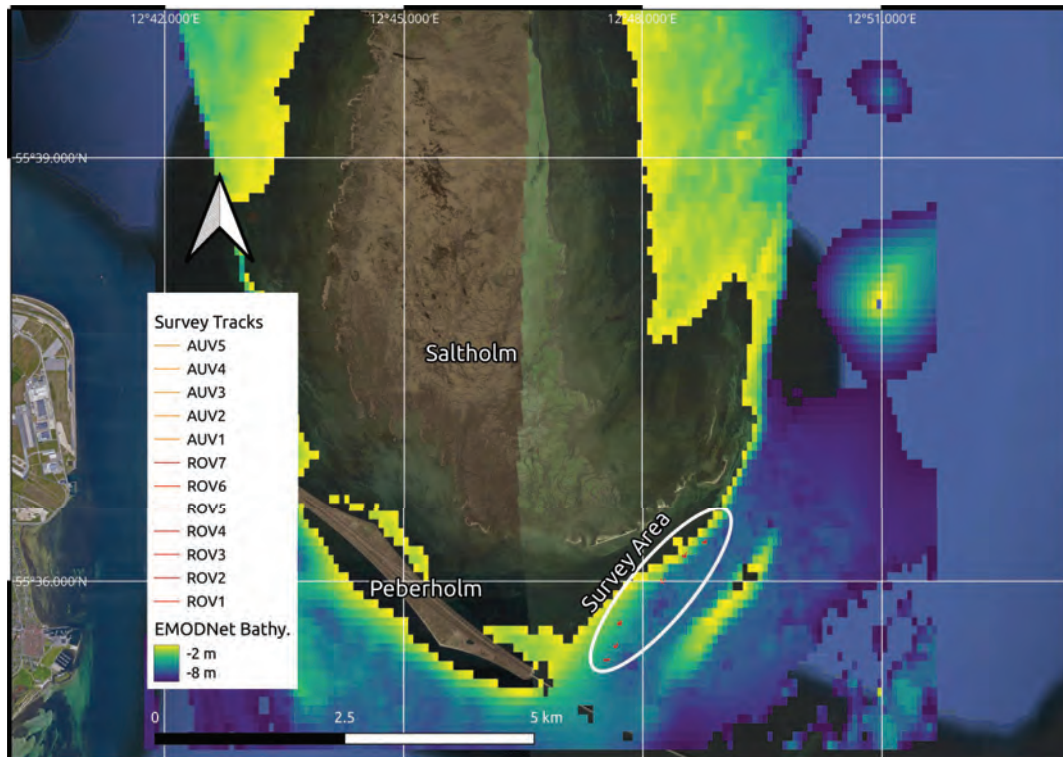


Figure 3.1. The Øresund survey area. Bathymetry data from EMODNet was used to select the survey site, as well as in consultation with colleagues at DTU.

The fieldwork was conducted on 3rd of September 2020 onboard R/V *Havørreden*. The equipment used (Fig. 3.2) was Atlas Maridan's AUV, *Seagull*, and DTU's ROV, *Blue2*. Additionally, a new Ultra Short Base Line (USBL) system, the MicroRanger2 from Sonardyne, was included to track the underwater vehicles via a beacon and receiver system. Additionally, a downward facing GoPro camera was attached to the chassis of *Blue2*.



Figure 3.2. The Seagull AUV and Blue2 ROV aboard R/V Havørreden.

To support mapping activities, video mosaicking software has been developed to produce a composite view of the sea bottom given from a video. The software does not need positioning data to produce the mosaic, but attitude data for the camera can be used to align the orientation of the output in relation to North. The developed software is now available here: <https://github.com/DTUAqua-ObsTek/mosaic-library>.

By taking the North aligned result image and assigning ground control points to the corners based on the maximum and minimum GPS recorded from the USBL, a georeferenced image can be created.

Limfjorden

The Limfjorden site location (Fig. 3.3) was part of a combined aerial, diver and underwater eelgrass survey campaign conducted in May 2021. The goal for this survey was to see if observations of eelgrass could be made by the underwater platforms that could not be obtained via aerial observations (section 2.2).



Figure 3.3. The survey area selected in the Limfjorden was Lovns Broad.

The Limfjorden is subject to high nutrient input from surrounding farmlands, resulting in highly variable underwater visibility conditions. At times the apparent visibility was about 3 m, at other times it was less than 50 cm. Additionally, the area selected was undergoing a bloom of Moon jellyfish (*Aurelia aurita*) at the selected time of year (May 2021). These conditions proved challenging for acquiring useful image surveys of eelgrass.

The fieldwork was conducted on the 18th of May, 2021 onboard R/V *Fjordrejen*. The equipment used (Fig. 3.4) was the ROV *Blue2* equipped with the Waterlinked™ Short Base Line (SBL) acoustic positioning system. Additionally, a downward facing GoPro camera was attached to the chassis of the *Blue2*. The echosounder on the ROV was also working correctly and recorded range to bottom. Additionally, the ROV was run with an autopilot i.e., following a specified course, speed, and depth. The ROV was deployed in front of R/V *Fjordrejen*, which followed the ROV at a close distance (approximately 5 m).



Figure 3.4. The ROV Blue2 with downward facing GoPro attached to battery compartment aboard R/V Fjordrejen.

3.2 Results

3.2.1 Øresund Campaign – deep water

AUV Surveys

The AUV *Seagull* was deployed at 5 locations along the coast of Saltholm and at 4 of these locations it was able to perform bottom photography transects. During the deployments, the USBL beacon was attached to the AUV for tracking of the vehicle underwater. The AUV itself collects the final GPS and heading before diving, then uses dead reckoning to perform the transect. The imaging data provided by Atlas Maridan were geotiff images with georeferencing assigned from the dead reckoning data. The imaging for the four transects are displayed in figures 3.5-3.8.

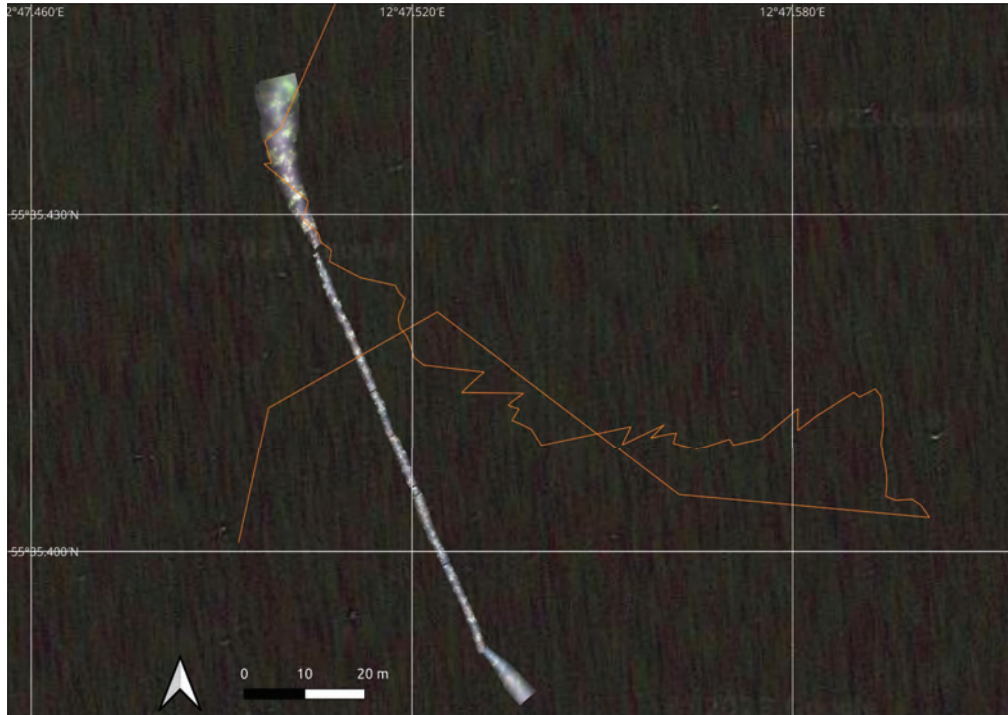


Figure 3.5. AUV Transect 1. The image line runs south-east. The orange line is the recorded USBL trajectory of the AUV.

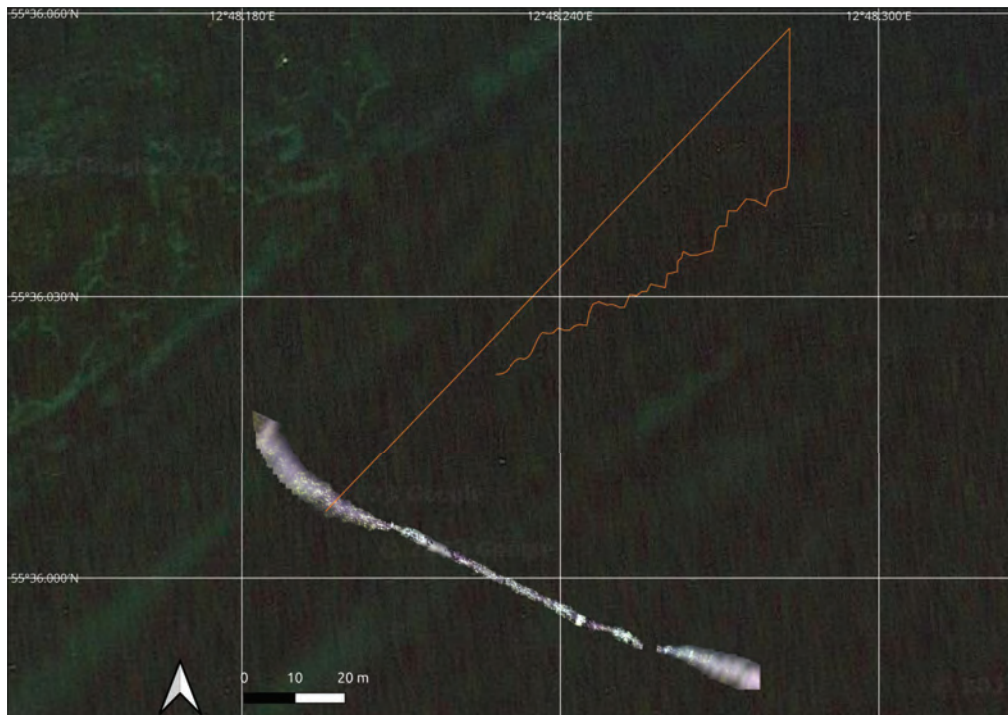


Figure 3.6. AUV Transect 2. The image line runs east by south-east. The orange line is the recorded USBL trajectory of the AUV.

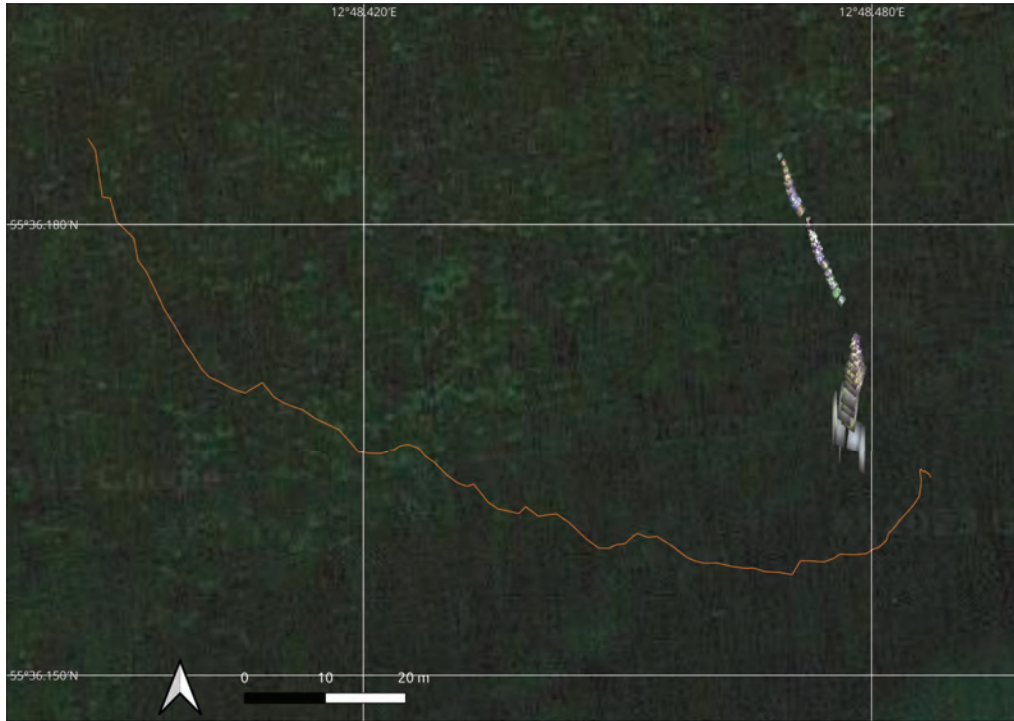


Figure 3.7. AUV Transect 3. The image line runs south. The orange line is the recorded USBL trajectory of the AUV.

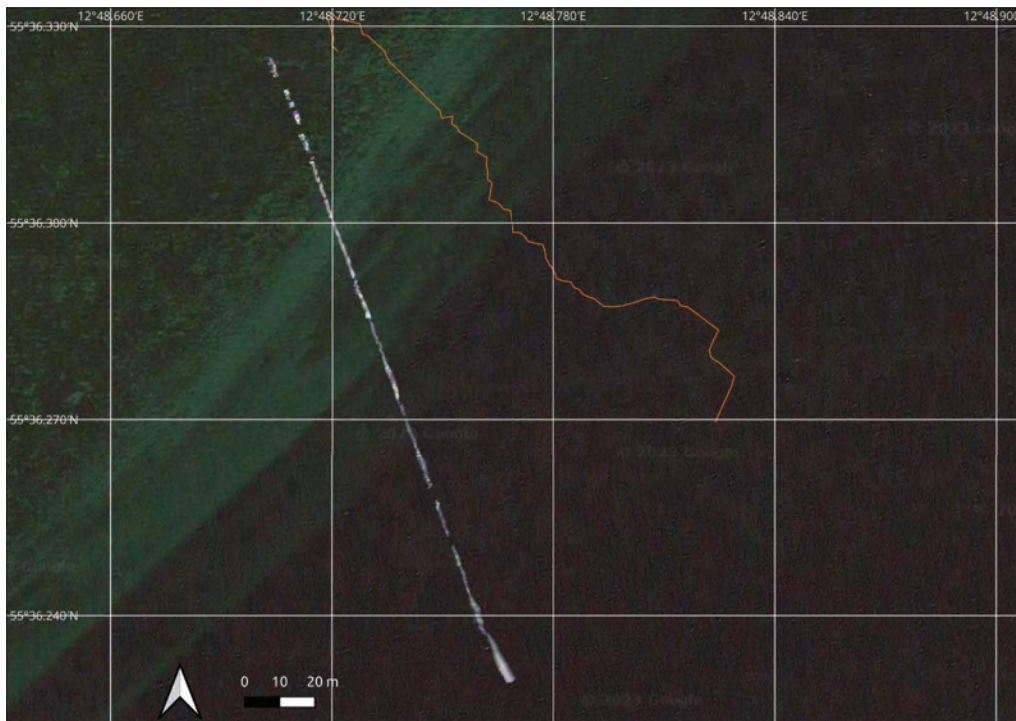


Figure 3.8. AUV Transect 4. The trajectory runs southeast. The orange line is the recorded USBL trajectory.

The quality of the image line can be seen when looking at cut-outs from the full trajectory, figure 3.11 provides some examples for the AUV data.

ROV Imaging

The video mosaicking software was used to generate image mosaics from the collected down-facing GoPros (Fig. 3.9). Since the echosounder was not working correctly during the survey, appropriate georeferencing values for the mosaic could not be made. However, the coinciding GPS log from the USBL shows similarities between the built mosaic and the actual path of the ROV (Fig. 3.9 and 3.10).



Figure 3.9. An example mosaic produced by the software on the downward facing GoPro. The software uses no external information, besides an initial camera orientation to align the image with north.

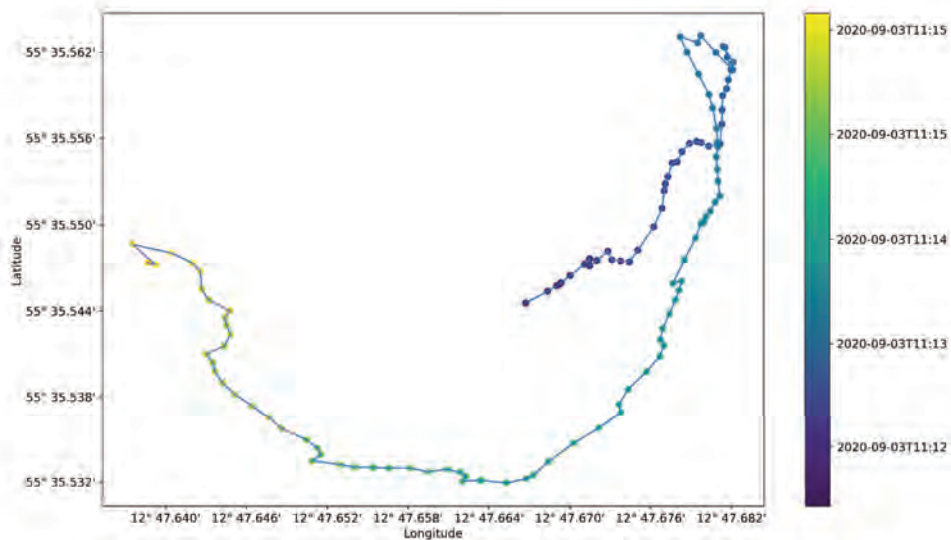


Figure 3.10. The associated GPS for the mosaic in figure 3.9. The loop in the top right corner corresponds to the loop made in the top right corner of the mosaic.

Eelgrass Observations

By inspecting the collected images in a Geographic Information System (GIS) and comparing with the vehicle trajectory and modeled bathymetry, observations of eelgrass can be made (Fig. 3.11).

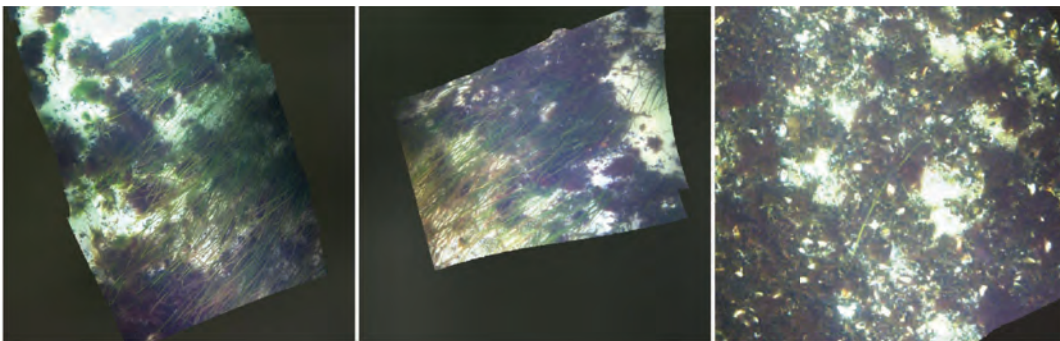


Figure 3.11. Eelgrass observations in AUV data, patches at 2.1 m (left), 4.4 m (middle), and single blades at 5.9 m (right).

3.2.2 The Limfjorden Campaign – turbid water

ROV Imaging

Due to the Moon jelly bloom, mosaicking via feature registration was not possible as the features around the jellies caused scaling issues with the algorithm. Instead, a georeferencing method was used by fusing the ROV's distance to bottom, the calibrated horizontal and vertical field of view of the downfacing camera, and the GPS position provided by the SBL and R/V *Fjordrejen*. The datasets were approximately aligned on a unified time series with the downfacing video, and a mosaic of GeoTiff images was created. Due to the presence of noise in the SBL

position dataset, the GPS from R/V *Fjordrejen* was used with a time-offset applied to the data. The resulting mosaic is provided in figure 3.12.

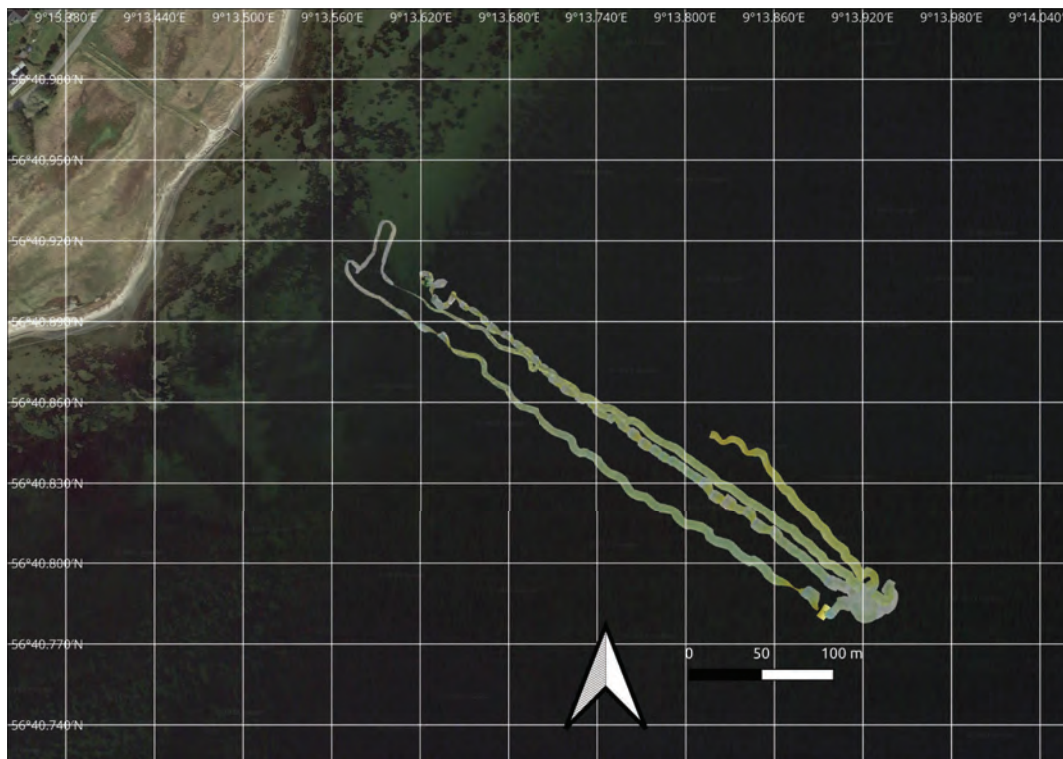


Figure 3.12. ROV imaging performed in the Limfjorden, Lovns Broad.

Eelgrass Observations

The general area surveyed by the ROV was mostly mussel beds. The ROV's distance to the bottom was too far in the deeper regions, reducing the visibility of the bottom. However, in the shallow regions the visibility was good, and observations of very sparse eelgrass were made in about 1.7 m water depth (Fig. 3.13).

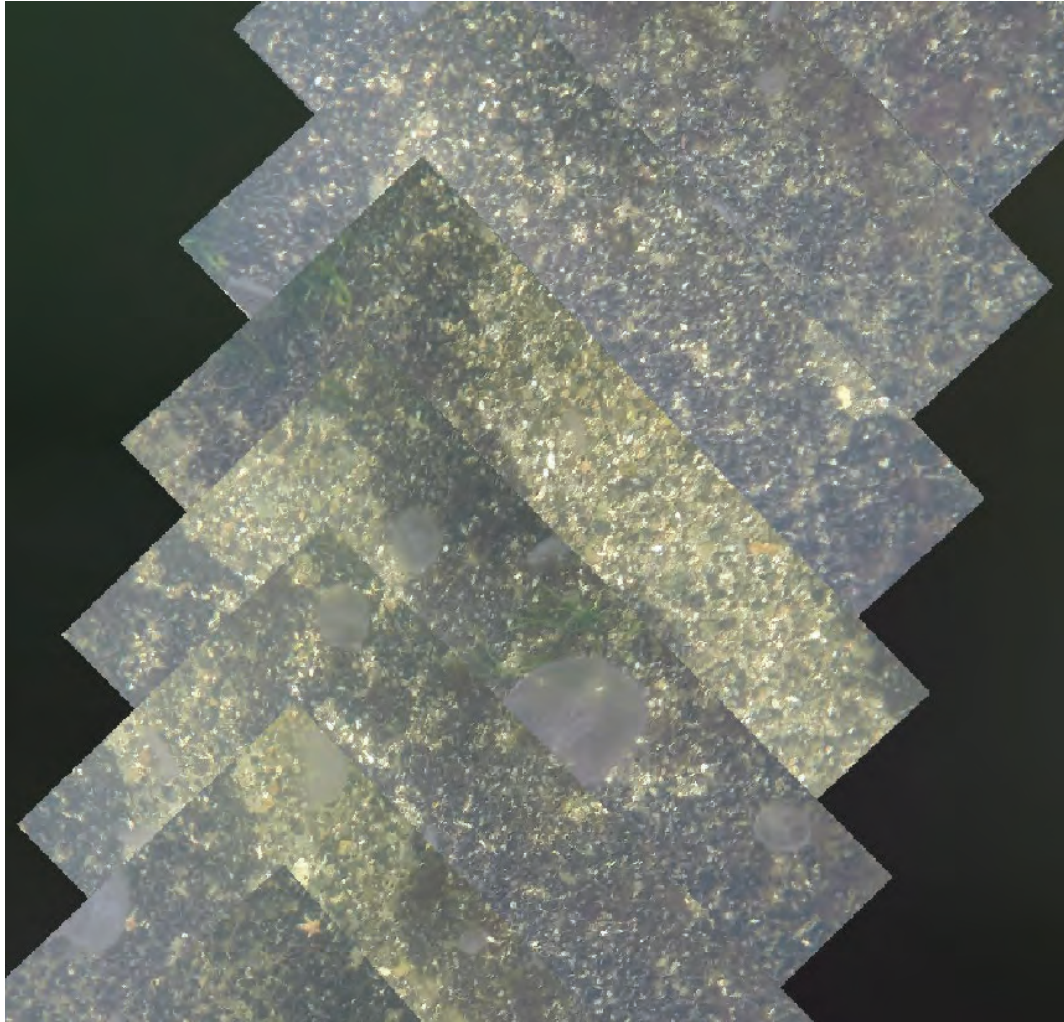


Figure 3.13. Eelgrass observation made at approximately 1.7 m water depth.

3.2.3 Underwater Vehicle Survey Effort Analysis

Survey area and resolution from the GeoTiff images were estimated using the Geospatial Data Abstraction Library (GDAL). These metrics were compared with the approximate duration between deployment time and recovery time extracted from the GPS data logs (see Table 3.1).

The resolution and area covered is determined by the distance of the vehicle to the bottom. The AUV has better terrain following capabilities than the ROV, so the resolution is more consistent across the entire transect.

Both vehicles require a small boat for deployment, surveying and retrieval operations, and additional setup time must be allocated for calibration of acoustic positioning equipment if the system is intended to be portable and transferable across multiple boats.

The time taken to process the collected data into a GIS compatible format should also be considered. The AUV data comes in image/Keyhole Markup Language (KML) file pairs, which can be immediately viewed in Google Earth™. However, the files must be further processed into a

unified GeoTiff image if the unique area coverage is to be estimated. Excluding the development time for the software programs used (primarily GDAL), the rendering of the image/KML pairs into a GeoTiff file is roughly 5 s per pair. Calculating the area coverage and other statistics can then be easily made by any GIS platform.

Table 3.1. Survey statistics extracted from the AUV surveys in the Øresund and the ROV survey in the Limfjorden. Coverage is calculated by the hour.

Transect Name	Resolution (mm ² / pixel)	Area (m ²)	Duration (h)	Survey Effort (m ² / h)
AUV Track 1	2.25	272	0.22	1234
AUV Track 2	2.25	366	0.05	7088
AUV Track 3	0.24	59	0.05	1083
AUV Track 4	6.25	274	0.59	458
ROV Track 8	6.72	8446	1.17	7221

On the other hand, the ROV data had to have specific methods developed to obtain the GeoTiff files for geospatial analysis. The pipeline, which includes: 1) frame extraction from the video, 2) alignment of the ROV data with the GoPro data, 3) GeoTiff image generation from position, camera orientation, distance to bottom, and calibrated camera intrinsic parameters, and 4) GeoTiff mosaicking, takes about 1 hour per hour of video footage obtained.

3.3 Discussion

Our research indicated that unoccupied and autonomous underwater systems offer a viable alternative for mapping in areas with unclear or deep water where aerial methods may be less effective (section 2.2). The resolution of the output GeoTiff images is very high: approximately 2.5 mm/pixel for the AUV and ROV (averaged across the transects). Eelgrass was observed in all three datasets, and within expected depths for the areas (<6 m for Øresund and <2 m for the Limfjorden). The AUV showed promise in giving stable control at low altitude and relatively long transects in comparison to the ROV but was subject to drift and is difficult to find and recover. On the other hand, the ROV provided immediate video quality feedback and was easy to control but is limited in range by the tether and is a less stable camera platform; especially when trying to maintain a constant distance to the bottom.

The biggest challenge to underwater bottom imaging and mapping is the precision and accuracy of the positioning system. As can be seen in figures 3.5-3.8, the recorded USBL trajectory for the AUV is significantly different from what the AUV's dead reckoning system estimated. The AUV simply uses the last known GPS it had before diving, and the first GPS it receives when surfacing and interpolates a trajectory between these two points based on a first order model relating propeller RPM to forward speed. This means only the start and end of the AUV transects can be trusted, as the model does not account for drift due to wave and current forces. This is generally shown in the USBL data as a curving line, however the absolute error between the USBL position and the AUV GPS position also shows that the USBL is not reporting an accurate position. This is due to the shallow water condition the USBL was deployed in, and the

absence of appropriate calibration and installation procedures that are necessary for accurate positioning. Similarly, the SBL positioning system also produced noisy data that was difficult to use as georeferencing data.

4. Improving existing GIS models for eelgrass distribution (WP3)

SDU and DTU Aqua have over the years developed a GIS tool to describe the distribution and spreading potential of eelgrass in different Danish water bodies (Lovns Broad, Løgstør Broad, Nissum Broad, Lillebælt, Odense Fjord, Roskilde Fjord, and Horsens Fjord). The GIS tool is based on nine environmental parameters (table 4.1) that are decisive for the reestablishment of eelgrass, such as sediment stability, light and oxygen conditions, as well as the presence of macroalgae, lugworms and already existing eelgrass (e.g. Canal-Vergés et al. 2016, Flindt et al. 2016). An individual raster layer in the GIS tool represents each parameter. Some layers are based on model output (MIKE 3) from advanced simulations of hydrodynamic forcing with current and wave dynamics (Kuusemäe et al. 2016), while other layers are based on field observations. The input data is classified into five ranges, according to how much a specific parameter affects the eelgrass establishment potential: 1) Optimal, 2) Good, 3) Threshold, 4) Poor and 5) Very poor. Afterwards a weighed overlay function is performed, resulting in an accumulated value for stress impact on the eelgrass recovery process and hence, the distribution potential of the eelgrass.

Table 4.1. Predictive parameters included in the eelgrass GIS tool with associated thresholds for eelgrass recovery potential as proposed by Flindt et al. (2016). Twc: Shear stress. LOI: Loss of ignition.

Parameter (layer)	Unit	Recovery				
		Very poor	Poor	Threshold	Good	Optimal
T_{wc}	$N m^{-2}$	>1	0.7-1.0	0.5-0.7	0.2-0.5	0.0-0.2
Sediment LOI	%	>10	5-10	2-5	1-2	0-1
Resuspension	Frequency	> daily	daily	monthly	Biannual	< Biannual
Benthic light	$\mu E m^{-2} s^{-1}$	0-100	100-200	200-300	300-400	> 400
O ₂ limitation	Period	3 Week ⁻¹	2 Week ⁻¹	Weekly	Monthly	< Monthly
Opp. Macroalgae	$g C m^{-2}$	>26	13	10	6	< 2
Non-opp. Macroalgae	$g C m^{-2}$	>26	13	10	6	< 2
Lugworm	$g WW m^{-2}$	>50	40	25	10	<9
Eelgrass	$g C m^{-2}$	< 3	< 7	< 14	< 28	> 28

In this work package we have been looking into various aspects of optimization of the GIS tool currently used for annual EIA's in Natura 200 areas of the Limfjorden. WP3 dealt with the following three lines of work that all contributes to a better implementation of the GIS tool in the future:

- 1) The improvement of the interpolation method used to create the input layers for the GIS tool that are based on either point specific field observations (eelgrass) (section 4.1.1) or model derived layers originating from DHI models (section 4.1.2),
- 2) Further improvement of model derived layers with emphasis on the two of the most decisive input layers light and shear stress (section 4.2), and
- 3) Testing the possibility of introducing an UAV derived eelgrass distribution layer to the GIS tool as a more precise and cost-efficient alternative to the interpolation-based layer (section 4.3)

4.1 Improved interpolation of data into model layers

4.1.1 Field collected data

The layers representing the spatial distribution of eelgrass, opportunistic macroalgae and non-opportunistic macroalgae used in the GIS tool are based on point observations obtained from video transects. The “spline with barriers” interpolation method (using depth contours as barriers) has been used to create continuous areas from these discrete point observations. The method shows good results in areas with homogeneous vegetation distribution (continuous beds) and a simple bathymetry. The accuracy of the method however decreases in dynamic areas with heterogeneous vegetation patterns and a complex bathymetry such as the Limfjorden. This is due to the reason that a) interpolation of distant point observations fail to account for abrupt changes and changes occurring over short distance such as scattered patches of submerged aquatic vegetation and b) neighboring points will not influence each other if they are separated by a bathymetry line, even if they have the same depth value.

As these conditions are very often applicable in the areas where the GIS model is implemented as a part of EIA's of dredge fishing, an aim of this project has been to develop a new and more suitable interpolation method for transforming point data into layers of the model.

The issue of neighboring points not influencing each other if they are separated by a bathymetry line, can be diminished by performing an additional ‘inverse distance weighted’ (IDW) interpolation in a loop for each depth interval using only the two nearest points. Figure 4.1 shows an example of different interpolation results using only the ‘spline with barrier’ method and the ‘spline with barrier’ method with the additional IDW interpolation of eelgrass point observations.

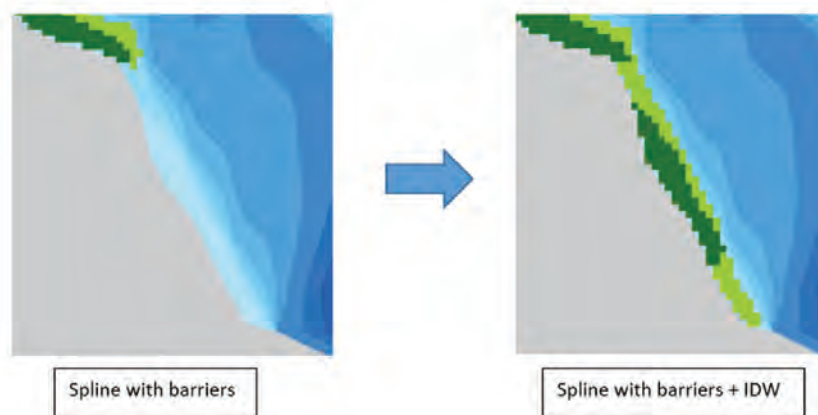


Figure 4.1. Example of interpolation of eelgrass using Spline with barriers (left) vs. Spline with barriers + IDW interpolation (right).

The described method of combined spline with barriers and IDW, was performed using different build-in interpolation tools (e.g. Spatial Analyst IDW interpolation tools in ArcGIS, QGIS and the MapInfo IDW Interpolator) which however, appeared quite labor intensive and still lacked accuracy due to the lack of options to adjust specific parameters. Only the ‘stats’ package in R in combination with a weighting factor (idp) of 2.5, performed separately for each 1-meter depth intervals showed better results. This was achieved using a 30x30 m bathymetry raster and, for

each depth interval, creating a new raster object within that depth interval. The IDW interpolation can then be applied to this new raster, and when all depth intervals are estimated, the raster layers are merged into one.

4.1.2 Model derived data layers

Other predictor variables included in the GIS tool are based on a combination of empirical data derived from the national marine survey program, and data derived from hydrodynamic and biogeochemical modelling. The latter was based on models developed by DHI for the Danish Ministry of Environment for managing the water framework directive (e.g. Erichsen and Birkeland 2019, 2020).

In this section we analyse the potential of improving the data layers representing benthic light and shear stress derived from modelling results by improving the methods of interpolation. Both variables are depth dependent and critical for calculating the eelgrass recovery potential, in particular along coastal areas such as Danish fjords where depth gradients can be steep and where the predicted eelgrass recovery may be limited to a relatively narrow stretch along the coastline. We use the Limfjorden as an example on data layers derived from model simulations that can be improved using interpolation techniques. In the Limfjorden, the eelgrass GIS tool has previously been applied in three of the Natura 2000 areas, Nisum Broad, Løgstør Broad and Lovns Broad (Fig. 4.2).

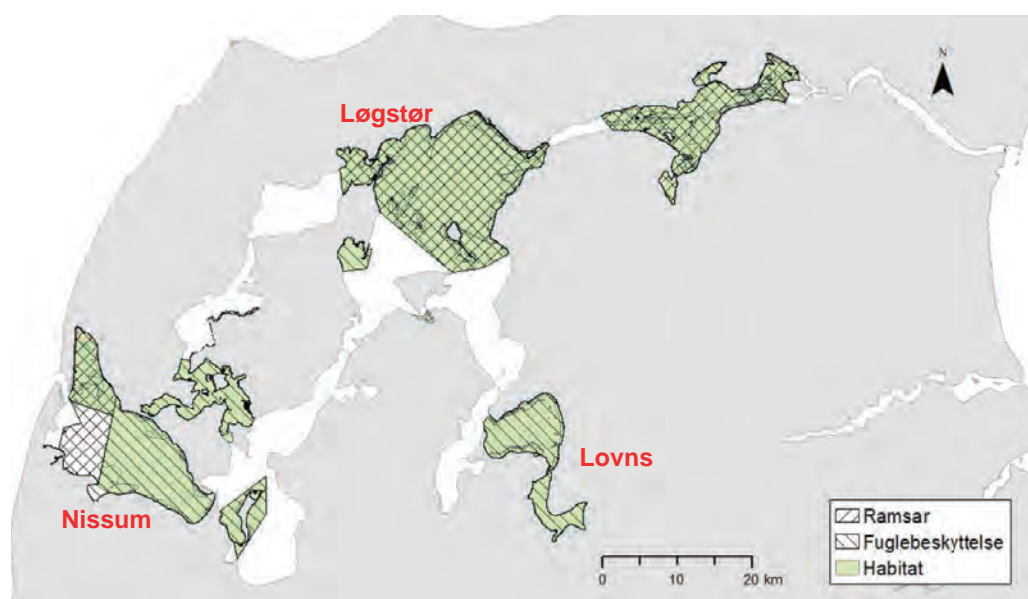


Figure 4.2. Location of Natura 2000 areas in Limfjorden including Nisum Broad, Løgstør Broad and Lovns Broad.

Originally, data on benthic light and shear stress used in Flindt et al. (2016) were acquired from DHI as extracted values from the hydrodynamic and wave models (shear stress) and from the biogeochemical model (benthic light) both developed for Limfjorden by DHI for the Danish EPA (Erichsen and Birkeland 2019, 2020). Data extraction was done from a previous version for the Limfjorden model where the grid resolution in some parts of the Limfjorden since then has been improved.

In papers by Flindt et al. (2016) and Canal-Vergés et al. (2016), light at seabed extracted from the MIKE models in Odense Fjord and the Limfjorden respectively are shown as photosynthetic active radiation (PAR) in the unit $\mu\text{E}/\text{m}^2/\text{s}$. The unit represents the average light at the seabed in the period from 1st of April to 31st of October and for the seasonal photoperiod (PC: Paula Canal-Vergés May 2022). For simplicity here we define the seasonal photoperiod as the time between sunrise and sundown, despite other definitions exist. Data originally provided by DHI for benthic light was in the unit E/m^2 representing the accumulated benthic light in the same period. For shear stress the unit was N/m^2 representing the average for the same period.

The following interpolation issue has been identified: Previous applications of benthic light and shear stress data extracted from the MIKE models have been applied without further processing. This means that the triangular representation of the computational grid in the modelling domain is maintained in the application of the data in the original eelgrass tool and in the presentation of maps in the published papers and reports (example in fig. 4.3). Extracted data from MIKE should instead be processed (interpolated) before the data is applied in the eelgrass GIS tool. Using the “raw” triangular grid from MIKE introduces an unintentional spatial inaccuracy. In this report section, interpolation routines are tested and discussed.

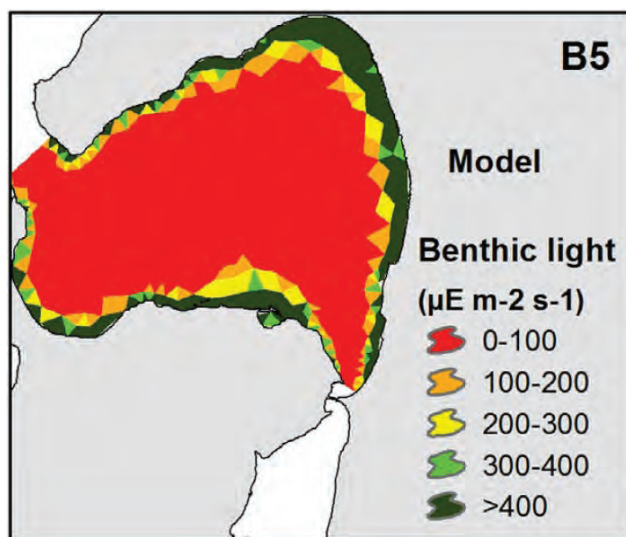


Figure 4.3. Example from Canal-Vergés et al. (2016) where data represent simulated benthic light extracted from a biogeochemical model in Lovns Broad, Limfjorden.

Interpolation of data extracted from the MIKE Model is necessary since each triangle element in the model grid varies in size and represents a mean value within the areal extent of each triangle. We tested 4 different methods for interpolation including Universal Kriging, Ordinary Kriging, Inverse Distance Weighting (IDW) and Spline. The 4 different methods for interpolation of simulated shear stress are shown as maps of Nissum Broad (Fig. 4.4), and as profile graphs extracted from a selected transect (Fig. 4.5). Additional comparisons between extracted data of shear stress and benthic light with interpolated values for other sections of the Limfjorden as examples are shown in figures 4.6 and 4.7.

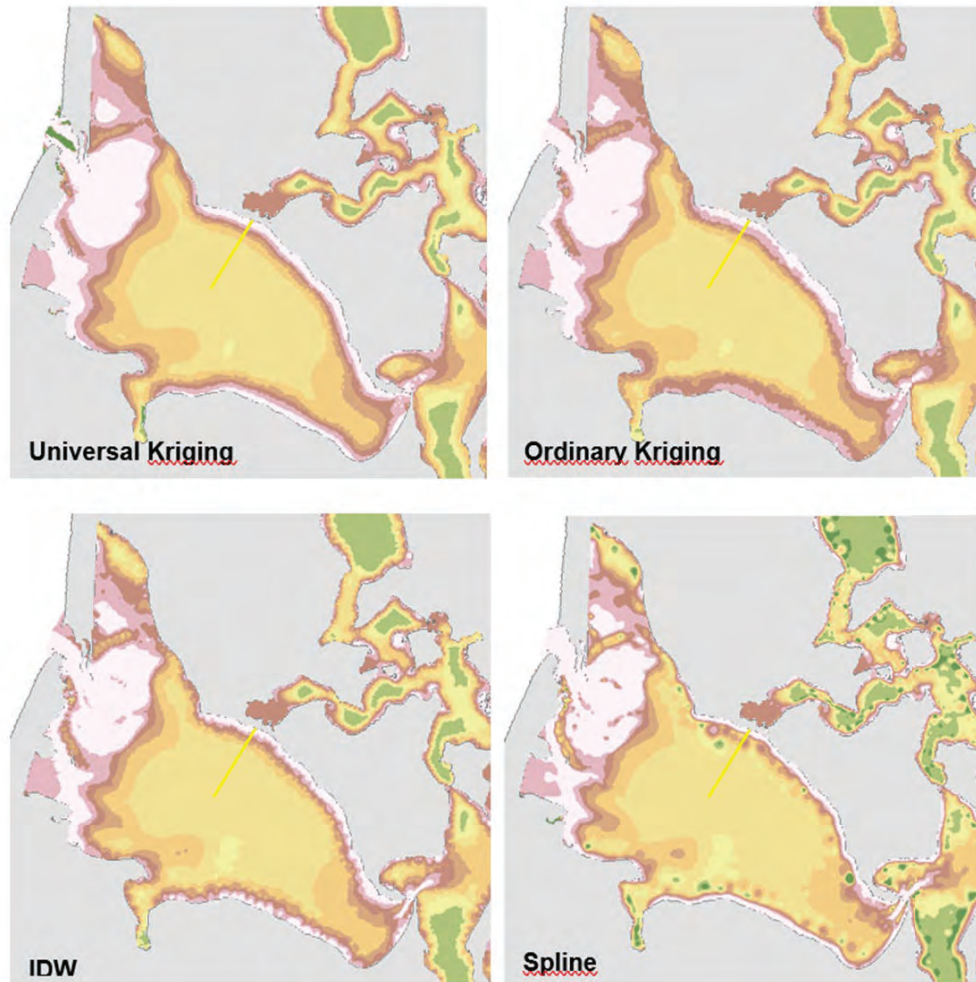


Figure 4.4. Example of interpolation of simulated shear stress in Nissum Broad using 4 different interpolation methods: Universal Kriging, Ordinary Kriging, Inverse Distance Weighting (IDW) and Spline. Yellow line indicates a selected transect for value extractions shown in figure 4.5.

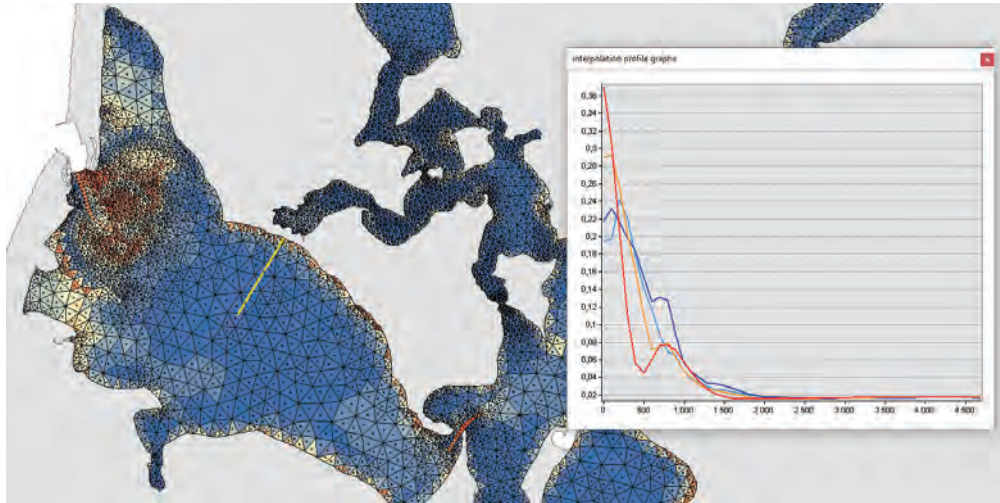


Figure 4.5. Shear stress extracted from the triangular flexible mesh in the MIKE model. Colors represent shear stress. Dots represent triangle centroids. Yellow line indicates where profiles from different interpolation routines are extracted as shown in graph: lightblue=Universal Kriging. Dark-blue=Ordinary Kriging. Orange= Inverse Distance Weighting (IDW). Red=Spline.

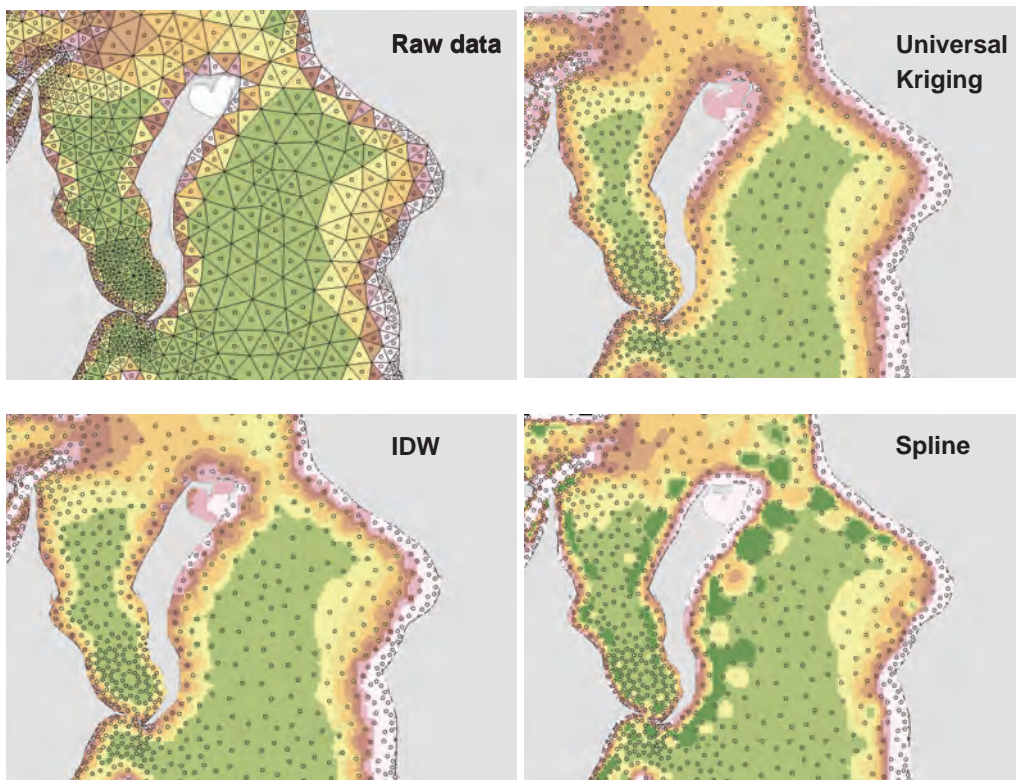


Figure 4.6. Example of different interpolation methods applied to a central section of the Limfjorden. "Raw data" refers to raw data extracted from the MIKE model before interpolation. The 3 interpolation methods include "universal kriging", IDW and Spline. The colour scale is the same in all plots.

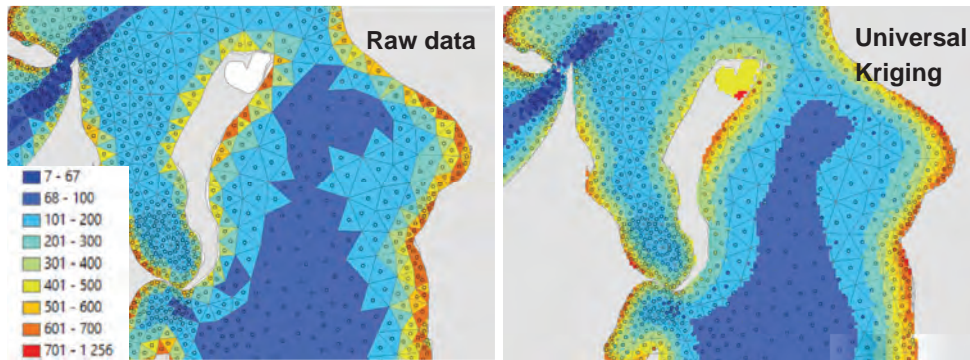


Figure 4.7. Comparison of extracted raw data of light at seabed extracted from the MIKE model with interpolated values using Universal Kriging.

4.2 Further improvement of model layers – light and shear stress

Both benthic light and shear stress are depth dependent and critical for calculating the eelgrass establishment potential, in particular along coastal areas such as Danish fjords where depth gradients can be steep and where the predicted eelgrass recovery may be limited to a relatively narrow stretch along the coastline. Therefore, besides the interpolation method covered in the previous section, this section will cover further identified issues related to the model layers light and shear stress. These are:

Model bathymetry issues - For benthic light and shear stress to be optimally interpreted (and interpolated) along often narrow zones of the coastline where prime eelgrass habitats are located, bathymetry data in MIKE need to be representative. However, comparison of the interpolated bathymetry values from MIKE with the depth data used by DTU Aqua (in a 100x100m resolution) reveals that the bathymetry representation in MIKE along the coast are biased.

Light parameter issue - The use of simulated light at the seabed originally acquired from DHI's biogeochemical model is sensitive to the depth issues described above. If bathymetry data is biased along coastal depth gradients, this is directly affecting the simulated light at the seabed and the error may be unacceptable high when applied in the eelgrass GIS tool. Instead, simulated KD is proposed as a depth independent variable. Based on KD values, benthic light can be re-calculated using more accurate depth data.

KD calibration issues – When comparing the simulated KD values with corresponding measured KD values at NOVANA station in Nissum Broad, Løgstør Broad and in Skive Fjord (the closest NOVANA station to Lovns Broad), respectively, it appears that the simulated values in particular in Løgstør Broad and Skive Fjord are biased relative to the measured values during the growth season April to October. To compensate for this bias, adjustment factors reflecting the mean deviation between simulated and measured KD for the period April to October 2010-2016, are applied to adjust the simulated KD values for each of the three basins Nissum, Løgstør and Lovns Broad. These adjustments assume that the horizontal variation in mean simulated KD values within each basin, despite the observed bias, still represent the relative horizontal variations of the actual KD.

The three identified issues above will be covered in the following.

Bathymetry representation in MIKE

The Bathymetry data in the MIKE model for the Limfjorden was extracted and interpolated using universal kriging and compared with the depth data used by DTU Aqua available in a 100x100 m resolution (Fig. 4.8). The bathymetry data set used by DTU Aqua is a composite data set used by the former counties surrounding the Limfjorden. The MIKE bathymetry is by definition more simplified since the computational grid in MIKE has coarser resolution than the original depth data. The comparison of the interpolated bathymetry data from MIKE (methodology covered in section 4.1.2) with the DTU Aqua data set shows a distinct deviation in particular along the coastal depth gradient covering a zone of up to 1 km where differences in depths are more than 1 m (in some cases up to several meters) (Fig. 4.9).

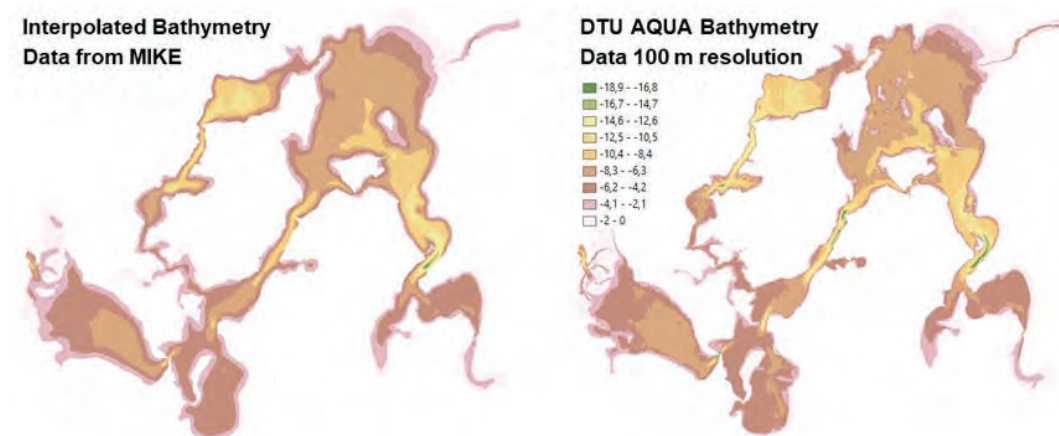


Figure 4.8. Left: Bathymetry data extracted from the MIKE Model for the Limfjorden and interpolated using Universal Kriging. Right: Bathymetry data used by DTU Aqua with a spatial resolution of 100 m

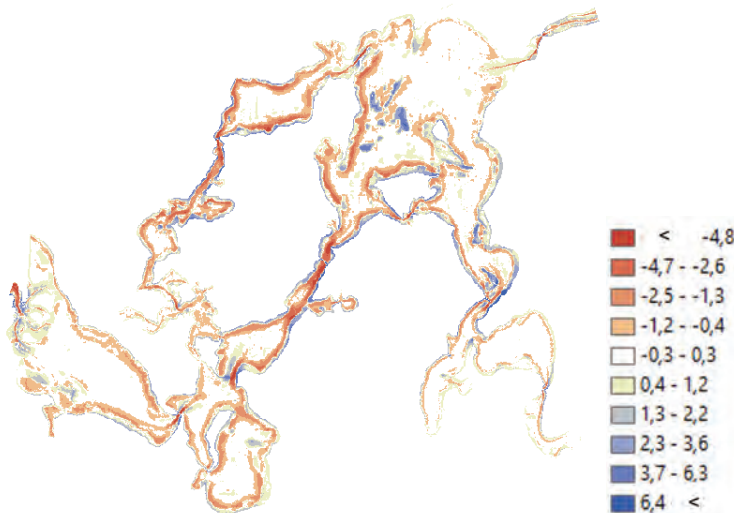


Figure 4.9. Calculated differences between bathymetry extracted from the MIKE model for the Limfjorden and interpolated, and the bathymetry data used by DTU Aqua.

Both simulated benthic light and simulated shear stress are depth dependent variables, which means that the inaccuracies or bias in depth representation in MIKE can be critical for these variables if they are used e.g., to predict the spatial extension of suitable habitat for eelgrass

along narrow stretches of coastlines. The implication for benthic light means that a more appropriate variable extracted from the MIKE model would be the simulated light attenuation coefficient KD (or alternatively KD converted from the derived variable Secchi depth) which are broadly independent of the water depth. By using KD instead, benthic light can be calculated based on more accurate depth data. This approach is demonstrated in the coming section.

For shear stress, this is however more complicated since this variable is highly depth dependent. In addition to depth, the wind (and wave) exposure of the coastal or shallow areas is a contributing factor including the direction of wind/waves and the length of the stretches of open water the wind/waves can act/develop before encountering a potential eelgrass habitat. To correct the bias introduced on shear stress due to in-accurate bathymetry representation in MIKE we therefore propose to re-run the calculation of current and wave induced shear stress for the Danish marine coastal waters using input from the calibrated hydrodynamic models and wave models developed for the Danish Environmental Protection agency for management of the WFD and a more accurate bathymetry representation. However, this task is beyond the scope of the current study.

KD Calibration evaluation

The measurements and simulated results of the light attenuation (KD) from the MIKE model for the Limfjorden for the period 2002-2016 can be accessed via <https://rbmp2021-2027.dhigroup.com/>. For Nissum and Løgstør, KD measurements exist for NOVANA stations Nissum Broad (VIB3702-0001) and Løgstør Broad (VIB3708-0001). For Lovns Broad the closest station is Skive Fjord (VIB3727-0001) (Fig. 4.10). Comparisons between measurements and simulation results are shown in figure 4.11.



Figure 4.10. Locations of NOVANA stations from which KD measurements were used to compare to simulated results.

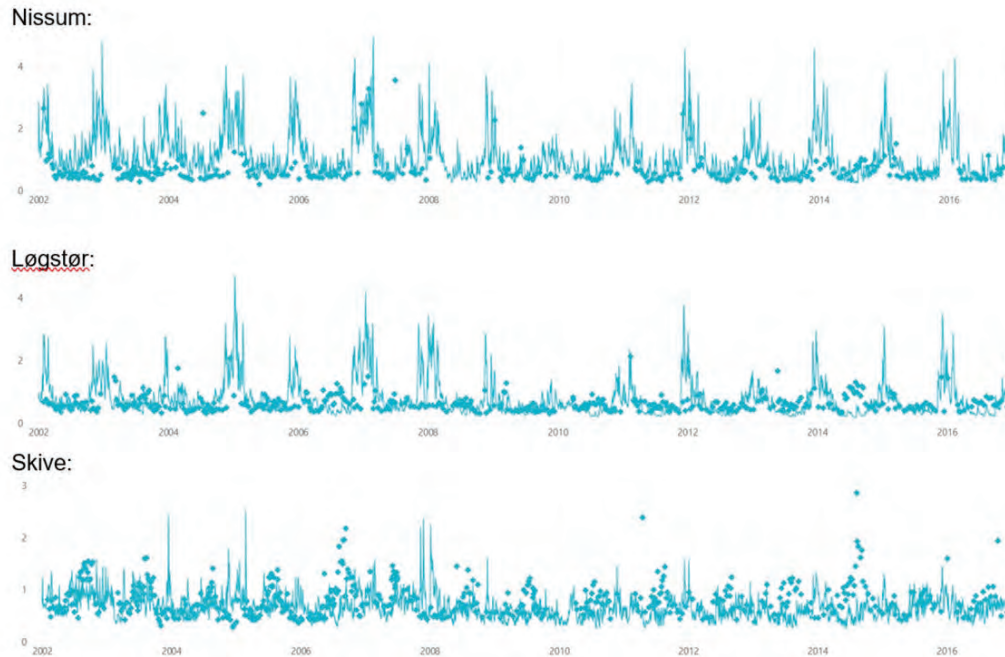


Figure 4.11. Comparisons between measured and simulated light attenuation coefficients (KD) for three NOVANA stations in Nissum, Løgstør and Skive Broad (Fig. 4.10).

In general, for Løgstør Broad and Skive Fjord and for the period 2010-2016 during April to October, measured KD values are ca. 50% higher than simulated values (Fig. 4.12). For Nissum Broad the KD values are similar, model values being only slightly higher. Winter values are not considered here since they are not used in the eelgrass GIS tool. The measured KD values for April to October extracted for the three stations are shown in figure 4.12. There are no clear indication of changes or developments in KD since 2000.

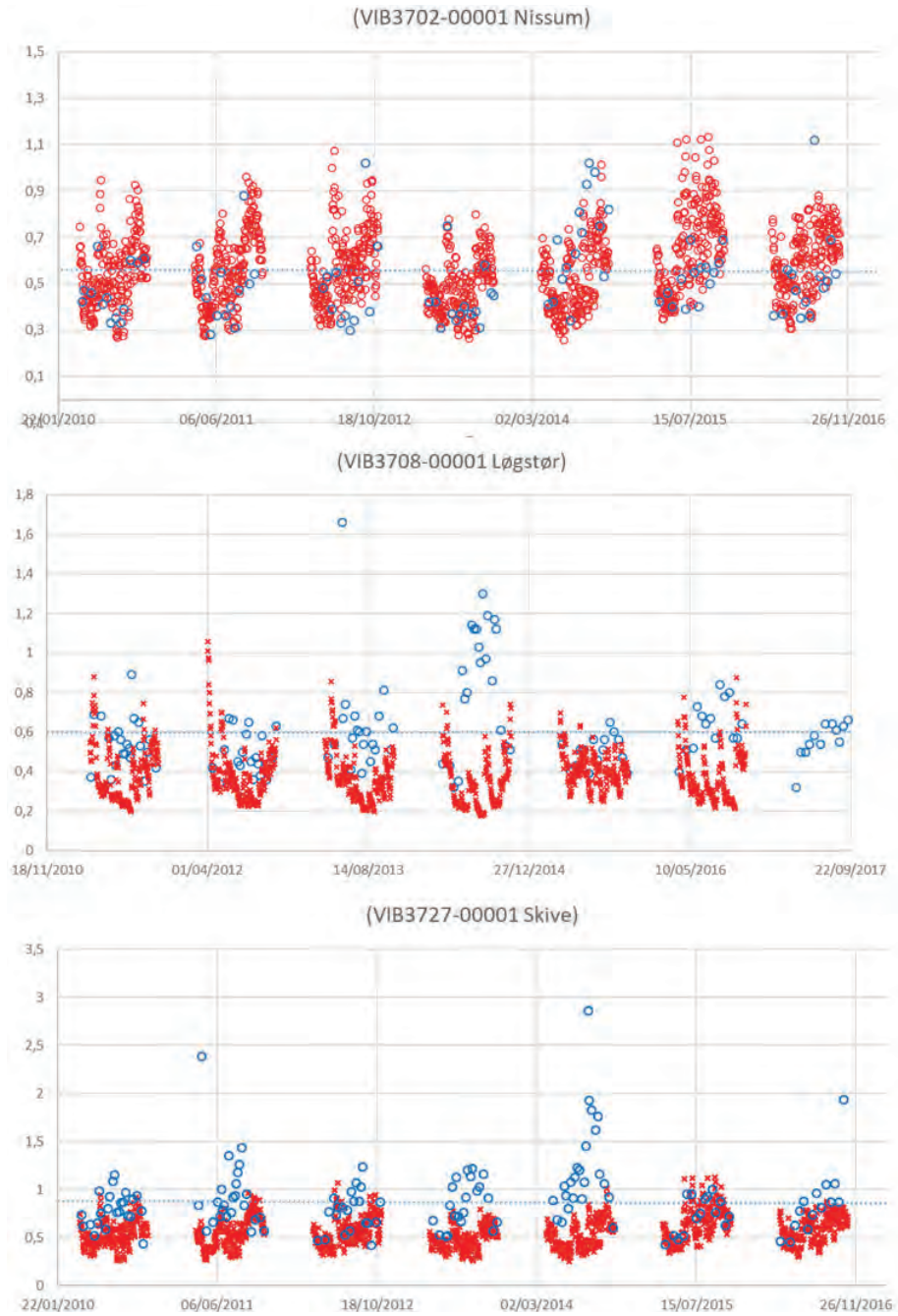


Figure 4.12. Comparison between measured (blue) and simulated (red) light attenuation coefficients (KD) for 3 NOVANA stations in Nissum Broad, Løgstør Broad, and Skive Fjord, respectively, from 2010 to 2016. Only values during the growth season April to October are included.

Re-Calculation of benthic Light

Re-calculation of benthic light based on more accurate bathymetry data was done using simulated Secchi depth converted into KD using the conversion equation proposed by Markager 2004. This conversion has been used previously by Staehr et al. (2019) for developing a national light index for an eelgrass model for predicting potential eelgrass habitats in Denmark, based on data of both measured KD and Secchi depth (SD) from the national monitoring program.

KD values can be calculated from model Secchi depths (SD):

$$KD = 2.3/SD \quad (\text{Markager 2004})$$

A time series representing photosynthetic active radiation (PAR) for 2010-2016 used as a forcing in the Limfjorden model, was provided by DHI as hourly values in the unit $\mu\text{E}/\text{m}^2/\text{s}$. Mean values for the period 1st of April to 1st of October for all 7 years 2010-2016 were calculated, considering daylight light hours:

Mean of Annual means +/- St.dev: 789 +/- 19 $\mu\text{E}/\text{m}^2/\text{s}$

Based on comparison in the previous section of the simulated KD values with corresponding measured KD values at NOVANA station in Nissum Broad, Løgstør Broad and in Skive Fjord, respectively, adjustment factors were calculated for each basin. The station in Skive Fjord was assumed to represent Lovns Broad. Adjustment factors were calculated based on the deviation between calculated mean of measured KD values and calculated mean of simulated KD values for the period 1st of April to 31st of October (2010-2016), for each of the NOVANA stations (Table 4.2). These adjustments assume that the horizontal variation in mean simulated KD values within each basin, despite the observed bias relative to measurements, still represent the relative horizontal variations of the actual KD within each basin.

Table 4.2. Adjustment factors applied for adjusting mean simulated KD values within each of the 3 basins: Nissum, Løgstør and Skive (~Lovns) marked in grey. Mean simulated values for additional NOVANA stations Kås, Nibe and Venø are included.

Location	Station	KD mean	KD mean	Adjustment factor
		2010-2016 (apr-oct) model	2010-2016 (apr-oct) measurement	
Nissum Br	VIB3702	0.588	0.514	0.874
Kås Br	VIB3705	0.480		
Løgstør Br	VIB3708	0.379	0.605	1.594
Nibe Br	VIB3711	0.454	0.595	1.311
Venø Bugt	VIB3720	0.457		
Skive Fj	VIB3727	0.560	0.893	1.594

As a last step, recalculation of light at seabed I_z relative to light at the surface I_0 was done using Lamberts Beers equation:

$$I_z = I_0 * e^{-z*KD}$$

Where depth z refers to total water depth and is based on the detailed depth data from DTU Aqua for the Limfjorden (Fig. 4.8, right), and KD are the interpolated values described above including the adjustment factors presented in table 4.1 and using the Universal Kriging interpolation method described in section 4.1.2.

The results for the three locations in the Limfjorden, including Nissum Broad, Løgstør Broad and Lovns Broad, are presented in figure 4.13-4.15.

Conclusion

The analysis presented in this section shows that the data layers in the eelgrass GIS tool developed by Flindt et al. (2016) and Canal-Vergés et al. (2016) representing benthic light can be improved by the use of a combination of bathymetry data with a high spatial resolution, by re-analysing the simulated light attenuation coefficients relative to measurements and calculated adjustment factors for individual areas, and by applying suitable methods for interpolation of simulated (and adjusted) light attenuation coefficients (KD).

For wave and current induced shear stress, no simple analytical method can be proposed. Instead, we propose that the simulated shear stress is re-calculated based on input from the hydrodynamic model (currents) and wave model (wave length and height) developed for the Danish marine coastal waters for the Danish Environmental Protection Agency, using more accurate bathymetry data.

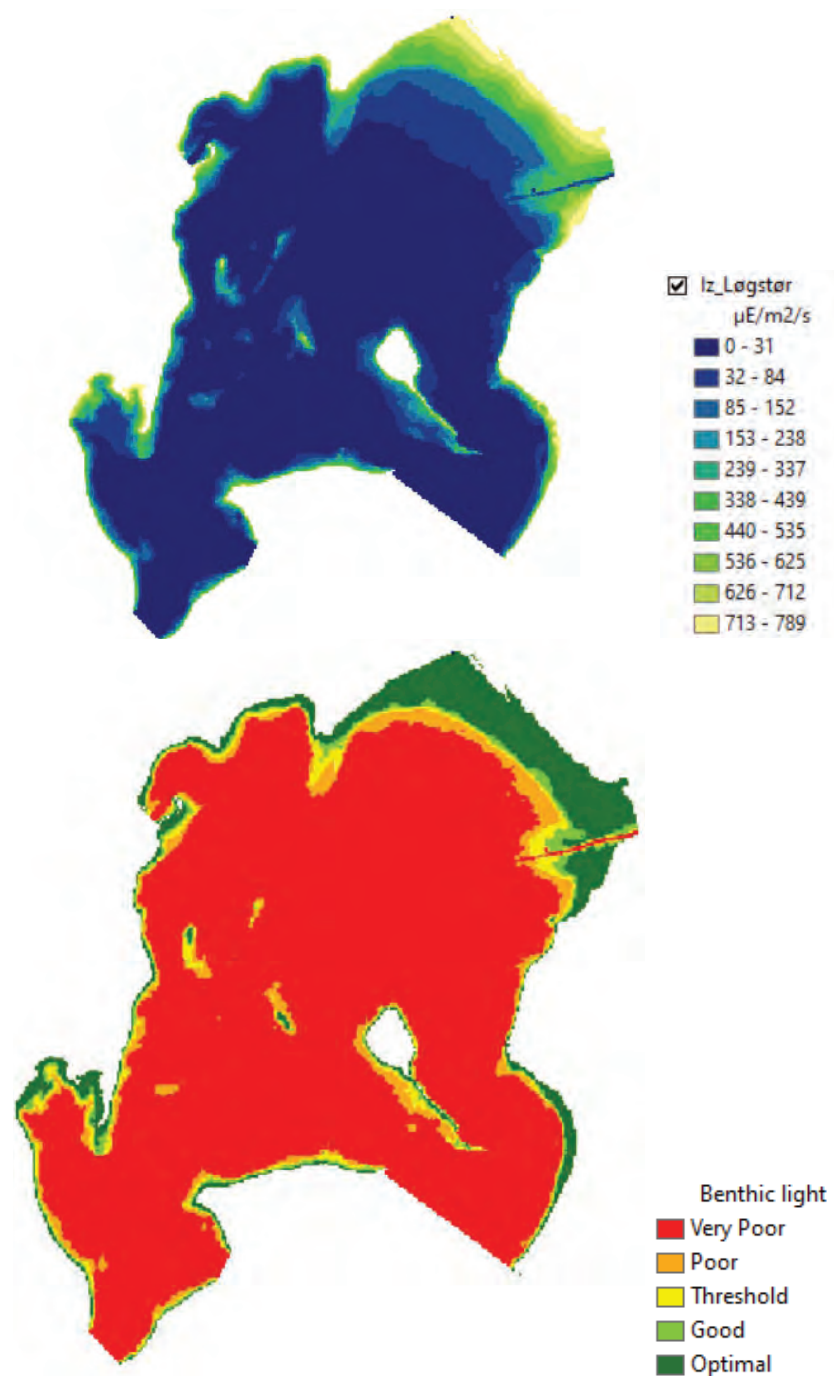


Figure 4.13. Top: Recalculated light at the seabed in Løgstør Broad using high resolution bathymetry data, and extracted, adjusted, and interpolated simulated KD values. Bottom: Classification of benthic light into 5 categories following Flindt et al. (2016) and Canal-Vergés et al. (2016).

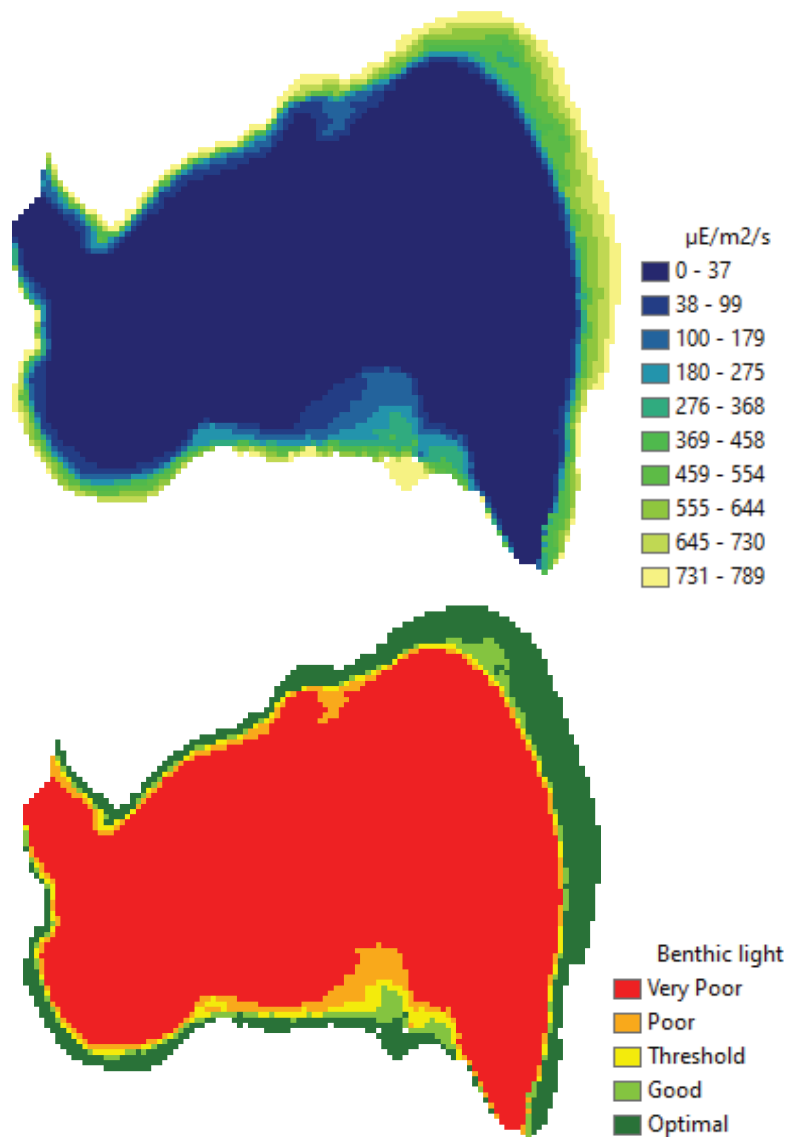


Figure 4.14. Top: Recalculated light at the seabed in Lovns Broad using high resolution bathymetry data, and extracted, adjusted, and interpolated simulated KD values. Bottom: Classification of benthic light into 5 categories following Flindt et al. (2016) and Canal-Vergés et al. (2016).

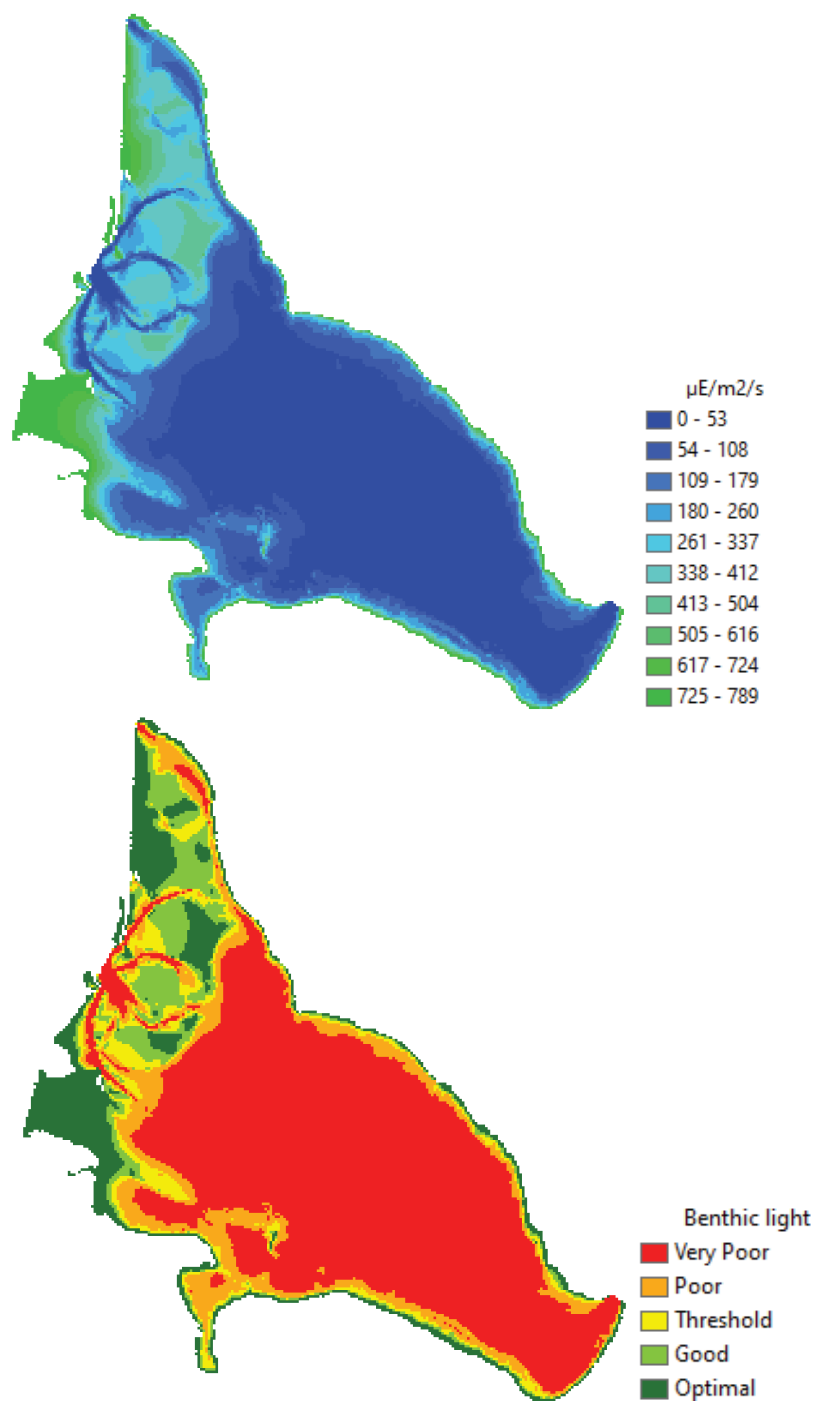


Figure 4.15. Top: Recalculated light at the seabed in Nisum Broad using high resolution bathymetry data, and extracted, adjusted, and interpolated simulated KD values. Bottom: Classification of benthic light into 5 categories following Flindt et al. (2016) and Canal-Vergés et al. (2016).

4.3 Implementing drone-data into GIS models

The UAV-based monitoring tool developed in section 2 allows the application of an eelgrass distribution layer to the GIS tool as a more accurate, time and labor efficient alternative to the interpolation-based layer described in section 4.1.1. With UAV-based monitoring, it is possible to generate eelgrass distribution layers of very high spatial resolution over relatively large areas, which especially in dynamic environments with fragmented eelgrass beds achieves higher accuracy of distribution values than an interpolation of point observations.

To test the possibility of creating a UAV-based eelgrass distribution layer that can be used in the GIS tool, we applied the UAV-based monitoring tool developed in section 2 to create an eelgrass distribution map of a 100 ha large area located along the southern coast of Lovns Broad. The site is characterized by shallow depths and a dynamic community of SAV species (mostly eelgrass) and bivalves (mostly blue mussels). The generated map was then converted into a raster layer format, used by the GIS tool. Finally, the outcome was compared with the interpolation-based layer, to assess the improved accuracy.

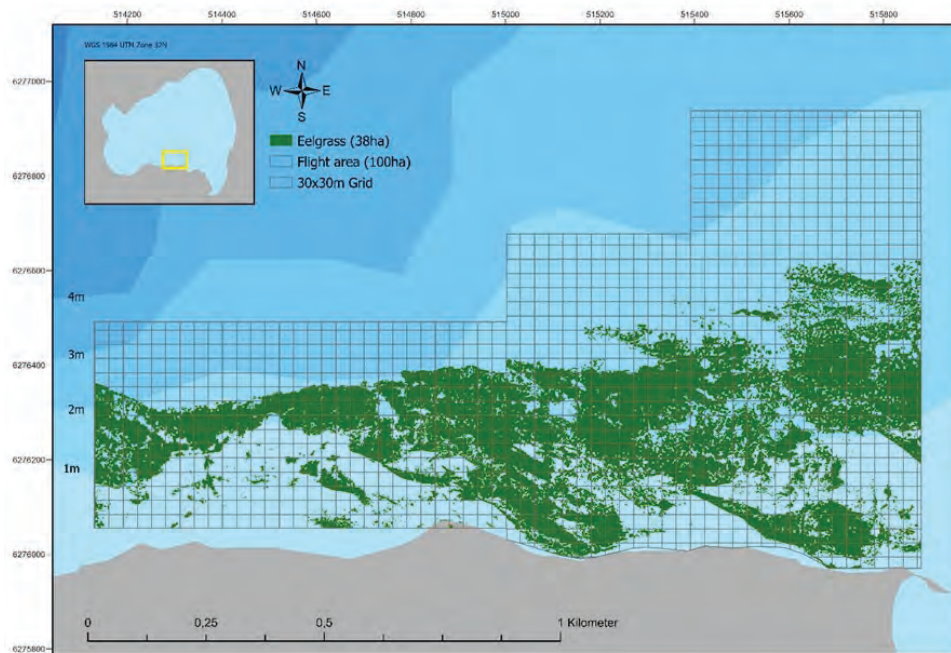


Figure 4.16. Detected eelgrass in the study area based on UAV monitoring with grid cells used in the GIS tool.

Out of the 100 ha, 38 ha were identified to have existing eelgrass cover (Fig. 4.16) (see more details in section 2.1).

In the GIS tool, each input parameter (one being existing eelgrass distribution) is represented by a raster layer classified into five ranges, according to how much the specific parameter affects the eelgrass establishment potential: 1) Optimal, 2) Good, 3) Threshold, 4) Poor and 5) Very poor (Flindt et al. 2016). Therefore, to fulfill the requirements of the GIS tool set-up, the high resolution (2.7 cm/pixel) UAV-based eelgrass cover map had to be converted into a 30x30 m square raster layer, where each square was classified into one of the five range classes. This

was done by creating a 30x30 m grid (Fig. 4.16) and calculating the percentage of eelgrass cover in each cell followed by a reclassification of each cell according to ranges given in table 4.3. The reclassification values were based on values from Flindt et al. (2016) given as g C m⁻² converted into first g DW m⁻² and then cover percent based on Fourqurean et al (1997) and Svane et al. (2021).

Table 4.3. Reclassification values for eelgrass coverage used to convert the UAV based eelgrass distribution into an input layer for the GIS tool. Based on Flindt et al. (2016), Fourqurean et al (1997) and Svane et al. (2021).

	Very poor (1)	Poor (2)	Threshold (3)	Good (4)	Optimal (5)
Coverage (%)	<1,27	<2,95	<5,90	<11,8	>11,8

After conversion, 56.8 ha were classified as being 'optimal' for eelgrass establishment, while 34.7 ha was classified as 'very poor' (Fig. 4.17). The eelgrass layer based on the interpolation method, on the other hand, resulted in 25.5 ha classified as 'optimal' for eelgrass establishment and 64.5 ha classified as 'very poor' (Fig. 4.18).

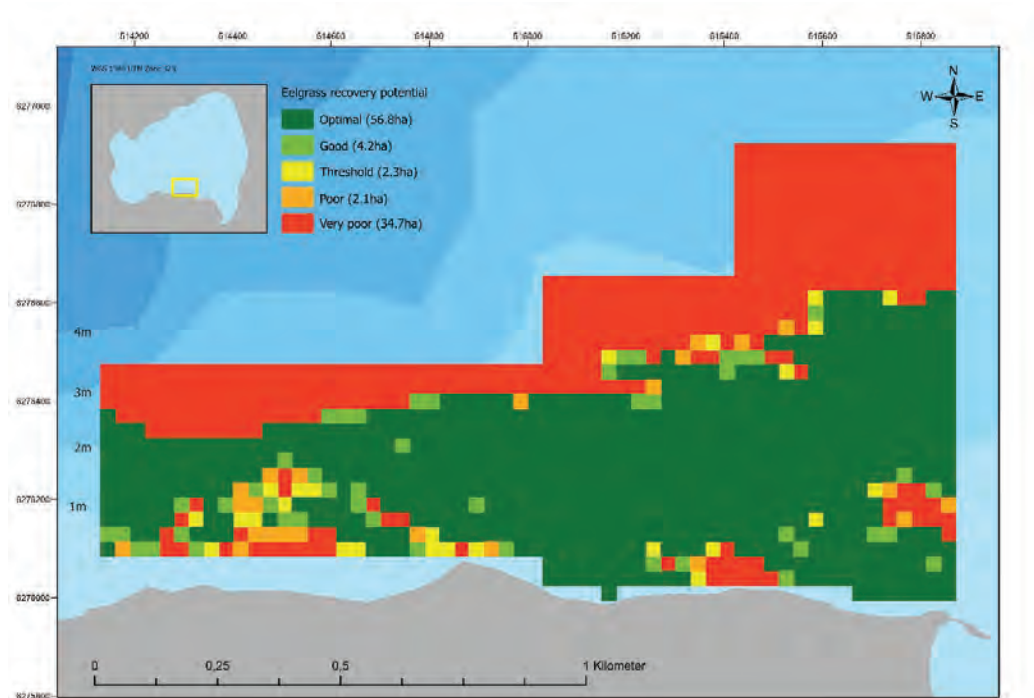


Figure 4.17. GIS-layer with classified eelgrass distribution based on UAV-derived data.

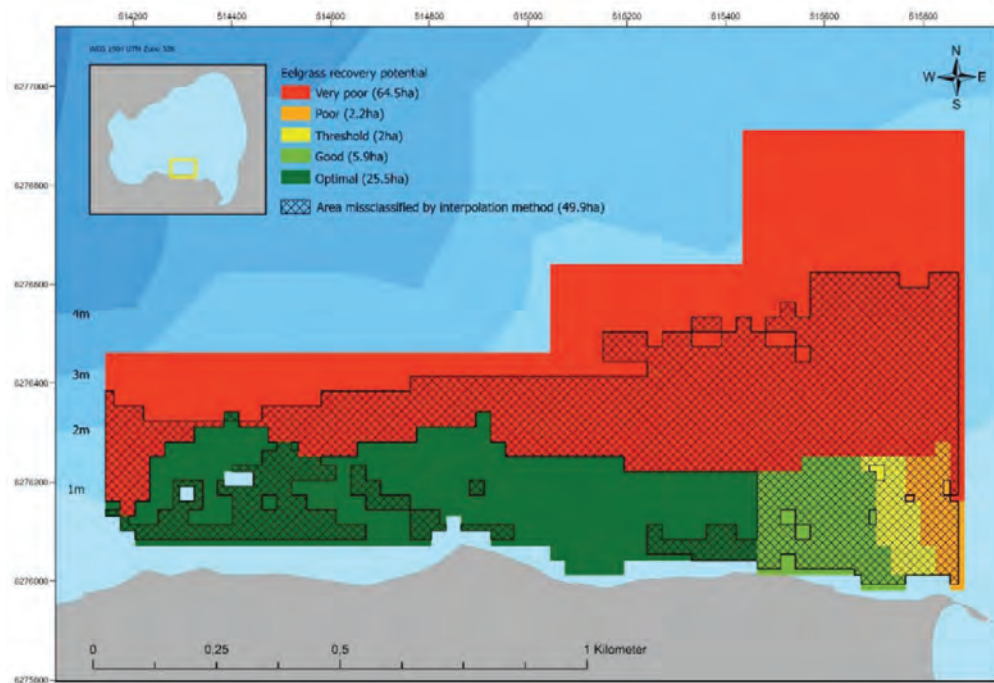


Figure 4.18. GIS-layer with classified eelgrass distribution based on the interpolation of point observation. Crosshatched area indicates misclassified area by the interpolation method.

In total, the interpolation method showed 49.9 ha of misclassification of which 32.8 ha ‘optimal’ and 2 ha ‘good’ conditions were incorrectly classified as ‘very poor’, ‘poor’ or ‘threshold’ conditions. This means that the UAV based eelgrass distribution layer provides the GIS tool with information on an additional 34.8 ha existing eelgrass in this study site of 100 ha. Compared to the interpolation-based method (section 4.1.1), that is an increase of 111%. Figure 4.18 shows the area that was misclassified by the interpolation method and figure 4.19 the area of eelgrass that is subsequently not considered by the GIS tool.

Based on this study, it can be concluded that for shallow-water dynamic areas with heterogeneous eelgrass growth patterns, the GIS-layer based on UAV monitoring qualifies as a more accurate alternative to the layer based on the interpolation of point observations. Because monitoring shallow and heterogeneous areas using the traditional in-water methods is difficult in the first place, it is suggested to cover these areas using UAV-based monitoring methods (given the higher accuracy and accessibility possibilities using UAVs), while traditional in-water techniques are better suited for deeper and more homogeneous environments.

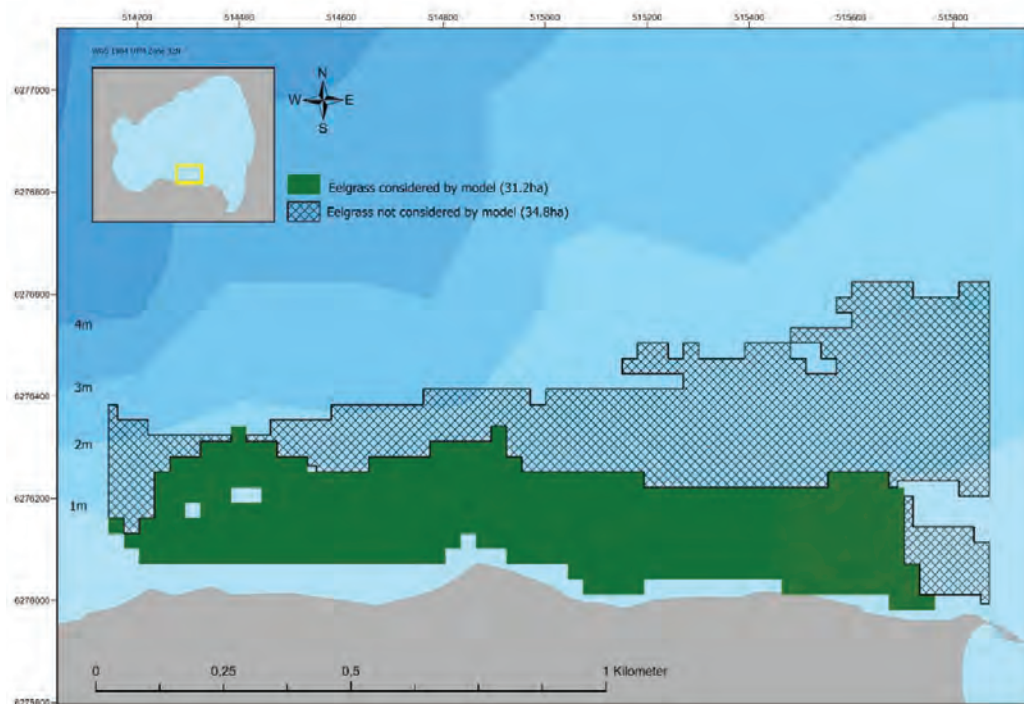


Figure 4.19. Green: Area of eelgrass distribution considered by the GIS-model, based on interpolated point observations. Crosshatched: Area of eelgrass distribution not considered by the GIS-model when the input layer of eelgrass distribution is based on the interpolation model.

5. Conclusions and recommendations

Conclusions

The overall aim of this project was to investigate various ways to optimize the current approach in eelgrass mapping and monitoring, primarily in relation to EIA's in Natura 2000 areas subjected to dredge fishing activities, but with the potential to be implemented in e.g., environmental management. The approach was to investigate the potential of implementing new technological tools in the field (i.e., UAVs, ROVs and AUVs) as well as to optimize existing eelgrass models currently used in EIA's for different water bodies in Denmark.

The results show that an UAV-based monitoring of eelgrass habitats can contribute significantly to large-scale eelgrass monitoring by providing data of high spatial resolution and accuracy in a labor and time efficient way. Using an off-the-shelf drone (DJI Phantom 4 RTK) with a conventional RGB sensor in combination with a fit-for-purpose image analysis approach, UAVs were found useful in both turbid and deep-water habitats, with the possibility to map eelgrass efficiently until 2-3 m in Limfjorden and 5.5 m depth in the Kattegat. The results also showed that multispectral sensors can be useful in some cases to detect eelgrass in turbid and deep waters. However, they are also more sensitive to environmental conditions, especially those affecting the water surface, such as wind and light reflections. Therefore, the significantly higher image resolution, and the resulting ability of covering more area in less time, makes the conventional RGB sensor a more reliable tool when mapping eelgrass in those environments.

With small, customized adjustments, the light-weight multi-rotor UAVs are also highly useful for ground truthing missions providing high-quality imagery for data validation in the following image analysis process. Using either a spool-line or fixed-line camera-setup attached underneath the UAV for ground truthing in coastal waters proved a feasible way of collecting ground truthing imagery in a systematic way, whereas setups relying on the drone to land on water, were not considered reliable.

For achieving the best possible classification of UAV-derived images of submerged eelgrass beds, the study provides a solid OBIA (object-based-image-analysis) workflow that will help practitioners select the appropriate classifiers and algorithm-related hyper-parameter tuning. The high accuracy of the different tested classifiers showed that OBIA has great potential when used for the classification of submerged eelgrasses in Danish waters. By decreasing uncertainties and time and effort spent on choosing the most appropriate classifier set-up, the use of UAV-based techniques in coastal monitoring programs might become more widespread, resulting in more accurate spatial information about existing eelgrass habitats and their growth/decline over time.

In areas beyond the depth suitable for UAV-based mapping, our results indicate that unoccupied and autonomous underwater systems offer a viable alternative for mapping, although, in contrast to the UAV-based monitoring, these systems are at the current stage challenged by the precision and accuracy of the data. Alternatively, the traditional method with a camera on a towed sledge can still be considered, although, in the setup used in the EIA's, this method only provides point observations and not actual areal mapping. For this, the study provides a new improved method for interpolation of point-based data using 'inverse distance weighted' (IDW)

interpolation in a loop for each depth interval using only the two nearest points. IDW is an interpolation method that estimates non-surveyed areas based on observations in the immediate vicinity. The further an observation is from the non-surveyed area the less impact it has, meaning that closer points will have greater weight. Compared to the previously used “spline with barriers” (using depth as a barrier), the method is especially useful in areas with heterogeneous vegetation patterns and a complex bathymetry such as the Limfjorden as it a) accounts for abrupt changes and changes occurring over short distance such as scattered patches of submerged aquatic vegetation and b) as neighboring points with the same depth value will still influence each other even if they are separated by a bathymetry line.

At the end, combining different methods i.e., UAVs to cover the shallow waters and ROVs or traditional in-water methods, such as towed cameras, to cover deeper waters; seems to be an effective methodology for eelgrass mapping on a water basin scale (e.g., Lovns Broad). By such, the resources needed can be slightly reduced, compared to the current method of EIAs, while the provided data will be of significantly higher accuracy and resolution. Specifically, we found that comparing the current method (video transect) to a scenario where the depth range 0-3 m of the broad are instead mapped by drone (44 hours), and the deeper parts (>3 m) are still based on video transect (30 hours), the mapping could be done with slightly less resources (6 hours). Of much more importance is however the significantly higher accuracy and resolution of the drone-based mapping compared to the current interpolation of point observations that does not always align with the actual eelgrass distribution.

Additionally, the in-field methods for eelgrass mapping can be combined with the use of dynamic models to add extra value in a management perspective, for instance in the case of the GIS tool, used in the EIAs to evaluate areas with good eelgrass establishment potential. Here, the study showed that implementation of UAV-based data, as a more accurate alternative to the currently used point-based interpolation, resulted in a big improvement of the eelgrass layer, that is being used as one of the input layers in the GIS tool. Thus, in a 100 ha test site in the southern part of Lovns Broad, the UAV based eelgrass distribution GIS layer showed 34.8 ha more eelgrass than the layer based on point-based interpolation (31.2 ha), corresponding to an increase of 111%.

Further possibilities to improve the GIS tool were found related to the model layers representing benthic light and shear stress. For light, our analysis shows that the data layers in the eelgrass GIS tool representing benthic light can be improved using a combination of bathymetry data with a high spatial resolution, by re-analysing the simulated light attenuation coefficients relative to measurements and calculated adjustment factors for individual areas, and by applying suitable methods for interpolation of simulated (and adjusted) light attenuation coefficients (KD). For wave and current induced shear stress, no simple analytical method was achieved. Instead, we propose that the simulated shear stress is re-calculated based on input from the hydrodynamic model and wave model developed for the Danish marine coastal waters for the Danish Environmental Protection Agency, using more accurate bathymetry data.

Besides large-scale eelgrass mapping, the result of the study shows the potential of UAVs for various other applications related to eelgrass monitoring. For instance, we show that seasonality related changes in eelgrass bed cover, as well as the effects of various stressor (e.g., ice cover, epiphytes, drifting macroalgae) can be monitored at high detail over relatively large areas

in an easy and economically feasible way due to the high spatial resolution, spatial accuracy and temporal flexibility provided by UAVs. UAVs can then be used to visualize eelgrass cover gain and loss between time steps in different scenarios, and thereby act as an easy quantifiable tool to assess eelgrass performance. A specific application for this is in the work of eelgrass restoration, where the growth performance of transplanted eelgrass shoots can be assessed in a relatively easy way compared to more demanding diver-based investigations.

Recommendations

To incorporate UAV-based eelgrass mapping into monitoring programs, it is important to consider aspects that facilitate repeatability, data comparability and easiness of its application. Based on the findings of this project, we suggest a setup that fulfils this, and at the same time is robust, widely applicable, and cost-efficient. In terms of hardware, we recommend a light-weight multi-rotor UAV equipped with a high resolution RGB camera and an RTK module in combination with a customized ground truthing setup.

The variety of features using light-weight multi-rotor UAVs allows for an application in a multitude of monitoring missions; from collecting ground truthing data over low altitude flights for small scale change detection and stressor analysis to large scale monitoring missions. The lightweight multi-rotor UAVs are usually equipped with RGB cameras of very high resolution (>20 MP), on was in this study proven to be superior to more advanced narrow band but lower resolution multispectral cameras when monitoring submerged eelgrass in the turbid or deep waters of coastal Denmark.

It is also recommended to opt for a UAV with an RTK receiver module, that allows for highly precise positioning of the UAV and thereby increases the spatial accuracy of the obtained data. Thus, RTK corrected data enables precise mapping and identification of even the smallest changes in eelgrass bed extent, as well as the highly precise collection of ground truthing data, which becomes especially important in environments of scattered growth forms or mixed habitats. For the easiest use of the RTK module, we furthermore recommend an RTK-network subscription.

For ground truthing, it is suggested to use a simple underwater camera system that can quickly be mounted underneath the same UAV used for aerial monitoring. For larger ground truthing missions and the application of additional loggers, it is suggested to invest in a system carried by a larger UAV, such as the Matrice 600.

For flight planning and processing of UAV-based imagery, different software is needed. We highly recommend planning and executing flights using flight mission planning software that allows for easy export and sharing of survey missions. In this project we used the software UgCS as it is compatible with many UAV models and allows for customized payload arrangements. For aligning and combining single georeferenced images to create orthomosaics over large areas, advanced photogrammetric software (e.g., Agisoft or Pix4D) is also needed. To analyze orthomosaics, we recommend using a development environment for object-based image analysis such as eCognition Developer software. At the end, to further process, analyze or visualize the produced data in the form of maps, a GIS software is needed. Depending on the user's needs, it can be chosen between open-source solutions (e.g., QGIS) or more advanced software such as ArcGIS, that provides a wider range of features.

While, due to its versatility, cost-efficiency and applicability, the suggested set-up is based on a multirotor UAV platform; in the future, other platforms, such as fixed-wing or hybrid UAVs can be recommended for long-term reoccurring survey campaigns, when focusing solely on large-scale monitoring of eelgrass beds (e.g., EIA's related to the mussel fishery). Here, the higher acquisition costs and efforts for acquiring special flight permits are paid off by the increased efficiency during data collection. While data processing and analysis workflows can be performed in the identical way when using a fixed-wing UAV instead of a multirotor UAV, the increased complexity of the UAV flights in terms of take-off and landing and maneuverability must however be taken into consideration. The collection of ground-truth imagery for a large-scale fixed-wing UAV-based monitoring campaigns is still recommended to be done with a multirotor UAV, using method presented in this report. Also, for monitoring purposes that do not require large scale mapping, such as low altitude flights for small scale change detection and stressor analysis, the variety of features that the lightweight multi-rotors AUVs allow for, would in many cases make these easy operatable platforms a more recommendable choice of equipment.

As a supplement to in-field observations, models are also valuable tools in a management perspective as they can for example describe the potential of eelgrass distribution in relation to the importance of key environmental indicators as the case for the GIS tool used in EIAs. However, for models to be reliable, the data they are based on needs to be of the best possible quality. In this study, we give specific solutions on how the data layers for two of the most important input layers, light and shear stress, could be improved, and thus, improve the overall output of the model. However, the proposed solution that the simulated shear stress is re-calculated based on input from the hydrodynamic model (currents) and wave model (wave length and height), using more accurate bathymetry data, was beyond the scope of this project. We therefore recommend this to be brought up in future projects of relevance.

References

- Canal-Vergés P, Petersen J K, Rasmussen E K, Erichsen A, Flindt M R, 2016. Validating GIS tool to assess eelgrass potential recovery in the Limfjorden (Denmark). *Ecological Modelling*, Volume 338, 2016, Pages 135-148, ISSN 0304-3800, [xhttps://doi.org/10.1016/j.ecolmodel.2016.04.023](https://doi.org/10.1016/j.ecolmodel.2016.04.023).
- Carstensen J, Krause-Jensen D, Markager S, Timmermann K, Windolf J (2013). Water clarity and eelgrass response to nitrogen reductions in the eutrophic Skive fjord, Denmark. *Hydrobiologia* 704: 293-309.
- Erichsen A and Birkeland M 2019. Development of Mechanistic Models. Mechanistic Model for Limfjorden. Hydrodynamic model documentation. Technical Note. December 2019. Prepared by DHI GROUP for Danish EPA.
- Erichsen A and Birkeland M 2020. Development of Mechanistic Models. Mechanistic Model for Limfjorden. Technical documentation on biogeochemical model. Technical Note. December 2019. Prepared by DHI GROUP for Danish EPA.
- Flindt M R, Rasmussen E K, Valdemarsen T, Erichsen A, Kaas H, Canal-Vergés P, 2016. Using a GIS-tool to evaluate potential eelgrass reestablishment in estuaries, *Ecological Modelling*, Volume 338, 2016, Pages 122-134, ISSN 0304-3800, <https://doi.org/10.1016/j.ecolmodel.2016.07.005>.
- Fourqurean JW, Moore TO, Fry B, Hollibaugh JT (1997). Spatial and temporal variation in C:N:P ratios, $\delta^{15}\text{N}$, and $\delta^{13}\text{C}$ of eelgrass *Zostera marina* as indicators of ecosystem processes, Tomales Bay, California, USA. *Marine Ecology Progress Series* 157:147-157.
- Greeve TM, Krause-Jensen D (2005). Predictive modelling of eelgrass (*Zostera marina*) depth limits. *Mar Biol* 146: 849-858
- Kuusemäe K, Rasmussen EK, Canal-Vergés P, Flindt MR (2016). Modelling stressors on the eelgrass recovery potential in Danish estuaries. *Ecological Modelling* 333: 11-42.
- Lange T, Oncken NS, Svane N, Steinfurth RC, Kristensen E, Flindt MR (2022). Large-scale eelgrass transplantation: a measure for carbon and nutrient sequestration in estuaries. *Marine Ecology Progress Series (MEPS)* 685: 97-109. <https://doi.org/10.3354/meps13975>.
- Lønborg, C., Thomasberger, A., Staehr, P. A. U., Stockmarr, A., Sengupta, S., Rasmussen, M. L., Nielsen, L. T., Hansen, L. B., & Timmermann, K. (2022). Submerged aquatic vegetation: overview of monitoring techniques used for identification and determination of spatial distribution in European coastal waters. *Integrated Environmental Assessment and Management*, 18(4), 892-908. <https://doi.org/10.1002/ieam.4552>
- Markager S (2004). Tekniske anvisninger for marin overvågning. Andersen, Markager & Ærteberg (red.). 1.3. Lyssvækkelse. 27-10-04.

Murray, C., and Markager, S. (2011). "Relationship between Secchi depth and the diffuse light attenuation coefficient in Danish estuaries," in Proceedings of the Baltic Sea Science Conference, St. Petersburg

Nielsen SL, Sand-Jensen K, Borum J, Geertz-Hansen O (2002). Depth colonization of eelgrass (*Zostera marina*) and macroalgae as determined by water transparency in Danish coastal waters. *Estuaries*, 25(5): 1025-1032.

Nielsen, M.M., Linden-Vørnle, M., & Petersen, J. K. (2019). Forvaltningsgrundlag for fiskeri af muslinger i Natura 2000-områderne Horsens Fjord og Lillebælt. Technical University of Denmark. DTU Aqua-rapport No. 343-2019

Staehr PA*, Cordula Göke, Andreas M. Holbach, Dorte Krause-Jensen, Karen Timmermann, Sanjina Upadhyay and Sarah B. Ørberg 2019. Habitat Model of Eelgrass in Danish Coastal Waters: Development, Validation and Management Perspectives. *Perspectives. Front. Mar. Sci.* 6:175. doi: 10.3389/fmars.2019.00175

Svane N (2020) Development of Analytical Methods Based on Drone Information. PhD Thesis.

Svane N, Lange T, Egemose S, Dalby O, Thomasberger A, Flindt MR (2021). Unoccupied aerial vehicle-assisted monitoring of benthic vegetation in the coastal zone enhances the quality of ecological data. *Progress in Physical Geography* 0(0): 1-18.

Thomasberger, A., Nielsen, M. M., Flindt, M. R., Pawar, S., & Svane, N. (2023): Comparative Assessment of Five Machine Learning Algorithms for Supervised Object-Based Classification of Submerged Seagrass Beds Using High-Resolution UAS Imagery. *Remote Sensing*, 15(14), 3600.

Valdemarsen T, Canal-Verges P, Kristensen E, et al. (2010) Vulnerability of *Zostera marina* seedlings to physical stress. *Marine Ecology Progress Series* 418: 119–130. DOI: 10.3354/meps08828.

Technical
University
of Denmark

DTU Aqua
Øroddevej 80
DK-7900 Nykøbing M.

www.aqua.dtu.dk